Numerical analysis of surface settlements induced by a fluid-supported tunnelling machine

Masterarbeit zum Erwerb des
akademischen Titels Diplomingenieur der
Studienrichtung Bauingenieurwesen

Verfasst von
Schaunig Gerhard

verfasst am Institut für
Bodenmechanik und Grundbau
der Technischen Universität Graz

Betreuer der Masterarbeit:
Univ.-Ass. Dipl.-Ing. Franz Tschuchnigg

Begutachter der Masterarbeit:
AO.Univ.-Prof. Dipl.-Ing. Dr.techn. M.Sc. tit. Univ.-Prof. Helmut Schweiger

Graz, im Oktober 2012

Kontakt:
Schaunig Gerhard
schaunig@student.tugraz.at

Eidesstattliche Erklärung

Ich erkläre an Eides statt, dass ich die vorliegende Arbeit selbstständig verfasst, andere als die angegebenen Quellen/Hilfsmittel nicht benutzt, und die den benutzten Quellen wörtlich und inhaltlich entnommene Stellen als solche kenntlich gemacht habe.

Statutory Declaration

I declare that I have authored this thesis independently, that I have not used other than the declared sources / resources, and that I have explicitly marked all material which has been quoted either literally or by content from the used sources.

Graz, im Oktober 2012 .....

Schaunig Gerhard

Acknowledgments

At first I want to express thanks to all those who were supporting me throughout my whole studies, friends, colleagues, assistants and also professors. I would like to especially acknowledge the support of Mr. Tschuchnigg and Prof. Schweiger, whose patience and help throughout the duration of my thesis has been an essential contribution to final draft. Without all my supporters I would not have been able to graduate from university in this period of time.

I also want to thank Dipl.-Ing. Johannes Jaeger, Dipl.-Ing. Berner Thomas and Dipl. –Ing. Johannes Gfrerer (BEMO GmbH) for supplying me with the subject for my final thesis and all the necessary information related to it.

Finally I want to express my gratitude to my parents who contributed as much as they could for a successful completion of university. Without the support and the patience of my parents I would not have been able make it through 6 years of university.

Kurzfassung

Den Hintergrund der Arbeit bildet ein Projekt in der Leipziger Innenstadt in Deutschland. Das Projekt umfasst den Bau zweier U-Bahn Tunnel mit den jeweils dazugehörigen Haltepunkten. Beide Tunnelröhren wurden rund 10-15m unter der Oberfläche durch eine vollautomatisierte flüssigkeitsgestützte Tunnelbohrmaschine (TBM) hergestellt. Die Stützung der Ortsbrust erfolgte in diesem Fall durch eine Bentonit-Suspension, welche in die vorderste Kammer der Maschine gepumpt wird. Der Ausbau erfolgt durch Betonfertigteile, sogenannten Tübbingen, welche fest miteinander verbunden werden. Der hierbei entstehende Spalt zwischen den Betonfertigeilen und dem ausgebrochenen Boden wird mittels einer Mörtelinjektion verpresst.

Ziel dieser Masterarbeit war es, die Interaktion der Tunnelbohrmaschine und den die Maschine umgebenden Flüssigkeiten mit dem Baugrund zu simulieren und die Auswirkungen auf Oberflächensetzungen zu untersuchen.

Dabei wurde vorab eine Studie zu den verschiedenen Bauweisen von Tunnelbohrmaschinen, welche für den Betrieb im Lockergestein geeignet sind, ausgearbeitet. Anhand der Daten der TBM, zur Verfügung gestellt durch Alpine Bau GmbH, war es möglich, die genauen Setzungen sowie die Stützdrücke rings um die Maschine im Untersuchungsgebiet zu definieren. Basierend auf den bodenmechanischen Werten aus dem Geotechnischen Bericht für dieses Projekt, wurde eine numerische Analyse der Oberflächensetzungen und der Schnittkräfte mithilfe von PLAXIS 2D und 3D durchgeführt.

Die abschließenden Ergebnisse zeigen, dass die numerische Analyse mit den realen Bedingungen sehr gut übereinstimmt und die verschiedenen Drücke der flüssigkeitsgestützten TBM mit der gewählten Modellierungsweise simuliert werden können.

Abstract

The background of this thesis is a project in the city centre of Leipzig, Germany. Scope of the project was the construction of two tunnels to connect the metro stations “Bayrischer Haltepunkt” and “Hauptbahnhof” within the city centre. Both tunnels were constructed using a fluid-supported tunnelling machine so called “Hydro- or Mixshield” TBM (tunnel boring machine). A bentonite suspension is simultaneously used as medium for supporting the tunnel face and for disposal of the excavated soil. The subsequently installed lining in the back of the TBM is made out of pre-fabricated concrete segments. The gap arising between outer radius of the lining segments and the soil cut-surface of the tunnel is immediately filled with grout or a grout-like material.

The aim of this master thesis is on the one hand to investigate the influence of both fluids and the henceforth imposed pressure on surface and sub-surface settlements. On the other hand it was necessary to evaluate a suitable modelling method for shield driven tunnels, using PLAXIS 2D and 3D as software for the numerical analysis.

A pre-survey on the options of tunnel boring machines available for excavation in soil or loose rock was carried out to distinguish the mechanical devices and the construction sequences for such a type of mining machine. Furthermore, based on data from the city tunnel in Leipzig, it was necessary to evaluate the pressures acting around the TBM and to investigate the influence on surface and sub-surface settlements. Using simple analytical solutions, the pressure in-crease/decrease along the shield of the TBM could be estimated and further incorporated into the numerical analysis.

The concluding analysis shows that it is possible to accurately approximate surface and sub-surface settlements induced by a fluid-supported tunnelling machine. It further shows that the grout or grout-like material and the corresponding pressure influences the results strongly and if not evaluated correctly these can lead to significant differences at the numerical analysis.

Table of contents

1 Introduction

The aim of the following thesis is on the one hand to investigate the influence of slurry and grouting pressures around a fluid-supported tunnel boring machine (TBM) on surface and sub-surface settlements. On the other hand it was necessary to develop an appropriate numerical modelling-method for shield driven tunnels. The thesis aims on investigating the correlation of actual grout pressures and the input values used for the numerical analysis. Furthermore, a case study on the anisotropic behaviour of the tunnel lining was conducted and compared to results using isotropic properties. The data used for the thesis is based on the city tunnel in Leipzig (CTL), which is supposed to connect the metro stations “Bayrischer Haltepunkt” and the central station within the city centre. The twin tunnels and associated metro-stations were built in the years from 2004 to 2011 by company “Alpine Bau Gmbh”, which subsequently provided the data incorporated in this thesis.

The objective of this thesis was to investigate the influence of fluid-supported tunnelling, thus the subsequent grouting measures, tapering of the TBM and furthermore the anisotropic lining behaviour on surface and sub-surface settlements.

2 Mechanized shield tunnelling

2.1 Introduction

Growth of the cities and further development of infrastructure and transport technologies in the 19th century led to more and more congested areas within the urban settlements. Consequently new space needed to be found for further public transport systems. The sought for construction areas beneath the ground level led to the decisive invention of mechanized tunnelling machines. A huge step was achieved in modern way tunnelling by substituting manpower by mechanical excavation.

The development of tunnelling machines took place in the early 19th century in London. Sir Marc Brunel invented the principle of shield driven tunnels in 1806 in London, first as a solution to undermine the river Newa in St. Petersburg, which was then superseded and substituted by a cable stayed bridge instead of a tunnel. In 1825 Sir Marc Brunel´s shield was used for the construction of the first tunnel to be built underneath the Thames in London, which, after serious cases of flooding, got completed in 1843. Callodan was the first one to suggest compressed air to prevent the ingress of water into the tunnel, yet this technique was refused by Brunel. 26 years later, engineer Henry Greathead successfully undermined the Thames again, for the first time using steel fabricated lining rings. The construction of the 2.2 m wide tunnel was done without any difficulties and delays. Although the principle of compressed air was introduced years earlier, the first tunnel to be completed in such a manner was in 1886 for the “tube” in London. The invention of the compressed air method was a huge step forward for tunnelling in permeable soils underneath the groundwater level. Due to the existing pressure inside the cavity, the ingress of water could be

omitted. Consequently it was possible to construct tunnels, which yet have been impossible to be executed due to difficult soil conditions.

In the beginning of the 20th century almost all the shields were based on the principle of Henry Greathead. After the second World-War, the principle of mechanized shield tunnelling was further improved and in 1959 the method of a fluid-supported tunnel was successfully used for the first time for the construction of a sewer-channel. The development of mechanized underground excavation reached a top at the tunnel underneath the Elbe in Hamburg, where the diameter of the TBM (tunnel boring machine) reached a maximum of 14.2 m, which is until today the biggest machine ever used for underground tunnelling works.

(Maidl, et al., 2011)

2.2 Fluid-supported tunnelling machines

The following chapter shows the principle and the construction details of fluid supported tunnelling machines, focusing on the “Hydroshield” rather than earth-pressure-balance (EPB) machines.

Fluid supported tunnelling was first introduced by James Henry Greathead in 1874. Especially in high permeable soil, where air-pressurized support systems are very difficult to use, the development of a new tunnelling principle was needed to overcome the problems occurring in such ground conditions.

2.2.1 Development

Although the principle had already been introduced in 1874, the first slurry-shield to be built was a drainage tunnel by E.C. Gardener in 1959.

The development of slurry pressurized tunnelling machines almost simultaneously took place in Japan, Great Britain and Germany. In Japan Mitsubishi was the first manufacturer to build a slurry shield in 1970, likewise in Great Britain the Robert L. Priestley Company introduced the first bentonite-shield in 1971. In Germany Wayss&Freytag developed the “Hydroshield” system which had first been used for the Hamburg-Willhelmsburg collector underneath the Hamburg port. (Maidl et al.,2011)

2.2.2 Principle

When using fluid supported tunnelling machines, the tunnel face is supported with pressurized slurry, bentonite, a polymer suspension or in case of the EPB (Earth-pressure-balance) with the excavated material itself. In case of a fluid-supported TBM the suspension fluid is pumped into the closed excavation chamber, forming a “filter-cake” at the tunnel face and is balancing the earth and water pressure which is acting as force against the opening.

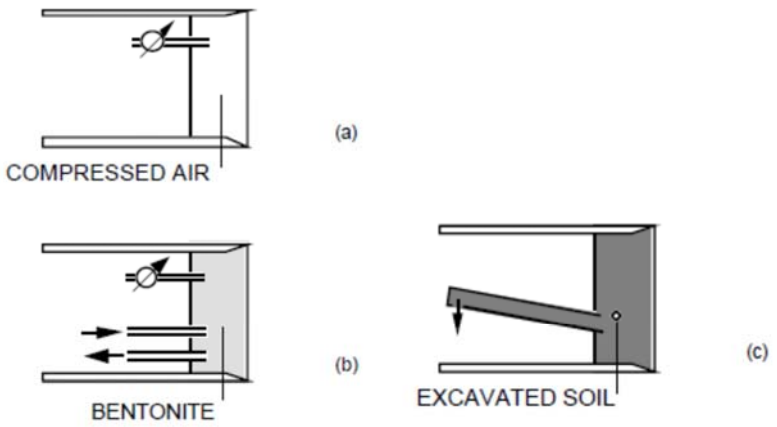

Figure 2-1: Fluid supported machines, principle **(Anagnostou, et al., 1994)**

The slurry simultaneously serves as transport medium, where the excavated material is conveyed through a hydraulic pipe system to a separation plant. Hence hydraulic pipes and hoses must be installed all along the tunnel to the tunnel face.

Beside the normal principle of using slurry or bentonite for stabilizing the tunnel face, there are some modified versions of fluid/slurry balance machines, which can be used for a wider range of ground conditions, as for example the Thixshield, Hydrojetshield or the typical Hydroshield, yet this thesis will only focus on the latter. In Europe the principle of the Hydroshield is the most well-known system for using fluid supported tunnelling machines

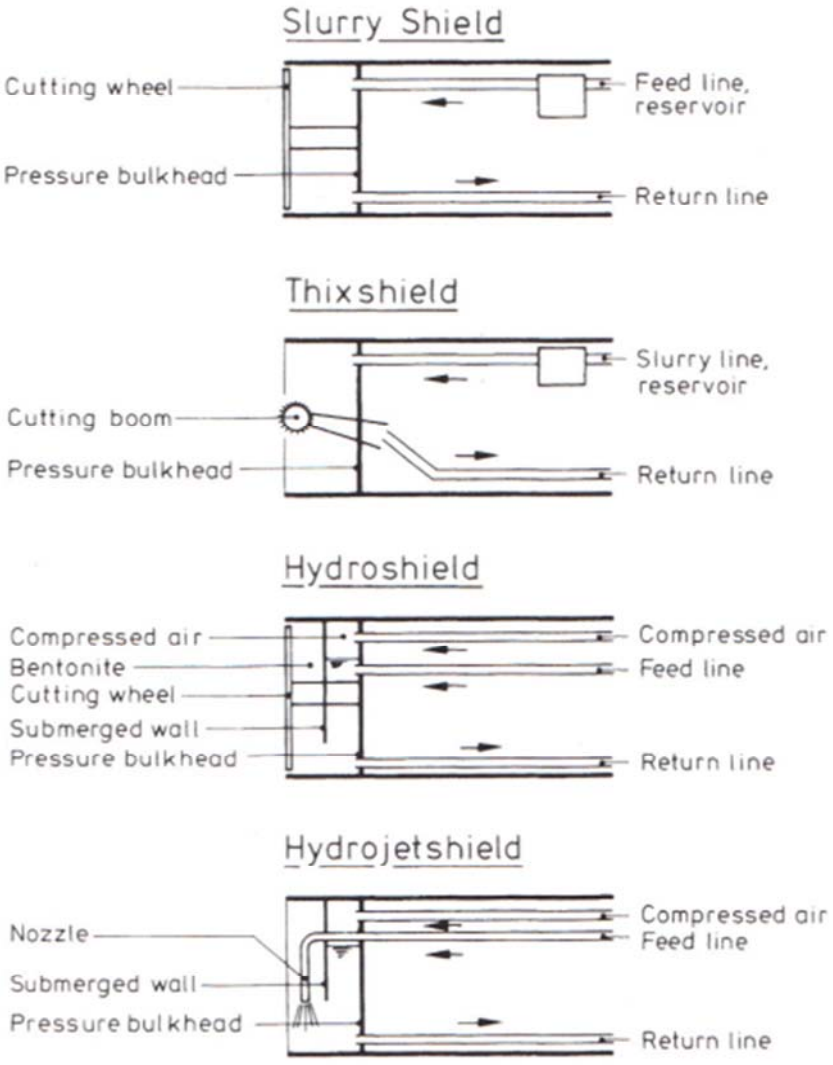

Figure 2-2: Operating principles of slurry-shields, see also Maidl et al. (2011)

2.2.3 Earth pressure balance machines

The following pages will only touch on the subject of earth pressurized tunnelling machines.

2.2.3.1 Principle

Using earth balance tunnelling machines, the tunnel face is supported with the excavated material itself which can be combined with additives.

The excavated material forms a cohesive supporting sludge within the excavation chamber (2), which is separated from the rest of the tunnel by a pressure wall (3). Supported with the excavated material, the face pressure is controlled by the rotation speed of a screw conveyor, which subsequently transports the mud onto a conveyor belt and out of the tunnel for further treatment and disposal.

(1) Cutting wheel
(2) Excavation chamber
(3) Pressure wall
(4) Screw conveyor
(5) Lining

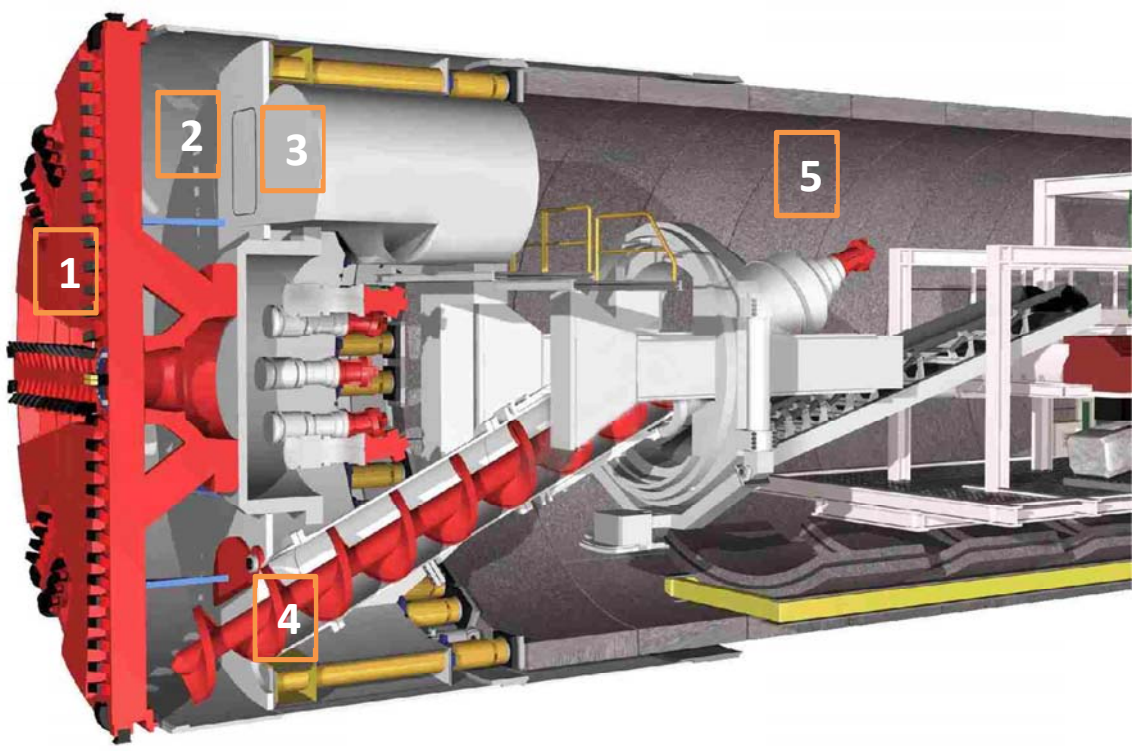

Figure 2-3: EPB tunnelling machine, Herrenknecht AG, www.herrenknecht.de, acess: 17.07.2012

2.2.3.2 Range of application

Tunnelling machines using earth pressure for stabilizing the face are best applicable for fine grained soil with a percentage of fine grains (<0.06 mm) above 30%. For coarse grained soils the torque force and support pressure increase disproportionally. Optimal ground conditions for using EPB machines are silty clayey and silty sandy soils. With an increased coarse grain percentage in the excavated material, the addition of water is not effective anymore and other additives need to be chosen for converting the soil into a pulpy, soft mud with low inner friction and low permeability for easy transportation on the belt conveyor.

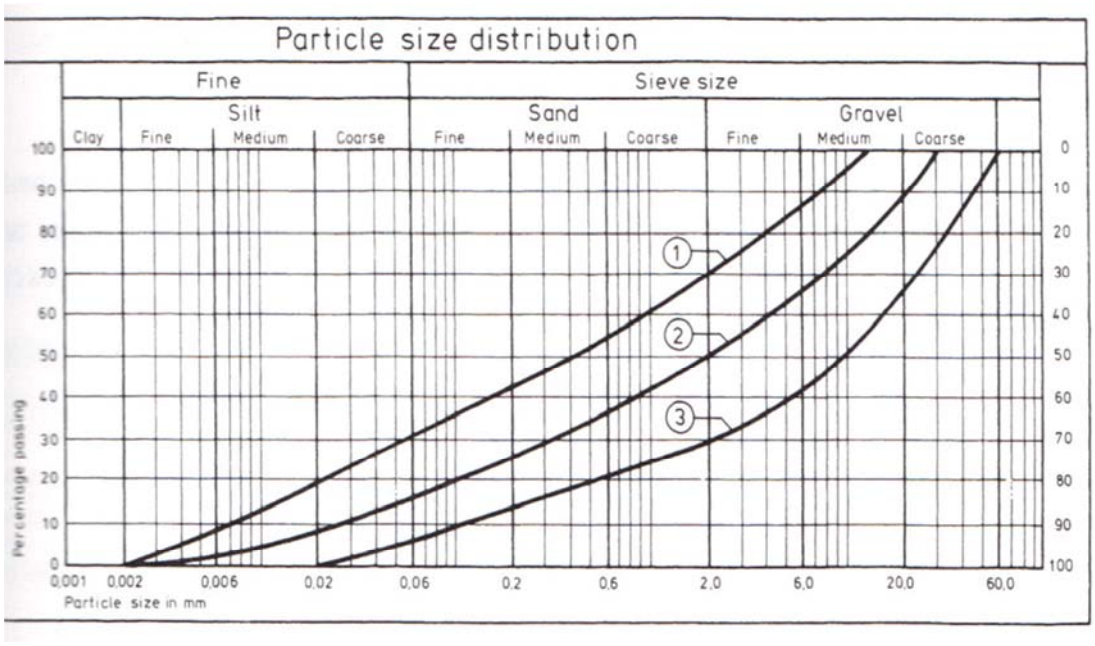

Figure 2-4: Range of application for a EPB-TBM **(Maidl, et al., 2011)**

If looking at figure 2-4, EPB machines are best applicable for soils above curve 1. Requirement for the range above 1 is the consistency index Ic = 0.4 – 0.75. For soils between curve 1 and 2 the permeability should not exceed a value of 10^-5 with a water pressure above 200 kN/m². Between curve 2 and 3, earth pressurized machines should not be used with acting water pressure. Underneath curve 3 the permeability is too high and an application of additives without effect. (Maidl, et al., 2011)

2.2.4 Hydroshield TBM

2.2.4.1 Principle

The Hydroshield concept is based on the slurry pressure balance principle. Soil is excavated with the cutter head which is surrounded with a bentonite suspension. The space in the back of the cutter head where the soil mixes with the slurry is called working chamber and is separated from the rest of the shield by a so called pressure-wall. The bentonite in the working chamber, supporting the tunnel face, is being pressurized with compressed air in the back of the chamber. Not applying the pressure on the fluid itself, it is being induced with an air cushion in the back of the working chamber. This chamber including the air-cushion is separated from the excavation chamber through a so called “dive-wall”.

The main technical difference between a normal “Slurry-shield” and the “Hydroshield”, is the pressure control. Whereas for the first machine the pressure is directly applied onto the fluid, it is being indirectly applied for the second one, which makes the support force independent from the bentonite quality and from the recirculated quantity of material being used. Hence unexpected loss of bentonite can be easily adjusted with the air-cushion in the back of the working chamber. (Maidl, et al., 2011)

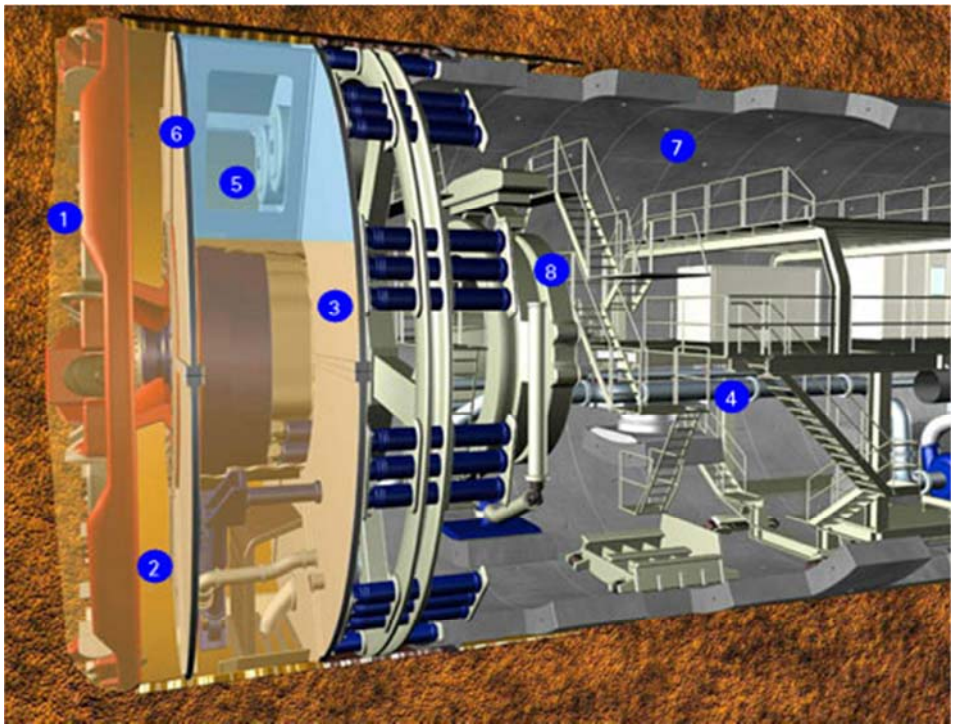

Figure 2-5: Hydroshield TBM (Thienert, 2010)

(1)Cutter head, (2)Working chamber, (3)Pressure Wall, (4)Feed line, (5)Air cushion, (6)dive wall, (7)Lining, (8)Drive

2.2.4.2 Range of application

The main field of application for Hydroshield tunnelling machines are coarse and mixed gravelly, sandy up to silty soil types. High permeable soils are leading to an uncontrollable disperse of slurry and neglect the arising membrane effect at the tunnel face due to the clayey minerals and the thixotropic properties of the bentonite. For soils with a higher permeability than 5*10^-3, there is a significant risk of slurry loss into the surrounding ground. It is possible to change the properties of the slurry or even the ground by using additives to overcome those problems, for e.g. adding fine grained particles or fillers to adjust the rheological properties of the material.

Yet, adding very fine particles or excavating in silty clays can lead to difficulties separating both fractions. (Maidl, et al., 2011)

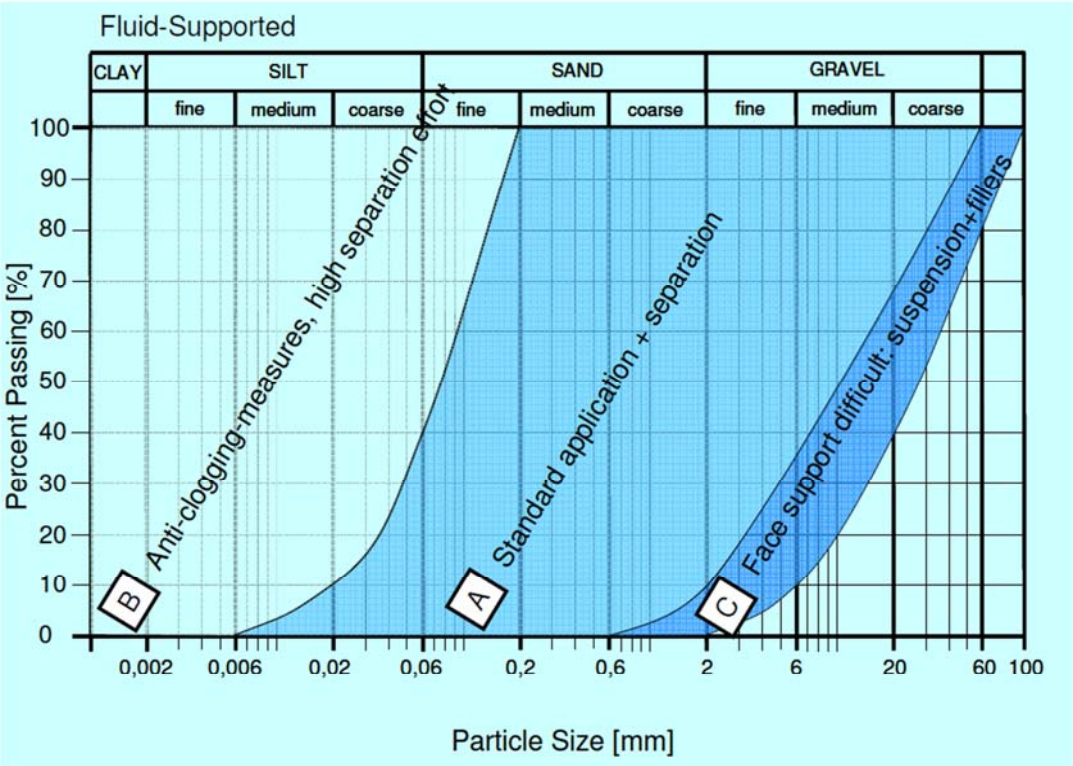

Figure 2-6: Range of application for Hydroshield tunnelling machines (Thewes, 2009)

Japanese slurry shields have been mainly developed for tunnelling in major cities near the shore. The top layer usually consists of fine sands and soft silty to clayey soils. Therefore the field of application for typical slurry shields ranges from silts, to silty sands and fine grained fluvial sands.

Figure 2-7 shows the range of application for Japanese slurry shields. For tunnelling in fine grained soils, the N-value for the standard penetration test should be below 15.

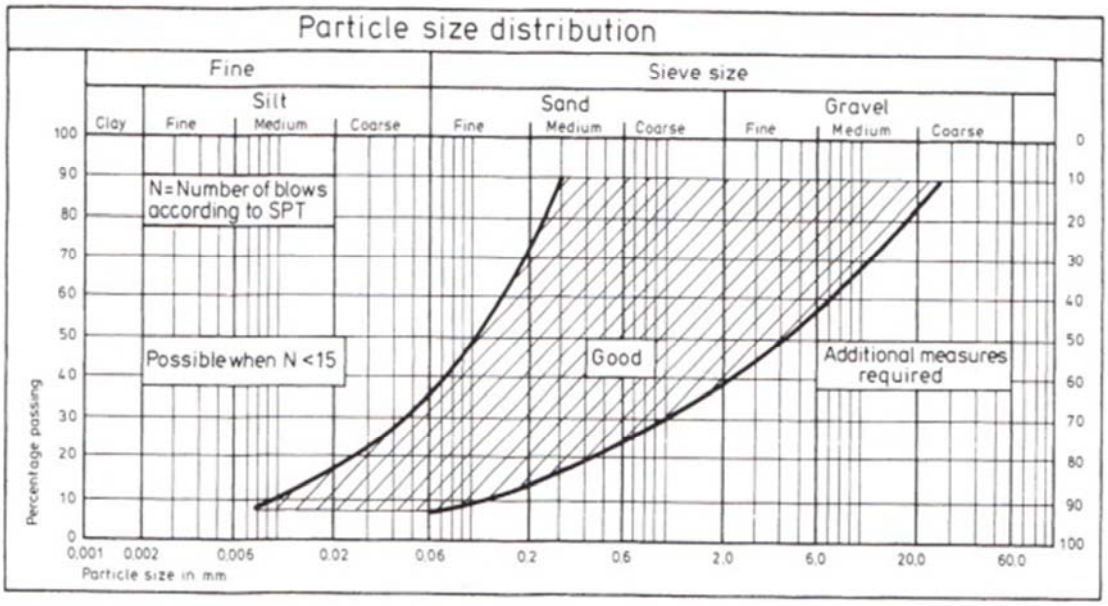

Figure 2-7: Range of application for slurry shields, see also Maidl et al. (2011)

2.2.4.3 Construction Sequence

The principle of the construction sequence when using a TBM (Tunnel boring machine), is fairly simple to describe, as the tunnel boring machine advances, precast lining segments made out of concrete are installed in the back of the TBM. Depending on the situation and on the overburden, the lining width and thereby the advance length of the machine ranges from about 1.5 to 2.0 m. The linings, so called “Tübbinge”, are installed with an erector attached to the TBM, hence while erecting one precast ring the excavation stops.

This may describe precisely the sequence when using a TBM in “normal” rock, yet when using a Hydroshield or a Slurry-TBM, the hydraulic issue for charging and discharging slurry needs to be considered as well. If bentonite or a polymer-suspension for stabilizing the tunnel face is used, the fluid is utilized as a transport medium for the excavated material, and therefore needs to be recycled and pumped back into the working chamber.

The following pictures show the sequence for the installation of 1 lining ring and the time needed for it. The width of 1 lining ring is 1.8 m.

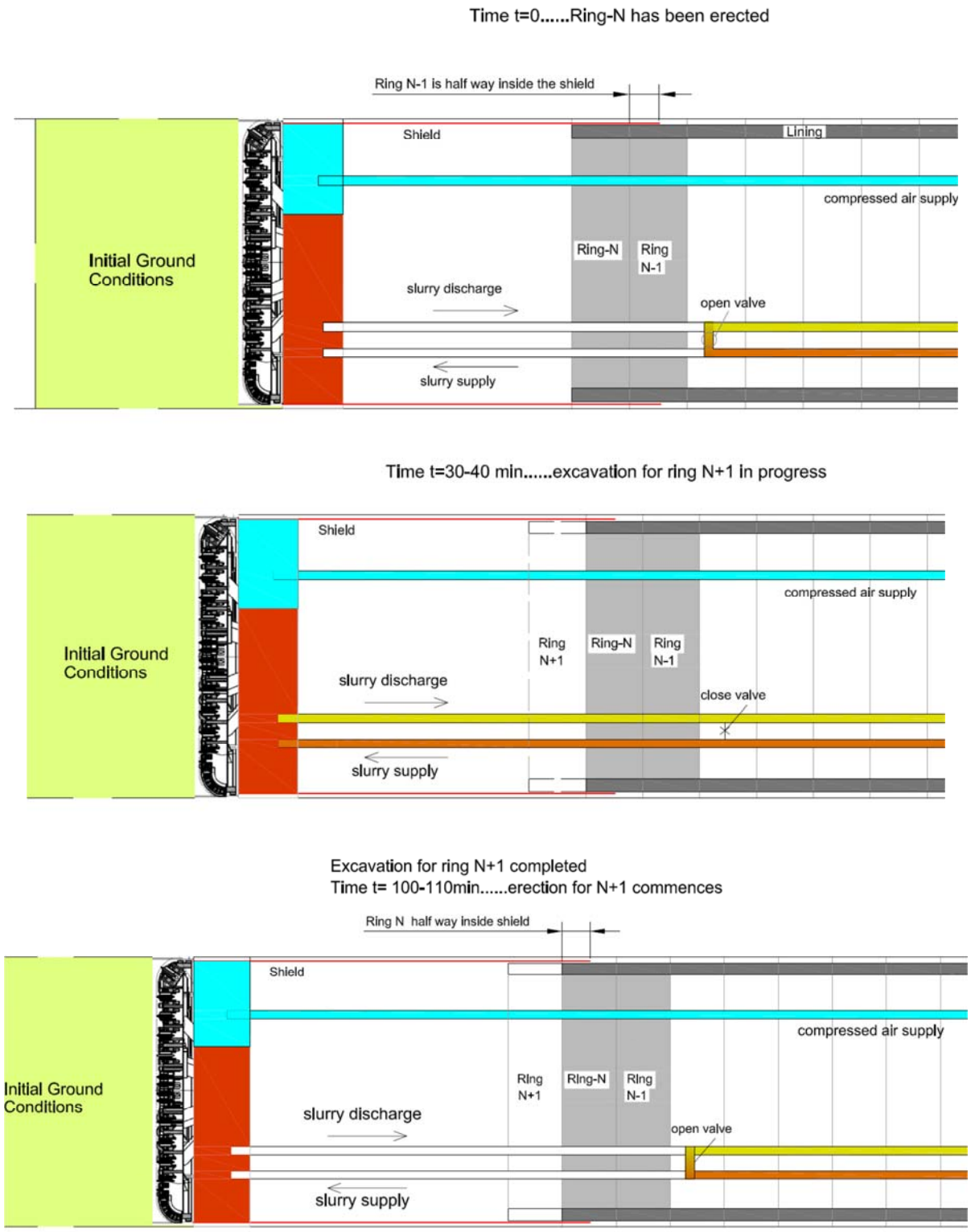

Figure 2-8: Construction sequence for a Hydroshield TBM

Figure 2-8 shows the installation process for 1 lining ring (width=1.8 m) and the time needed for it.

Advance time for 1 ring:

Assuming **ring-N** has just been erected, preparation for the next advance is completed and **time t=0**, the TBM is now starting its drive for **ring-N+1**. The advancing speed of the TBM is about **4-5 cm/min**, and it consequently takes **30-40 min** for the excavation of 1 lining ring with a width of 1.8 m.

After finishing the excavation, the valve for the slurry feed is being closed and the bypass between slurry-fed and discharge is being opened, thus preventing flow towards the working chamber. The slurry now circulates within the hydraulic system, but not being pumped into the working chamber. Meanwhile the face-pressure is maintained through the compressed air bubble in the back of the pressure wall.

Erection time:

The ring erection itself takes about the same, **30–40 min**, but including the time for opening and closing the valve etc., it takes approximately **60–70 min** in average. Hereby included is also the time for extending the slurry pipes and the plug for the electrical power supply.

Extension of bentonite supply pipes:

This is necessary for every 3/3/4# lining ring, as the pipe length is 6 m.

Time for extension of electrical supply = ~8 h

Timeline for grout injection at Ring-N:

Lining Erection	Timeline for ring-N	Grout Injection_Ring-N
Ring-N erection completed	**~ 0 min**	No Grout around ring N
Half of excavation for N+1 completed	**~15-17 min**	Grout starts surrounding ring N
Excavation Ring N+1 completed	**~ 35 min**	Half of the rin surrounded with Grout
Erection Ring N+1 completed	**~ 70 min**	Half of the ring surrounded with Grout
Preparation for Ring N+2 finished	**~ 100 min**	Half of the ring surrounded with Grout
Half of Ring N+2 excavated	**~ 115 min**	Ring-N completely surrounded with Grout

Figure 2-9: Timeline for the erection of 1 lining ring

The table presented in figure 2-9 shows the approximate time for 1 lining ring to be fully surrounded with grout. This is important if one considers consolidation, water filtration and further hydration of the grout around the lining segments.

2.2.4.4 Data based on the city tunnel in Leipzig

The data has been provided by company “Alpine Bau GmbH” .

On the basis of the data from the city tunnel in Leipzig (CTL, which is described thoroughly in chapter 4), advance and lining erection speed have been collected and elaborated, which is indicated in figure 2-10:

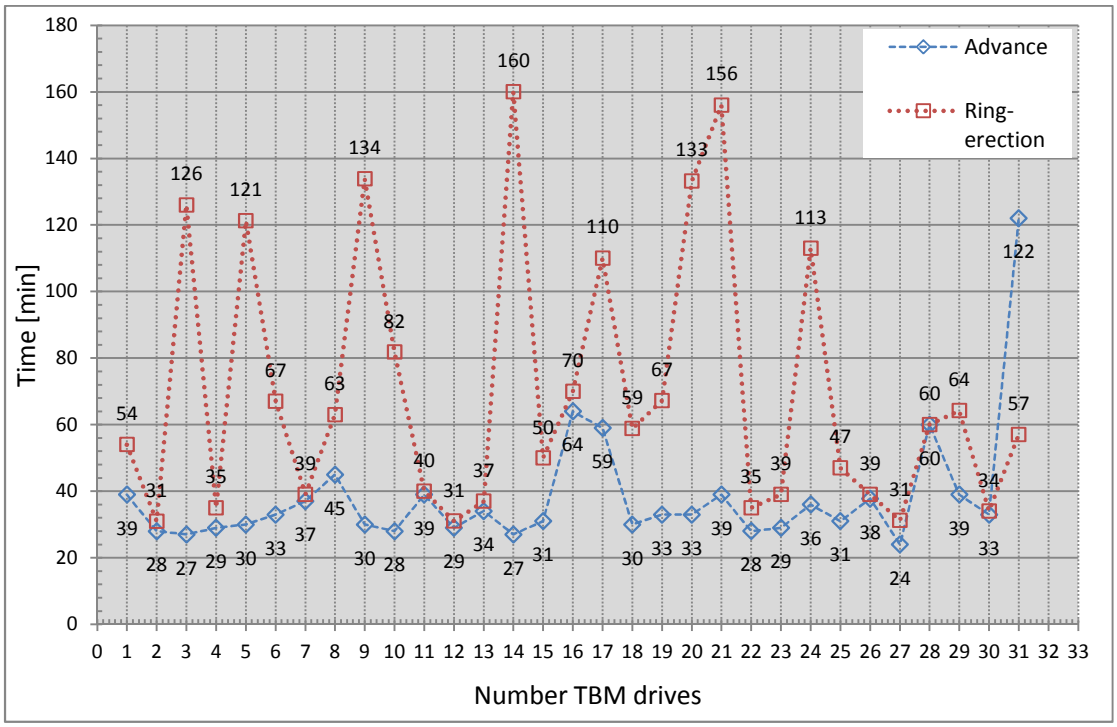

Figure 2-10: TBM advancing and erection speed on a chosen section of the city tunnel in Leipzig

Deducting from figure 2-10, the advancing speed of the TBM for 33 drives is quite constant, as for the ring erection it strongly depends whether there is a pipe, electrical supply extension or maybe a shift change.

The TBM drive constantly varies within 20 and 40 minutes, whereas for ring erection the time has a strong fluctuation due to the difficulties mentioned above.

Average Values of the TBM speed on the basis of figure 2-10:

TBM speed total [cm/min]	average advancing speed [cm/min]	average ring erection speed [cm/min]	daily advance rate [m/d]
1,7	**4,7**	**2,6**	**23,9**

Table 1: TBM advancing and ring erection speed

The time needed for the TBM to excavate one slice and erect a lining ring is important if one wants to consider the consolidation of grout behind the shield-tail. The water filtration of grout into the surrounding soil and thus the consolidation is a time dependent factor.

3 TBM-soil interaction

As the thesis deals with tunnelling in soil or loose rock, there is an interaction between the surrounding material and the machinery producing the void within this continuum. Unlike “normal” rock, soil is not stable when left unsupported.

Without explicitly explaining face-support calculation, the following chapter should only give an overview of the interaction between the TBM and the surrounding soil.

3.1 Deformations due to shield-tunnelling

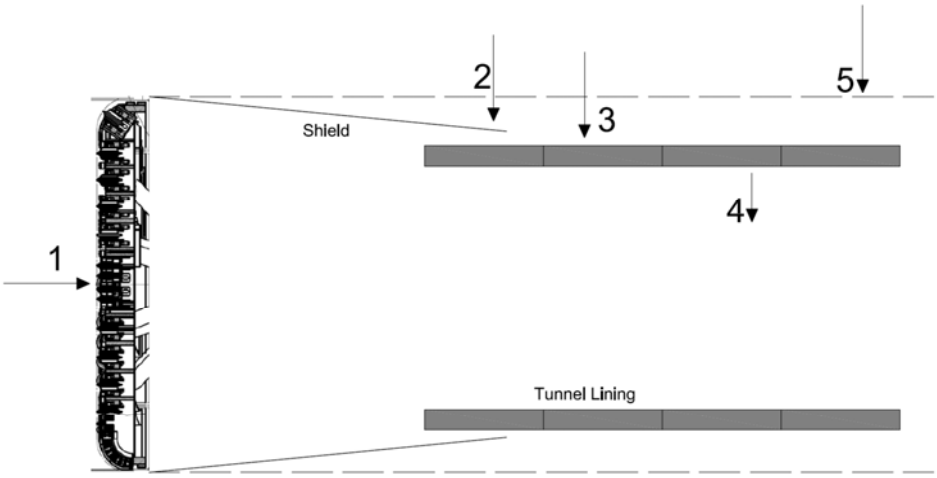

Figure 3-1: Deformations due to Shield Tunnelling

Settlements due to shield-tunnelling (see also Mair et al., 1997):

1 – Movement of the ground towards the face due to stress relief

2 – Radial movement towards the shield due to tapering or overcutting

3 – Settlements due to the gap between shield and lining

4 – Displacements of the lining

5 – Radial movements due to consolidation

If the face support is adequate, the first component of settlement for mechanised tunnelling is negligible. Therefore the second and third component is inducing most of the settlements for a machine driven tunnel. Consequently those two factors need to be investigated thoroughly. The displacement of the lining itself does not contribute significantly to surface settlements. Hence it will not be discussed more closely. Component number 5 is more important in clayey, silty grounds than in sands or gravely soils.

3.1.1 Empirical approach

The analytical approach to estimate the settlement trough can be very well approximated and described with a Gaussian-distribution curve. This will be mostly referred as empirical approach for evaluating surface settlements due to tunnelling. (Mair, et al., 1997)

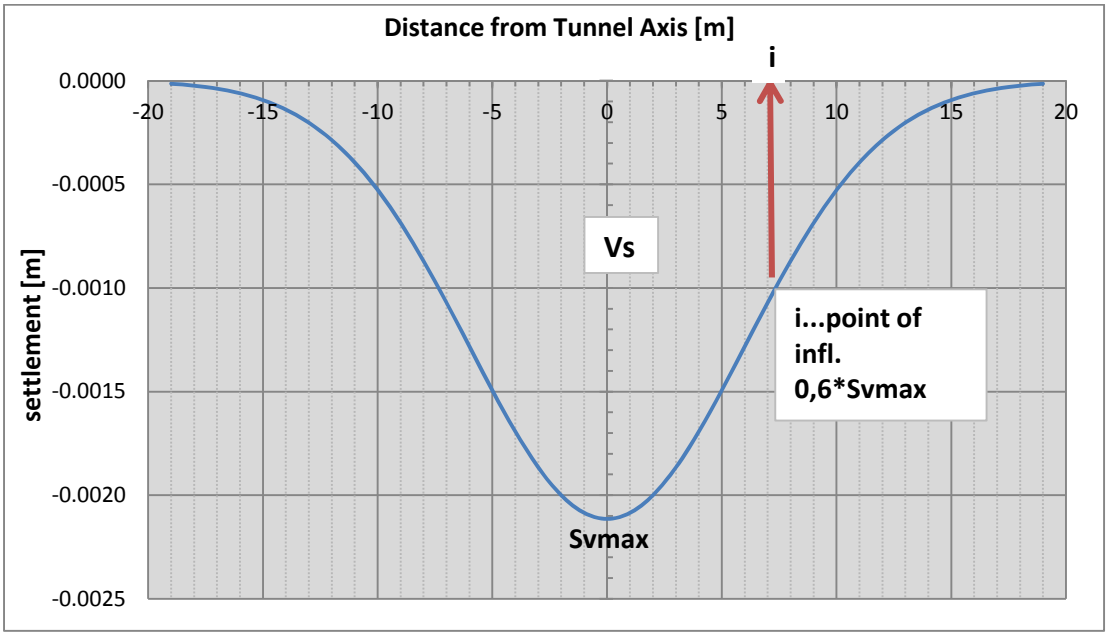

Figure 3-2: Gaussian settlement trough

Transverse settlement trough estimated with a Gaussian function:

$$S_{v(y)} = S_{v\max} * e^{-\frac{y\wedge 2}{2i\wedge 2}}$$

Where Svmax is the displacement above the tunnel axis and i is the point of inflection.

The area per unit length within this function will be called V_s. It is necessary to evaluate the volume loss per unit length, since the settlement curve is caused by the volume of soil which has deformed into the tunnel void after it has been constructed. V_t is the volume of soil which has been deformed into the void.

In undrained conditions one can easily say that $V_s \sim V_t$.

Therefore it is convenient to introduce a *Ground Loss Ratio* (GLR):

$$GLR = \frac{V_t}{A_t} = \frac{V_s}{A_t}$$

With At being the tunnel volume per unit length.

$$V_s = \sqrt{2 * \pi} * i * GLR$$

Hence,

$$S_{v\max} \approx \frac{A_t}{i * \sqrt{2\pi}} * GLR$$

For input, one needs two parameters, the point of inflection (i) and the Ground Loss Ratio (GLR).

O´Reilly and New (1982), showed that there is a linear dependency between the point of inflection and the tunnel depth. (Mair, et al., 1997)

$i = z*K$

with K being a parameter influenced by the ground conditions.

K for sand: 0,2 – 0,4

K for clay: 0,4 – 0,6

In layered ground i can be written as:

$i = K_1*z_1 + K_2*z_2$

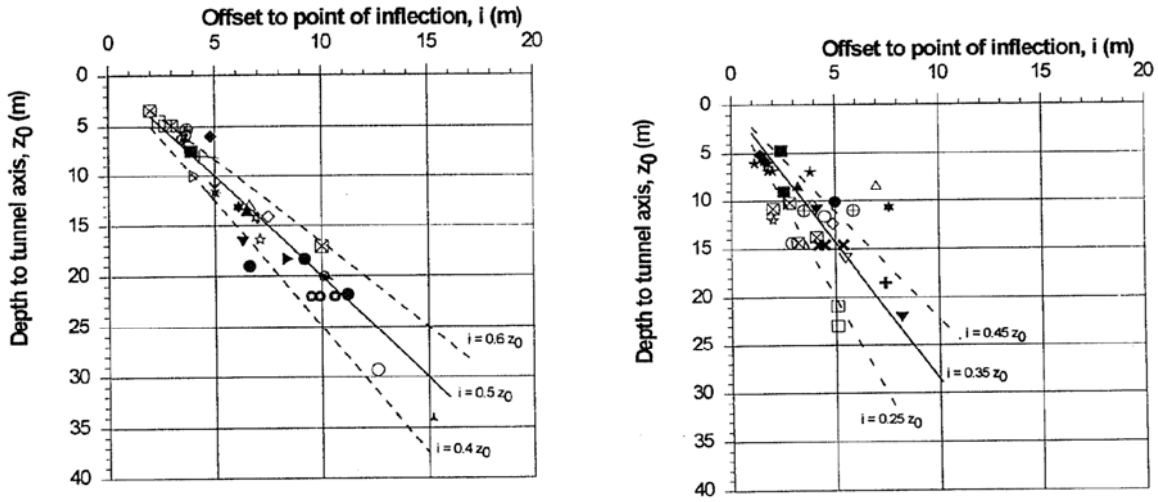

Figure 3-3: Point of inflection for clay (left) and sand (right figure) **(Mair, et al., 1997)**

The Volume Loss strongly depends on the construction procedure, the experience of the crew as well as ground conditions.

Nowadays values less than 0,5% can be achieved with slurry/earth pressurized machines by accurately controlling face and grout pressures.

Mair et al. (1997) suggests certain magnitudes for Volume loss due to tunnelling in soil or loose rock:

- Open face tunnelling in London stiff clay: 1-2%

- Spayed concrete linings (NATM) in London Clay: 0,5-1%

- Closed face tunnelling (slurry/earth pressure); for sand: 0,5-1% ,

  which can be even lower than 0,5% when pressures are carefully controlled by an experienced crew; in clay: 1-2%

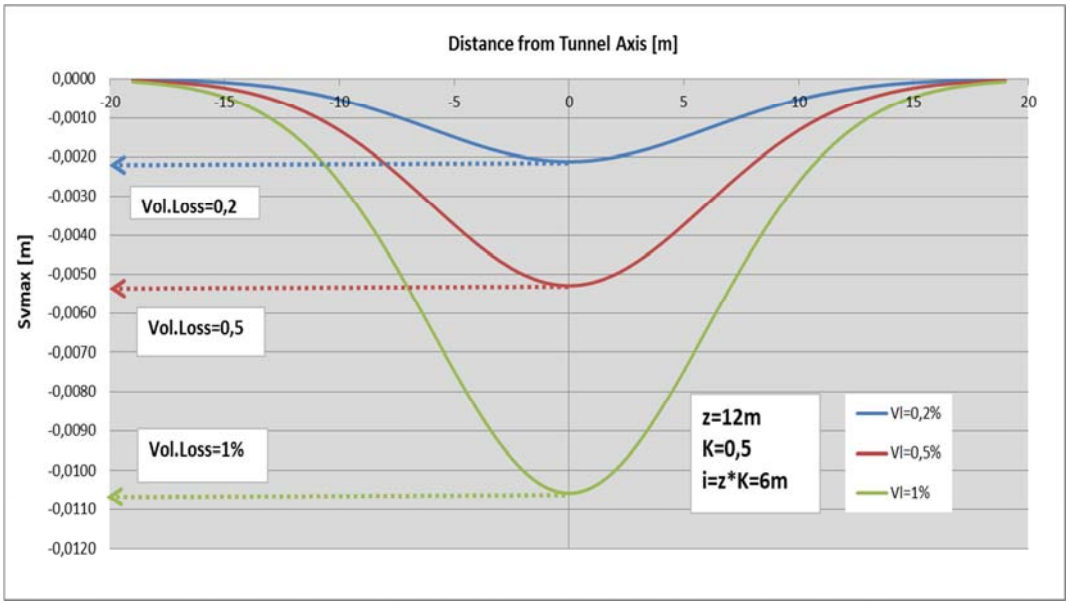

Figure 3-4: Gaussian settlement trough, z=12m, K=0.5

Figure 3-4 shows a calculated settlement trough for a tunnel depth of 12m and for different GLR values.

3.2 Face-support

Hereby only the face support with fluids/slurry will be discussed more thoroughly. Earth pressurized, or compressed air face support will be neglected as the tunnel investigated in this thesis was constructed using a Hydroshield-TBM.

If supporting the face with slurry or any kind of bentonite, the pressure of this fluid needs to sustain the active earth pressure as well as the piezometric water pressure. Because of its thixotropical properties, bentonite is very well suited for this kind of support system. Another material suitable for such kind of excavation technique is for example a polymer-suspension

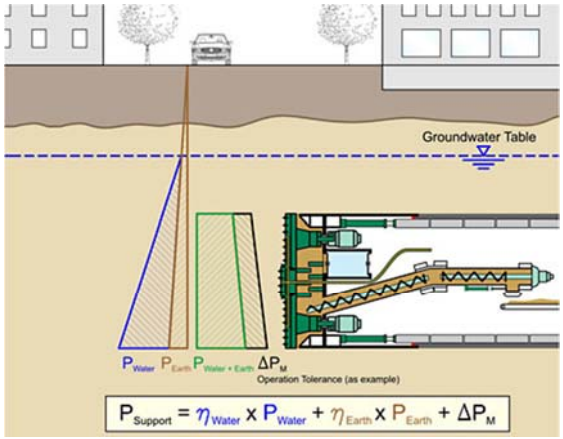

Figure 3-5: Face support pressure, www.facesupport.org, Babendererde Engineers, access: 5th of june 2012

Depending on the particle size distribution of the ground the bentonite suspension forms up a membrane at the face or penetrates a certain amount into the soil. In fine sands or silty grounds, the suspension will create a sealing membrane, whereas in coarse sand or gravely sands, the bentonite will penetrate through.

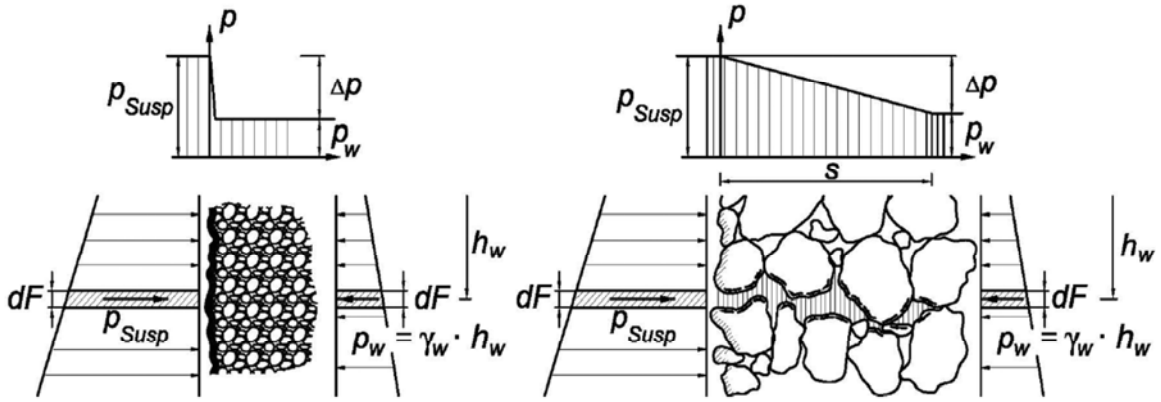

Figure 3-6: Membrane- (left) & Suspension stagnation model (right), **(Anagnostou, et al., 1994)**

In case of the membrane model, the bentonite will only penetrate a very small distance into the soil. Consequently no support force is lost.

The choice of the model has a great importance for the grout-consolidation in-between the gap of lining and the soil cut-surface.

In coarse sand or gravely sand the penetration of the suspension depends on the pressure difference between supporting and acting forces (dp), the shear strength of the bentonite (Tf) and the particle diameter d10.

The penetration distance is calculated as followed:

$$e = \frac{dp * d_{10}}{2 * \tau_f}$$

Due to its yield strength the penetration of the bentonite comes to a standstill after it reached the maximum penetration e_max.

This is important if one wants to consider water-filtration of the injected grout. The fresh grout is tending to consolidate due to the volume-loss of water filtration into the surrounding soil and thus experiences a decrease in pressure. The bentonite used as a supporting medium at the tunnel face will radially create a “filtercake” directly at the cut-surface of the soil, which then slows down the process of water filtration of the grout. Consequently it is necessary to consider the permeability of this filtercake formed due to the bentonite.

Thickness of the bentonite filtercake in respect with time (Thienert, 2010):

$$h_{fc} = \sqrt{2 * \frac{1-\alpha}{\alpha} * dp * k_{fc} * dt}$$

With:

h_{fc}	thickness of the filtercake
α	percentage of volume-loss (according to the filter-press experiment, DIN 4126)
d_p	pressure gradient (according to model, membrane- or stagnation)
k_{fc}	permeability of the bentonite “cake”
d_t	time interval

$$\frac{1-\alpha}{\alpha} \approx 0.3 \div 0.6 \text{.....} \textit{see also Thienert} \ (2010)$$

Permeability of bentonite:

k_{fc} = $2*10^{-10}$ *to* $2*10^{-11}$….see also Thienert, 2010 or Talmon et al., 2009

Pressure gradient d_p:

Acting water pressure = 85 kN/m²

Imposed slurry pressure = 185 kN/m²

- Membrane model, d_p = 185 – 85 =100 kN/m²

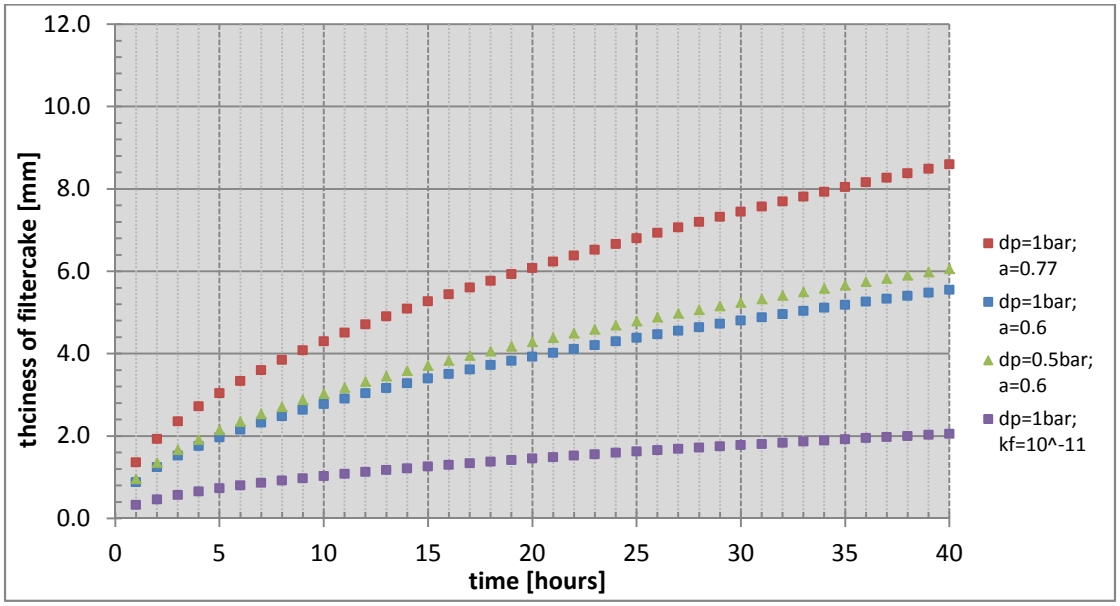

Figure 3-7: Thickness of bentonite filtercake with respect to time

The flow-resistance of the filtercake is thus calculated as followed:

$R_{fc} = h_{fc} / k_{fc}$ [s]

The flow-resistance is a time dependent value. It describes the resistance of water flow through a specific medium, in this case bentonite.

With:

h_{fc} = ~4 mm

$k_{fc} = 2*10^{-10}$ m/s

- $R_{fc} = 2*10^{7}$ s

If one wants to consider the consolidation of grout, the flow-resistance of the bentonite is thus very important, because it governs the amount and velocity of water filtration into the surrounding soil.

3.2.1 Support Force

For calculating the support force at the tunnel face, different kinds of models can be used. Models commonly used in Germany are the procedure in DIN 4085 which is using the failure mechanism of Piaskowski/Kowalewski. Using this model the tunnel is divided into horizontal strips, where the 3 dimensional earth pressure is calculated with the 2 dimensional approach reducing the loads with corresponding reduction factors.

Another model widely being used, is the failure mechanism developed by HORN (1969), which was further improved by *Anagnostou and Kovari (1994) using the silo-approach of JANSSEN and TERZAHGI.*

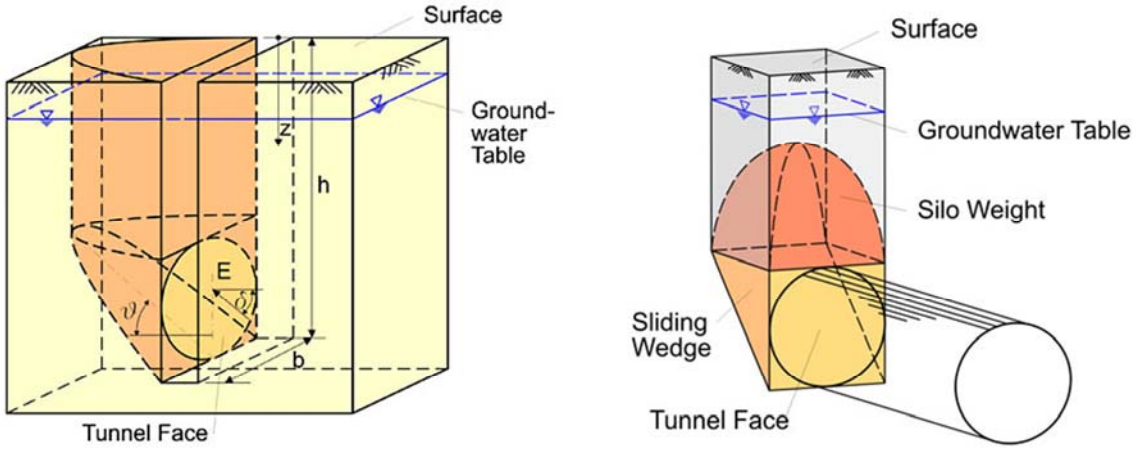

Figure 3-8: Face stability wedge, www.facesupport.org, Babendererde Engineers, access: 5th of June 2012

Necessary support force:

$$S = n_{a*} * E_a + n_w * W$$

With:

E_a…….active earth pressure

W……...water pressure

n_a, n_w……partial factors for safety

The calculation process itself is not being further discussed in this thesis. For more information on the analysis see also Anagnostou (1994), www.facesupport.org (access: 5th of June) or DIN 4085.

3.2.2 Monitoring of face-support pressure

For evaluation of the face-support pressure for the FEM calculation, data from the city tunnel in Leipzig has been used and elaborated, which was provided by company “Alpine Bau GmbH”.

In case of the city tunnel in Leipzig a Hydroshield/Mixshield TBM was used for the tunnel excavation. The equipment for measuring the face support as well as the grouting pressure is provided by the company also providing the slurry-pressure-balance machine, in this case the “Herrenknecht AG”. The measuring gauges are installed around the TBM, recording accurate values of all the pumping and injection pressures.

The computer connected with the TBM records the effective pressure 2 to 3 times per minute, which results in 180 values per hour. Hence the support pressure can be easily supervised and adjusted if necessary. The pressures are recorded using the unit *bar,* thus all the chart including grout or slurry pressures are labelled with *bar* at the vertical axis. 1 bar equals 100 kN/m².

Example values measured during the construction of the city tunnel in Leipzig:

The first two values describing time and location of the TBM, the third one is numbering the lining ring and subsequent values are measuring the slurry and grout pressures.

Time	Station	Tübbing No.	Slurry Pressure	Grout Pressure
14.08.2008 12:04	*500157,8726*	*5084*	*1,8831*	*2,96586*
14.08.2008 12:04	*500157,8726*	*5084*	*1,8831*	*2,96586*
14.08.2008 12:05	*500157,8726*	*5084*	*1,8831*	*2,96586*
14.08.2008 12:05	*500157,8726*	*5084*	*1,8831*	*2,96586*
14.08.2008 12:05	*500157,8726*	*5084*	*1,8831*	*2,96586*
14.08.2008 12:06	*500157,8726*	*5084*	*1,8831*	*2,96586*
14.08.2008 12:06	*500157,8726*	*5084*	*1,8831*	*2,86458*

Table 2: Extract from the monitored data of face pressures

Slurry pressure with respect to time:

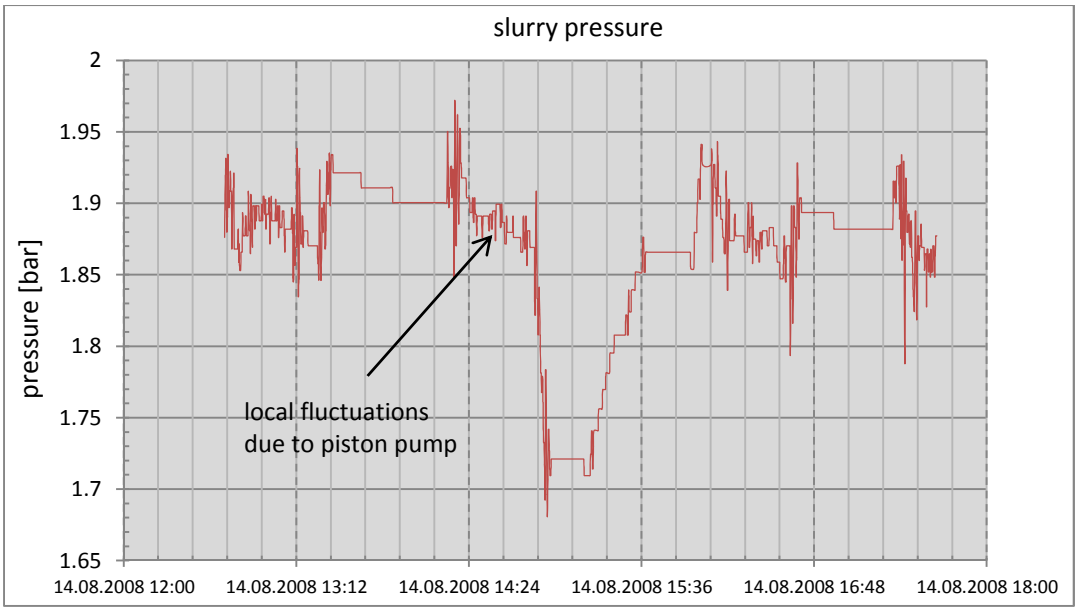

Figure 3-9: Example values of measured slurry face pressures

Plotting the face-support pressure against time, it will not show a constant pressure, as the unsteady strokes of the pump causes a certain fluctuation. Those cyclone or piston pumps (Figure 3-10), need a certain pre-pressure to convey the fluid all the way to the tunnel face, which causes the just mentioned variation in pressures. Figure 3-9 shows such an example of evaluated measured face-support pressures. In addition it is necessary to say, that the pressure is always measured at the crown of the TBM, which contributes to later analysis, because as an input-reference point one can easily take the tunnel crown.

Figure 3-10: Cyclon/piston pump, (http://www.habermann-gmbh.de, access: 12.05.2012)

3.3 Shield-soil interface

As already mentioned in *2.3.1*, in case of accurately controlled face support the induced settlements on the surface are mostly due to the radial movement of soil towards the shield or the lining.

For shield driven tunnels in general it is necessary to imply a certain overcut while steering through any kind of material. This is due to driving a curve in longitudinal direction. In soils or fractured rock there is no need to have a large overcut. That differs to mining in solid rock, where it is helpful and almost necessary for a TBM to have a certain amount of overcut. Figure 3-11 provides an example of the crown cutting-edge from the Hydroshield TBM used at the city tunnel in Leipzig. (for description of the city tunnel in Leizpig see chapter 4) The overcut for the example in figure 3-11 is 10.0 mm in diameter and 5.0 mm in radius.

As in case of a Hydro- or Slurry-shield TBM, the face is supported with a fluid-suspension, this fluid tends to flow into the gap arising between cut-surface and shield and is imposing a pressure onto the ground. From the tail of the TBM grout is injected to fill the gap between lining and cut surface, which is then also flowing towards the face and interacts with the slurry.

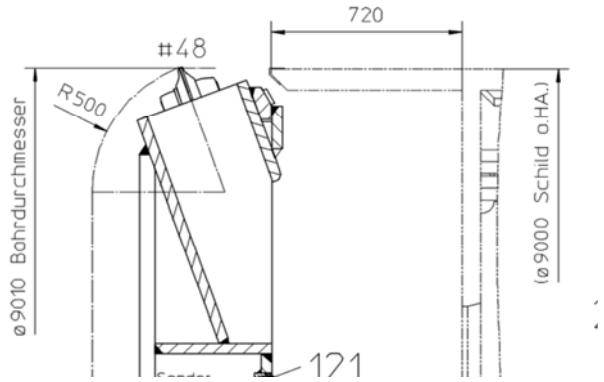

Figure 3-11: Cutterhead diameter including overcut

Consequently the whole tunnel boring machine is radially surrounded with fluids imposing a pressure onto the soil and implying a pressure-boundary condition in-between the shield and the cut-surface.

3.3.1 Tailskin grouting

Grout needs to be injected into the gap between lining and ground to achieve and immediate support of the prefabricated concrete rings. This is necessary to mitigate further displacement of the soil towards the lining, to maintain the natural stress in the ground and to improve the water tightness of the lining.

There are two possible ways to inject the grout into the annular gap arising from the excavation:

- Injection through grout holes in the lining
- Injection via tailskin

In modern shield tunnelling, the second option is the most common one. This is only possible with modern wire brush seals at the rear of the shield to prevent the grout from flowing into the machinery and working area.

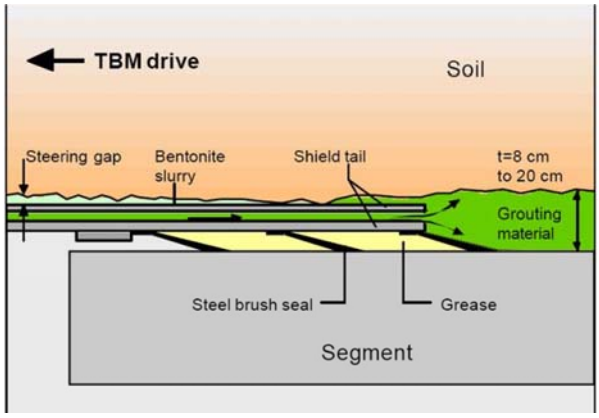

Figure 3-12: Grout injection (Thewes, 2009)

Injection through tailskin:

The grout is injected through 6 or 8 injection openings, which are radially arranged at the tailskin of the TBM (Figure 3-13).

Nowadays this way of injecting grout is state of the art in modern tunnelling methods. The gap arising behind the shield is immediately filled with grout to prevent further settlements due to movement of the soil towards the lining.

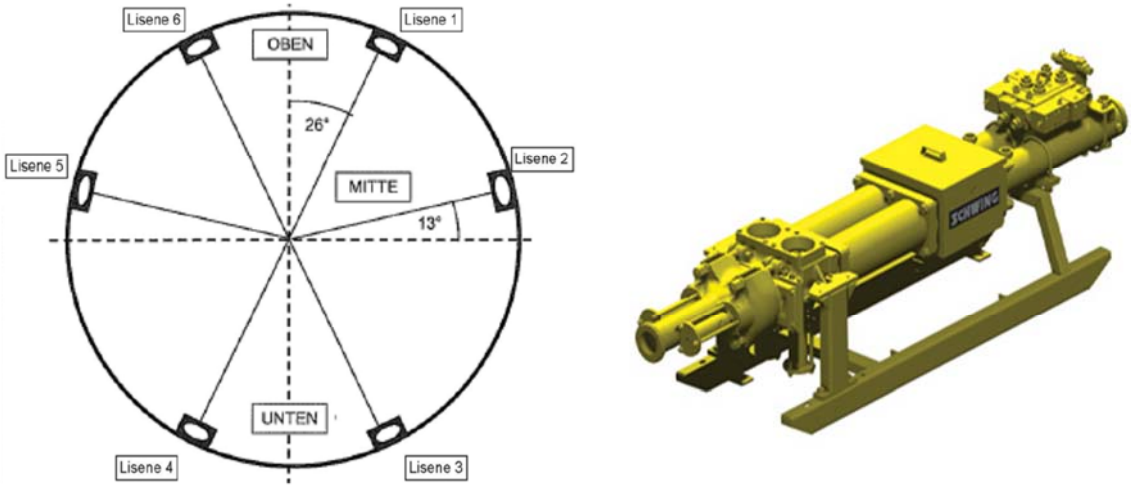

Figure 3-13: Injection openings (left) and grouting pump (right), (http://www.schwing.de, access: 16.07.2012)

Pumping Equipment, conveying pipes:

For conveying the grout from the mixing aggregate on the ground surface to the front of the tunnel, usually a double piston pump (for example from company Schwing, figure 3-13) is used. The pump capacity amounts to 10 m³/h, which is about 3 litres/sec. To ensure the quality and exact quantity of grout pumped into the tunnel, digital measuring systems are used which usually record two important parameters, the number of piston strokes and the weight of the grout storage tank. (Thienert, 2010)

3.3.1.1 Grout properties

Materials used for grouting:

- Cement containing products
- 2 component materials
- Cement-free grout

Products containing cement or cement like materials, are the most widely used grouting products for mechanized shield tunnelling. Thereby it is necessary to distinguish between active and conditionally active grout. The amount of cement for active grout lies above 200 kg/m³ whereas for conditionally active grout it is below 200 kg/m³.

The cement can either be CEM I, CEM II or a CEM III according to the requirements. (CEM=cement).

Composition for cementitious grout:

	Cement	**Sand 0-1 mm**	**Sand 0-2 mm**	**Gravel 2-8 mm**	**Bentonite Suspension**	**Volcanic ash**	**Water**
	Kg/m³	[kg/m³]	[kg/m³]	[kg/m³]	[kg/m³]	[kg/m³]	[kg/m³]
active grout	194	169	674	454	153	194	207
Conditionally active grout	120	169	674	454	183	268	177

Figure 3-14: Example for cement containing grout composition, (Thewes et al., 2009)

The injected grout has to fulfil certain properties. Most importantly the bedding of the segmental lining with grout has to be sufficient for immediate stress transfer around the circular opening. Therefore the material needs to have a basic stiffness and furthermore a certain slump for a smooth flow around the lining rings. On the counterpart, a high stiffness in the beginning leads to less plasticity and difficulties at conveying the material trough a hydraulic hose system (see also Thienert, 2010).

Usual requirements for cement containing materials:

Workability/ Plasticity	Slump (t=0h): 20 cm +- 5 cm (DIN EN 1015-3) Slump (t=8h): 15 cm +- 5 cm (DIN EN 1015-3)
Compression strength	t=24h >> 0.5 N/mm²
Shear strength	To avoid uplift and huge deformations Ty = 1 - 2 kN/m²
Young´s modulus	~ 5 – 10 MN/m²...(fresh injected grout has a lower stiffness)

Figure 3-15: Typical requirements for grouting material, (Thewes et al., 2009)

2-component grout:

2 components are separately pumped to the shield tail through injection openings, where they can mix and merge into 1 material. Difficulties can arise during standstill of the TBM, as it is possible that both fluids react within the conducting channel, which leads to choking and clogging of the openings.

Cement-free grout:

For information on cement-free grout see Thienert, 2010. The grout properties for the later numerical analysis are described in chapter 6.3.2.

3.4 Grout-flow around TBM and lining

Due to the overcut and tapering of the TBM, the injected bentonite slurry will flow along the shield and interact with the grout which is injected at the tail of the TBM. Due to the high pressure it tends to flow towards the face and pushing the slurry back to the face. Thus it will create a pressure-boundary interaction between the TBM and the surrounding soil. Hence a theoretical approach considering the flow around the TBM needs to be established. Bezuijen (2009) describes an approach for analytically evaluating those pressures and using it for implementation into the Finite Element Method.

3.4.1 TBM geometry

Figure 3-16 shows the shield and cutter head used for the city tunnel in Leipzig. The diameter of a TBM shield in the front is larger than at the tail. In this case, the front diameter is 9000 mm and the diameter in the back is 8970 mm, which implies a gap of 15 mm in radius. Adding 5 mm of overcut, a gap of 20 mm arises at tail of the TBM.

Cut radius = 9010 mm

Overcut = 5.0 mm

Tapering = 15.0 mm

Total gap at shield tail = 15.0 + 5.0 =20.0 mm

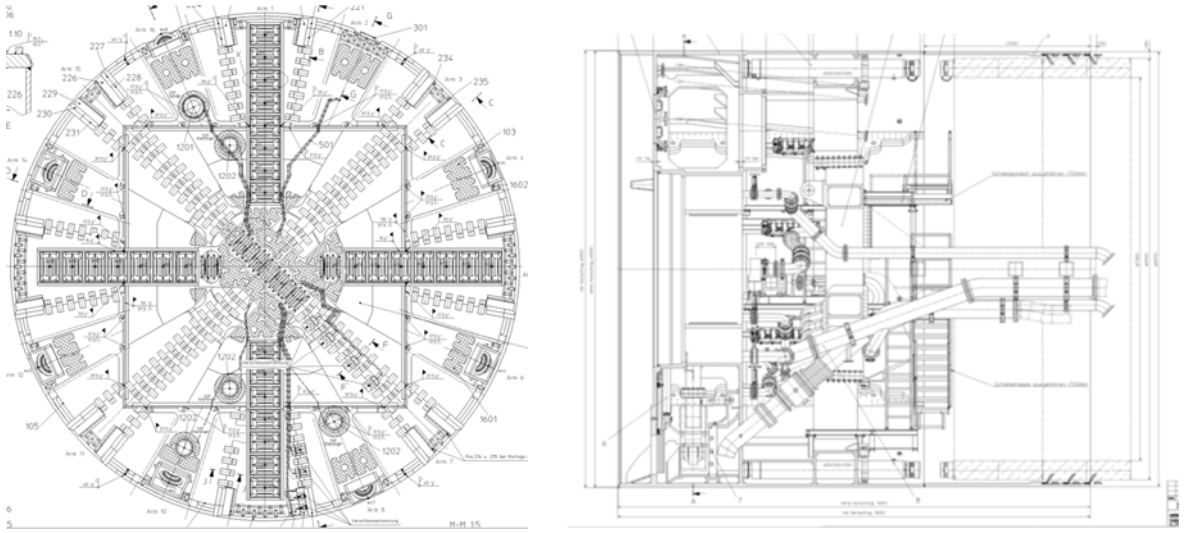

Figure 3-16: Hydroshield TBM used in Leipzig (ALPINE Bau GmbH)

3.4.2 Grout-flow theory

Assuming a perfectly circular opening in a linear elastic material, the equilibrium equation is derived by the equilibrium of radial and tangential forces at a finite element around the opening.

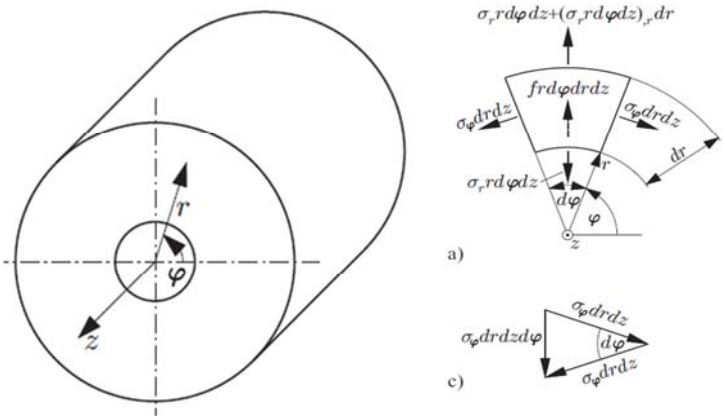

Figure 3-17: Circular hole in elastic mediu (Einführung in die Technische Mechanik, Balke, H., 2010)

The change of stress around the symmetrically bored hole subjected to a certain pressure can be written as (Bezuijen, 2009):

$$d\sigma = 2 * \frac{dr}{r} * G \qquad \text{.....(1)}$$

With:

d_r…..change in radius, displacement

r…….radius of excavated circular opening

G……shear modulus of soil around the tunnel

dσ…..change in stress

$$d\sigma = p - (\sigma' + \sigma_w) \quad \text{…….(2)}$$

With:

p.....subjected pressure onto the soil (grout or slurry)

σ´….effective stress of soil

σ_w….water pressure

see also (Bezuijen, 2009)

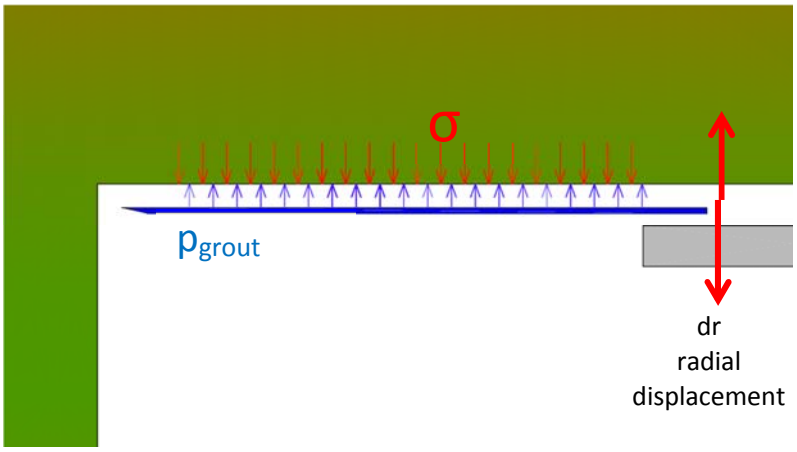

Figure 3-18: Displacement of opening in elastic medium

If the pressure subjected to the soil is higher than the effective stress including water pressure, the soil will be pushed away. Yet if the grout or slurry pressure is lower, there will be a displacement towards the shield or lining.

This only describes the change in stress at a certain point. Considering that the grout tends to flow within the arising gap towards the tunnel face, the pressure is supposed to experience a decrease. Not taking grout-consolidation into account, the pressure decline due to movement of either the grout or the TBM, needs to be based on the approach of a drop in pressure within closed flow-channels and is thus depending on the yield strength of the material itself..

The pressure decrease can be expressed as (Bezuijen, 2009):

$$dp = \frac{dx}{s}(\tau_y + \eta\frac{dv}{dy}) \text{ .....(3)}$$

with:

dp….change in pressure

dx…..incremental length along the shield

s……gap between shield/lining and soil

T_y…..shear stress of grout/slurry

n…….dynamic viscosity

dv/dy…velocity gradient in the flowing liquid (this part can be neglected assuming the gradient to be very low)

As it was already discussed before, due to a certain overcut, the gap at the front is not equal to zero. Consequently slurry tends to flow backwards. Assuming that grout will flow towards the face and slurry in the opposite direction, both liquids will meet and interact somewhere along the shield. The pressure distribution now depends on the overall flow direction of both.

3 potential situations could arise (Bezuijen, 2009):

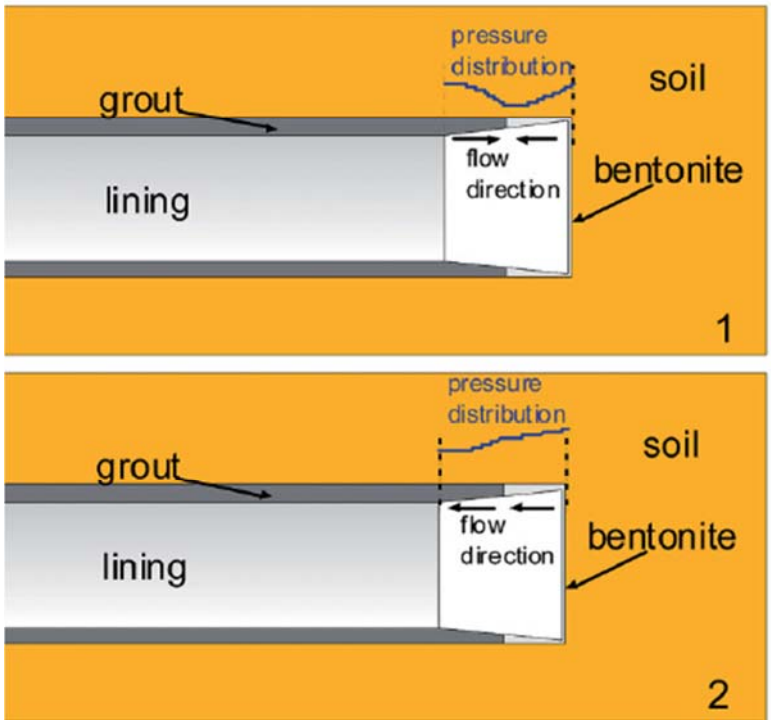

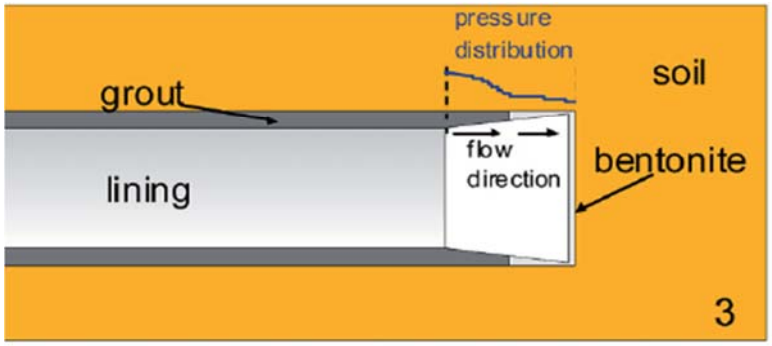

Figure 3-19: Potentials of grout flow along the TBM shield **(Bezuijen, 2009)**

1 – Grout is flowing towards the face and slurry is flowing backwards colliding somewhere along the shield.

2 – Bentonite flows backwards, pushing the grout towards the tail. Here the highest pressure will be at the face of the TBM

3 – The flow direction is towards the face, thus the grout pushing the bentonite to the front. The highest pressure will be at the tail of the TBM where grout is injected.

Since grout is always injected with a higher pressure compared to the slurry at the face, assumption number 3 would be the most realistic one. But as further analysis will show, a drop in grout pressure will immediately cause a different situation, leading to a decrease of pressure from the face towards the tail.

Using precise data it is possible to calculate the arising gap due to grout and slurry pressure. The cross sections analysed are described in a chapter 4.

With an overburden of 15 m and a water level a 6.5 m below surface, the effective stress at the crown of the tunnel is 191 kPa and the water pressure is 87 kPa, according to the soil profile for cross section I described in chapter 4.

Example evaluation:

The yield strength for grout and slurry was taken from Thienert (2010).

Shear Modulus soil, G	90	MN/m²
E-modulus-ur soil, E_{ur}	240	MN/m²
cut radius TBM, r	4,5	m
overcut	0,005	m
Delta_x	0,2	m
yield strength grout, τ_g	0,5	KN/m…see also (Thienert)
yield strength slurry, τ_s	0,03	KN/m²..see also (Thiener)
water pressure, σ_w	87	kN/m²
effective stress soil, σ'	191	kN/m²
grout pressure, P_g	320	kN/m²
stress difference, dσ	42	kN/m²

Figure 3-20: Parameters grout flow calculation

Assuming that the grout pressure is 320 kN/m² and the slurry pressure at the crown of the face is 185 kN/m², the arising gap and corresponding pressures are shown in figure 3-21 and 3-22. (The analysis using evaluated data from the city tunnel in Leipzig is shown in chapter 3.4.3)

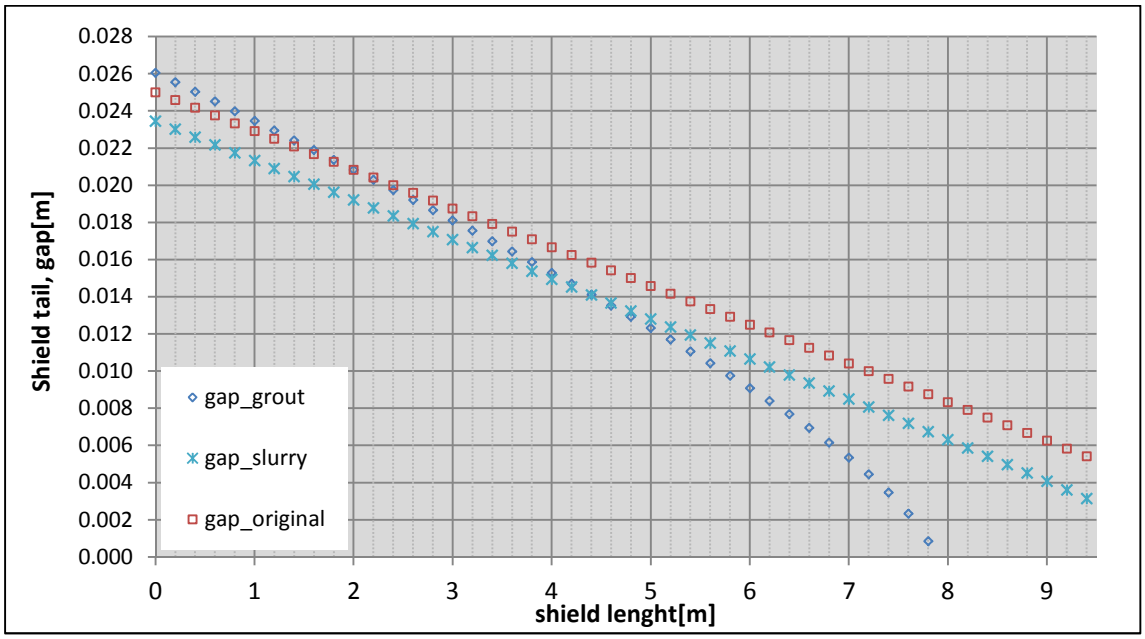

Figure 3-21: Arising gap due to grout and slurry pressure along the TBM

The interface between slurry and grout is approximately 5.2 m behind the tunnel face and the corresponding pressure distribution is shown in figure 3-22.

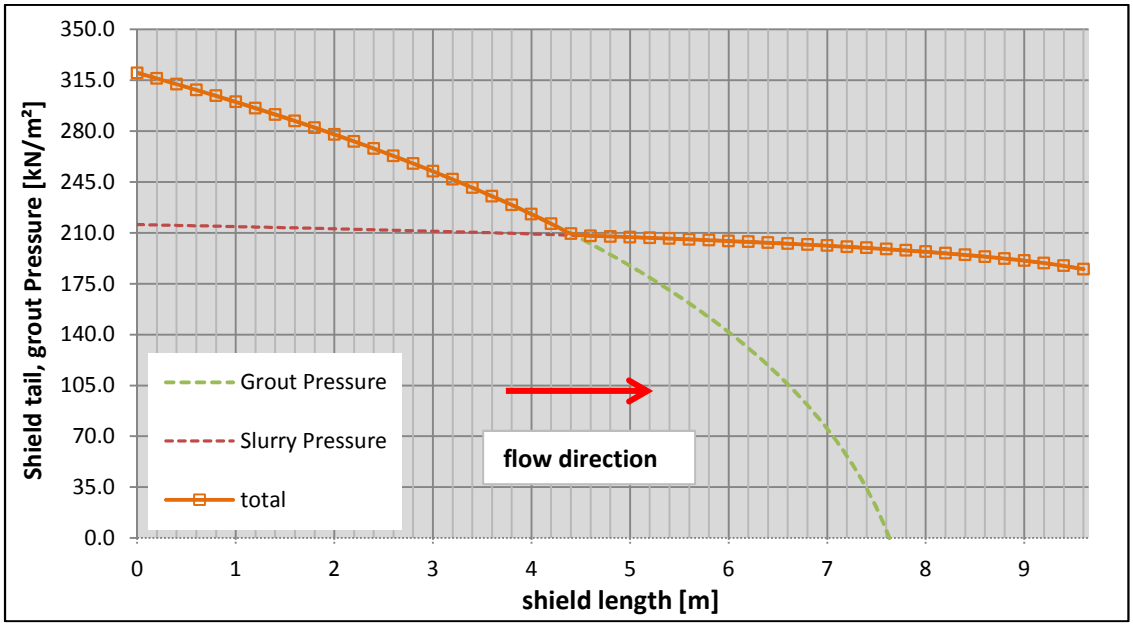

Figure 3-22: Pressure distribution along TBM shield

Assuming that the flow-direction is towards the tunnel face, the slurry pressure will increase further to the tail. Thus the lowest point of pressure is at the face of the tunnel and the highest one at the tail of the TBM. This consideration incorporates flow-assumption number 3 from figure 3-19. In chapter 3.4.3 one will see that this approach is not valid in this case and the following analysis will reveal the same.

3.4.2.1 Pressure distribution in the ground-lining gap

The theory for the calculation of grout pressures in-between the ground-lining gap is based on the water filtration and consolidation of the injected material.

The volume loss due to water filtration into the surrounding soil, which occurs at the grout-soil interface, causes a drop in pressures and a decrease of stresses around the circular opening. Consequently the grout will create a filter cake, which inhibits further consolidation and filtration of water into the soil.

While the TBM advances, short after the excavation commences fresh grout is injected and pressures increase. When excavation stops, no further grout will be injected thus leading to a consolidation, consequently to a decrease in pressure and a movement of the cut surface towards the lining or shield.

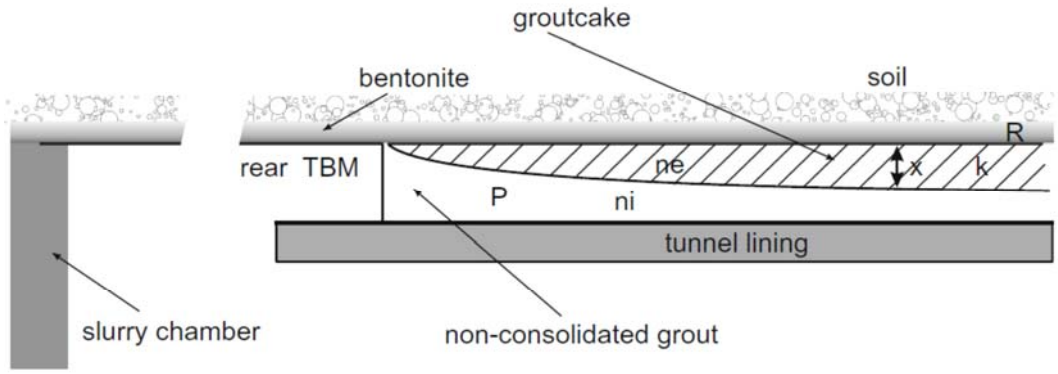

Figure 3-23: Consolidation of grout **(Talmon, et al., 2009)**

The filtration of water is highly influenced by the layer between grout and soil, which in case of a Slurry-TBM consists of a bentonite-soil mixture. Hence the layer in contact with the injected grout consists of a soil-bentonite composition and thus is less permeable than normal soil. This leads to longer filtration times as if there would be only soil. For calculating the exact amount of water loss it is necessary to consider the slurry-effect onto the soil, which means that there is a difference whether the bentonite forms a stable filter cake or will penetrate through the ground and stagnate at a certain pressure. See also chapter 3.2 and Talmon et al. (2009)

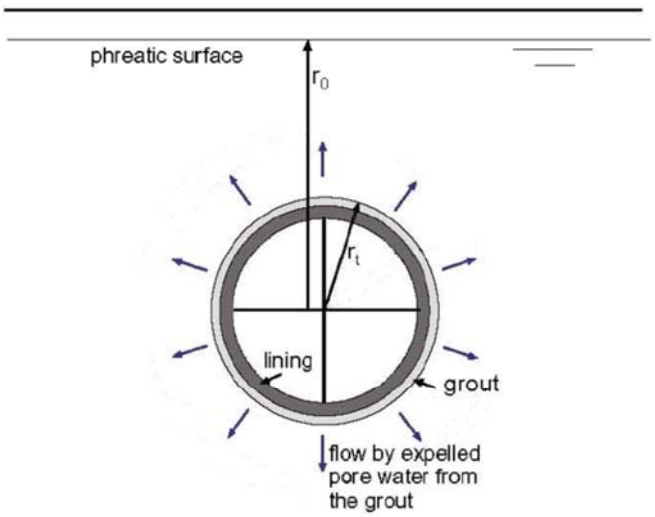

Figure 3-24: Filtration of water into surrounding soil **(Talmon, et al., 2009)**

Properties relevant for grout-consolidation:

- Permeability of bentonite-grout “filtercake”
- Porosity of grout, before and after consolidation
- Permeability of surrounding soil
- Shear modulus of soil
- Pressure difference between grout and pore water

The change in volume of the grout over time depends on the exposed area, the imposed pressure on the material and on the permeability of the interface layer between grout and soil (Thienert, 2010):

$$\frac{dV}{dt} = \frac{A * dp}{R_{fc} + R_{fm}}$$

With:

A exposed area

dp imposed pressure on the grout (depends on the penetration model > membrane or stagnation)

R_{fc} hydraulic resistance of the consolidating grout layer

R_{fm} hydraulic resistance of the bentonite layer including the soil

Integration with respect to t and inserting the boundary condition that the thickness of the consolidated grout h=0 for t=0, results in the equation giving the thickness of the grout layer:

$$h_{fc} = \sqrt{2 * \frac{1-\alpha}{a} * dp * k_{fc} * t + (h_{fc,o} + k_{fc} * R_{fm})^2} - k_{fc} * R_{fm}$$ (Thienert, 2010)

(h_{fc} equals to x in figure 2-23 on the previous page)

The pressure decrease is further calculated using the equations (2) & (3) in chapter 2.4.2.

For specification of the variables see chapter 3.2 and for the theory of grout consolidation see also Thienert (2010) or Talmon (2009).

3.4.3 Data evaluation on the basis of the city tunnel Leipzig (CTL)

The data from the city tunnel in Leipzig was provided by company “ALPINE BAU GmbH”, which was in charge of the main tunnel works for this project, starting in 2004. The project itself is described in chapter 3. Within this chapter the evaluation of grout and slurry pressures will be discussed more thoroughly.

2 cross sections were chosen for the elaboration of all the data, which is the section at km 2.760, further called as “Cross Section I”. It is situated along the very congested “Petersstraße” in the centre of Leipzig and one cross section, which is 150m further away close to the metro station “Markt”, later mentioned as “Cross Section II”.

Thus only the data within a certain time and range was collected and evaluated. This is advisable because the monitoring computer is saving approximately 10 pressure values per minute. For 1 day there are 14 400 rows of data, hence only a certain range of data should be taken for later evaluation to minimize the work.

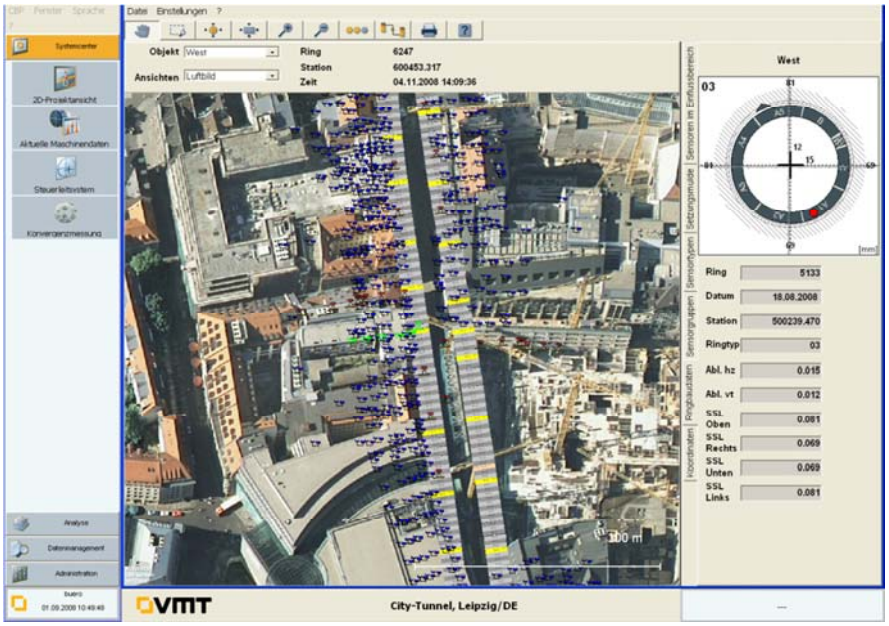

Figure 3-25: TBM monitoring software (Alpine Bau GmbH)

Figure 3-24 shows the monitoring software usually provided by the same company also delivering the TBM (in this case Herrenknecht AG).

3.4.3.1 Cross section I

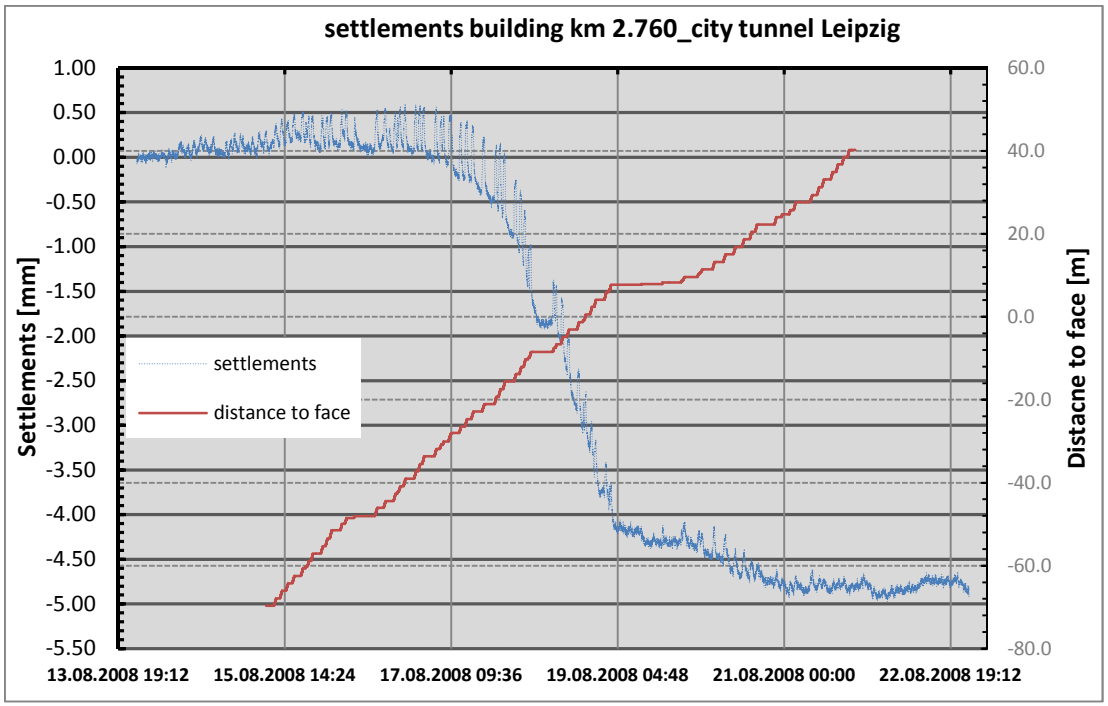

Figure 3-26: Settlements cross section I

In figure 3-24 one can see the settlements for the cross section at “Petersstraße”. The measurements were obtained from tube-levellers which are fixed to an adjacent building, thus giving movements of the building and furthermore of the foundation in about 9 m depth.

The decisive settlements due to undermining the building occur from the 17.8 to 21.8 (lining ring 5115 to 5149). Before that date it is obvious to see that there has been a certain heave while the TBM was approaching the building and the monitored section. The red line in figure 3-26 displays the distance from the tunnel face to the survey mark at km 2.760, showing that approximately 30 to 35% of settlements occur before the face has reached the station. Mair et al., 1997, concluded as an empirical estimation, the percentage of settlements before the face passed a point should be about 25-30%.

3.4.3.1.1 Slurry pressure

The face-support pressure is always measured at the crown of the tunnel. From the crown downwards, the pressure is increasing with depth. While excavation mode, the slurry normally has a density of about 11 – 12 kN/m³ and when regenerated usually 10.5 to 11 kN/m³. The density and the amount of regenerated suspension is a key factor for evaluating the volume of excavated soil.

The specified unit for all pressures measured at the TBM, is *bar.* 1 bar equals 100 kN/m².

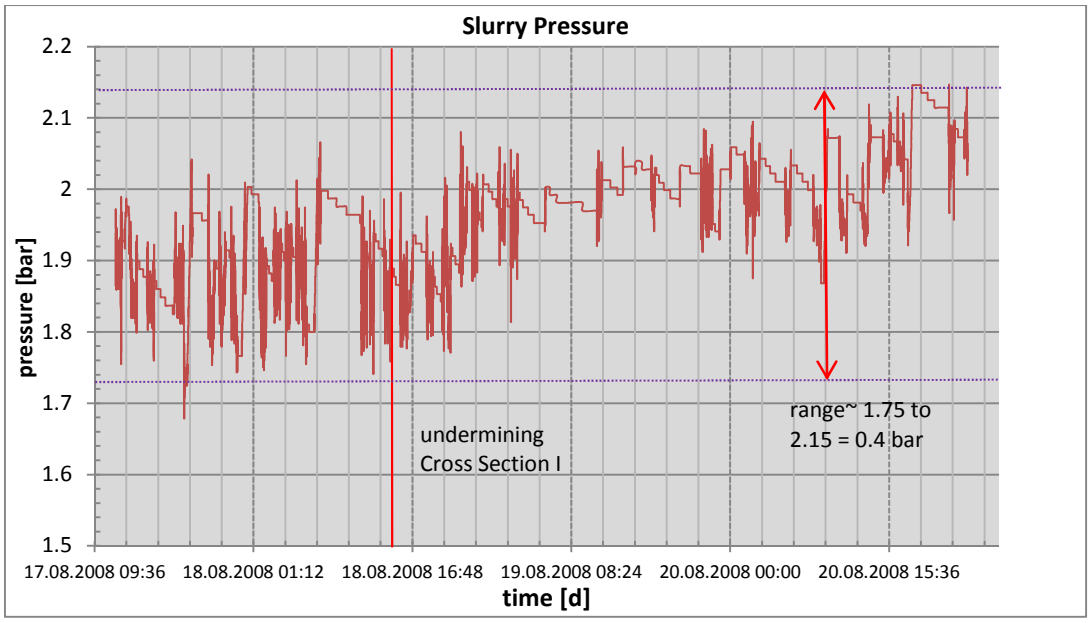

Figure 3-27: Decisive slurry pressures influencing settlements at cross section I

As already mentioned, the fluctuations during excavation are due to the strokes of the piston pump, conveying the slurry to the front of the TBM. The unsteady range of the pressures in figure 3-27 is a combination of the influencing strokes and the change from TBM-advance to ring erection.

In the figure above the pressure fluctuates within a range of about 0.4 bar. Thus for later FEM calculations no precise slurry pressure can be evaluated. This is not of great importance because the axial face pressure does not have such an influence on vertical settlements compared to the annular grout pressure. Nevertheless, an average pressure has been elicited from the data used for figure 3-27, resulting in a mean-value of roughly 185 kN/m² or 1.85 bar. The chosen cross section has been undermined on the 18.08 as one can also see in figure 3-27.

Mean slurry pressure value from 17.8 to 21.8

~1.80 – 1.90 bar

3.4.3.1.2 Grout pressure

The grout pressure fluctuates even more and making it difficult to verify realistic values for a FEM calculation. It is therefore necessary to take a closer look into the difference between TBM advance and lining erection.

As already mentioned above the grout is being injected via openings in the TBM shield tail, the value of pressure however is being measured at the beginning of the shield-tail, meaning that the measured values are not the actual pressures the grout is subjecting onto the soil (again all pressures are denoted in *bar).*

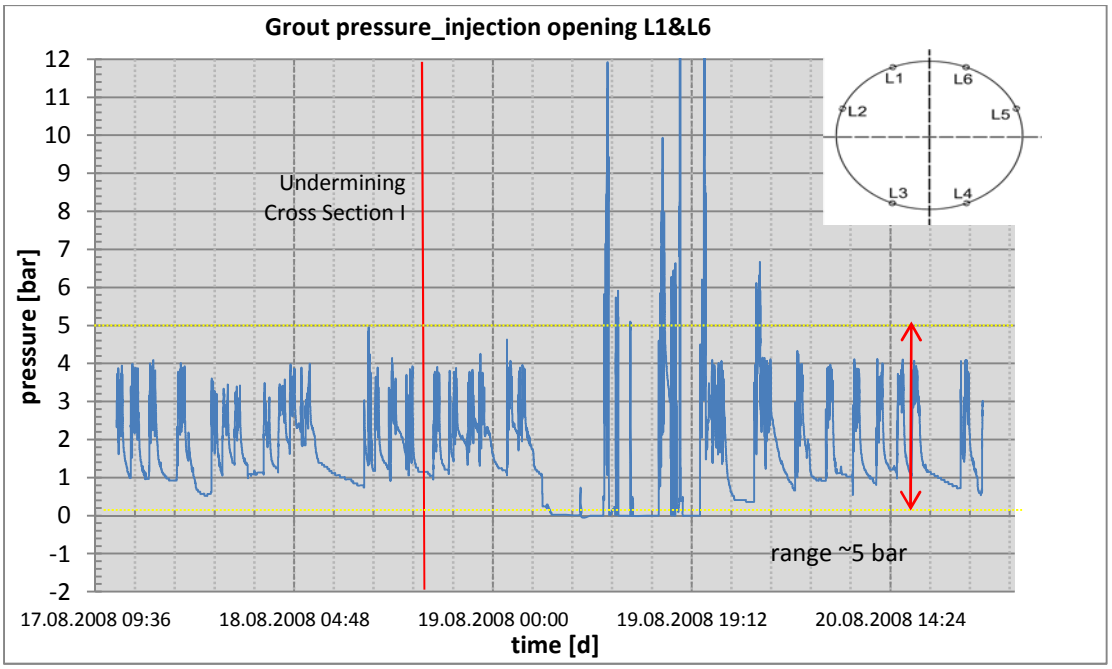

Figure 3-28: Decisive grout pressures cross section I

Consequently there needs to be a stress gauge measuring those pressures at the tail of the TBM, if there is no such equipment available, only a rough estimation on how much the pressure decreases can be made.

The actual measuring gauges are installed at the beginning of the injection openings, which is 4.5 m before the end of the shield tail (figure 3-30). Thus the injected material experiences a pressure decrease from the recording instrumentations to the actual opening at the end of the shield-tail, which can roughly be estimated with the equation mentioned in 3.4.2.

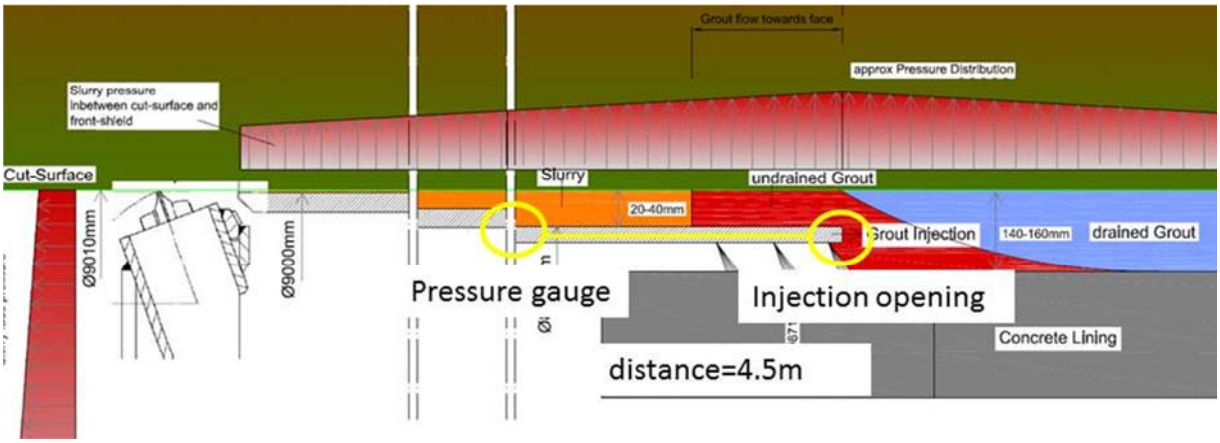

Figure 3-29: Grout injection-channel, pressure gauge

With respect to the yield strength of grout, it is possible to estimate the pressure drop with following equation:

$$dp = \frac{dx}{s}(\tau_y)$$

With:

dx = 4.5 m……...distance between measuring valve and injection opening

s = 0.06 m……...thickness of the injection opening

T_y……..yield strength of grout [kN/m²]

Ty [kN/m²]	dp [kN/m²]
0.3	22.5
0.4	30.0
0.5	37.5
0.6	45.0
0.7	52.5
0.8	60.0
0.9	67.5
1	75.0
1.1	82.5
1.2	90.0

Table 3: Pressure decrease along the injection opening with respect to the grout yield strength

As one can see above, the pressure decrease within the injection channels fluctuate in-between 20 and 90 kN/m² (0.2 to 0.9 bar). For further calculation an average value of about 0.5 – 0.6 bar was taken to evaluate the real pressures. Again an uncertainty range of plus minus 0.1 bar was chosen due to the unsteady strokes of the pump. On the correlation between vertical settlements and grout pressures it is visible that settlements almost only occur when no advancing takes places, thus during ring erection.

In figure 3-30 it is evidently shown that during excavation the building is experiencing heave, while during ring erection the low grout pressures lead to settlements. But it is not obvious that settlements are only induced due to the standstill of the TBM, since the advancing causes a change in the grain composition of the soil and thus in the stress distribution.

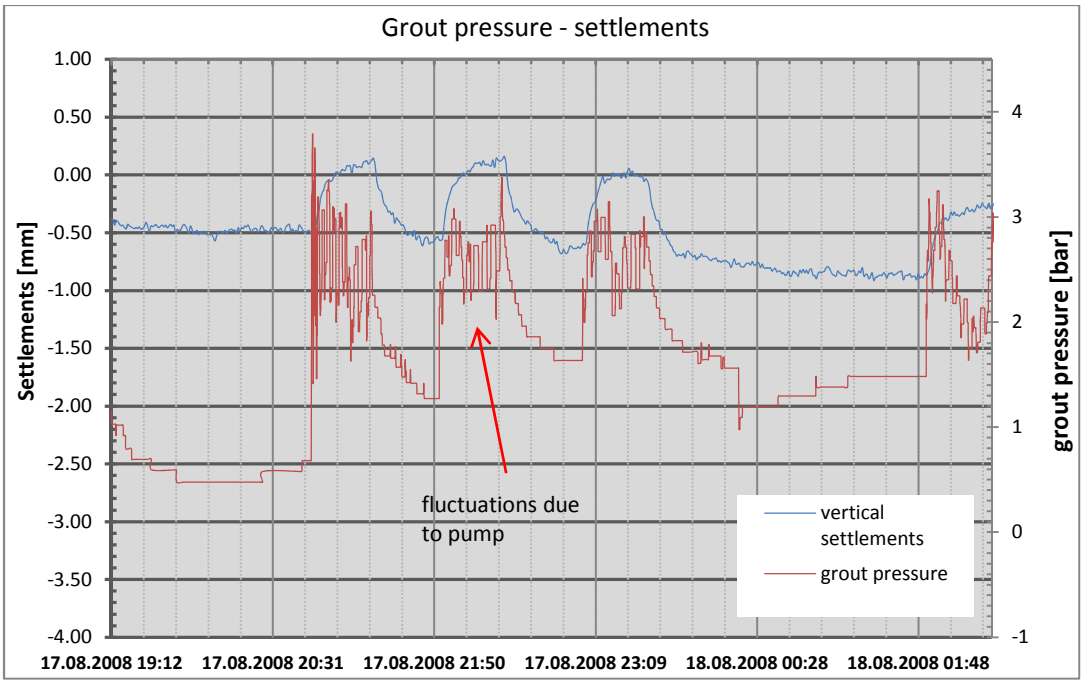

Figure 3-30: Correlation between grout pressure & settlement

Consequently the values had to be separated into an average pressure during TBM-advance and a pressure during ring-erection. Therefore 35 sections (lining-rings) from the 17.08 to the 21.08 (as per figure 3-26) were elaborated and the average value was calculated on the basis of the data used for figure 3-27 and 3-28. For the grout pressures during TBM-advance and ring-erection, the average value of Lisene 1 and 6 was taken. Lisenes 3 and 4 (which are on the base of the TBM) could be neglected as the gradient from the crown to the invert seemed to be very unsteady (case-study on the grout-pressure gradient in chapter 6.3.2.2)

Average grout pressure values for 35 TBM-drives:

Advance: 290 kN/m² or 2.90 bar (for Lisene 1 and 6)

Ring erection: 205 kN/m² or 2.05 bar

Average slurry pressure value for 35 TBM-drives:

~ 185 kN/m² or 1.85 bar (as per 3.4.3.1.1)

Those values should constitute the actual values of grout pressures at the tail of the TBM. Assuming that the grout pressures during ring erection contribute 70% to the settlements and the ones measured during TBM advance 30%, it is possible to elaborate the values for the input for the grout-flow assumption along the shield.

Average grout pressure values decisive for the settlements at cross section I:

	1	2	3
Mean Values cross section I	Excavation [bar]	ring erection [bar]	0.30*(1)+0.7*(2) [bar]
Grout pressure at measuring gauge	2,95	2,05	2,32
Grout pressure at end of shield tail (-0.5bar)	2,45	1,55	1,82

Table 4: Average pressure values, decisive for settlements at cross section I

Considering the values in table 4 to be average values of grout pressure, the fluctuations due to the pump contributes to the unsteady pressure distribution, thus it is moderate to say that the grout pressure lies within a lower and upper boundary.

Hereby:

Decisive grout pressure cross section I ~1.7 – 1.9 bar (while TBM drive partly 2.0-2.2 bar

Decisive slurry pressure cross section I ~ 1.85 bar

3.4.3.1.3 Pressure distribution along TBM shield for cross section I

On the basis of the previous evaluation of measured data and the previously described theory about grout pressures around a TBM, it is now possible to calculate an approximated pressure flow and distribution along the shield for cross section I.

Parameters (soil parameters see also chapter 4):

Shear Modulus soil, G	90	MN/m²
E-modulus-ur soil, Eur	240	MN/m²
cut radius TBM, r	4,5	m
overcut	0,005	m
delta_x	0,2	m
yield strength grout, Tg	0,5	KN/m²
yield strength slurry, Ts	0,03	KN/m²
water pressure, σw	87	kN/m²
effective stress soil, σ´	191	KN/m²
grout pressure, Pg I	180	kN/m²
grout pressure, Pg II	220	kN/m²
slurry pressure, Ps	185	kN/m²

Table 5: Parameters pressure distribution cross section I

The calculation is based on the soil properties for „Bitterfeld sand". Based on the evaluated measured data there could be 2 potential situations. The grout pressure (Pg) indicates the input pressure at the shield tail of the TBM.

2 potential situations for grout flow along the TBM shield:

Those 2 simulated pressure situations will later be referred as **Case A and B.**

- Case A: Grout pressure P_g = 220 kN/m², flow > towards tail
- Case B: Grout pressure P_g = 180 kN/m², flow > towards face

Resulting in 2 possible cases of pressure distribution along the TBM shield, indicated in the following figure:

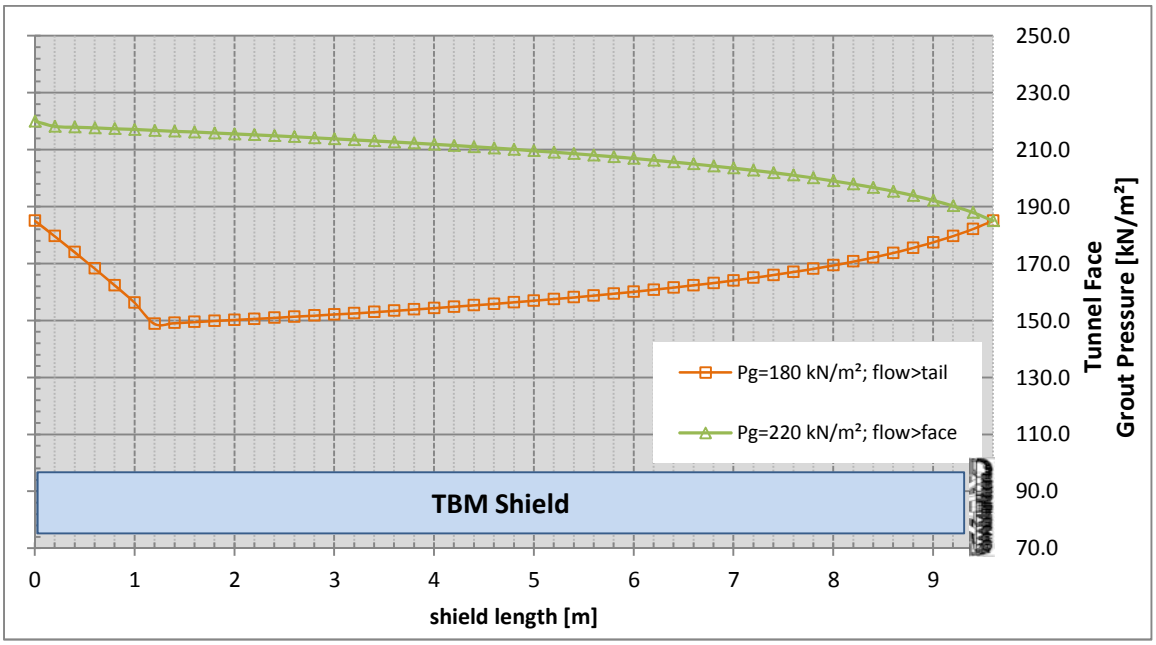

Figure 3-31: Pressure distribution along TBM shield, calculated

Figure 3-31 indicates that the assumption of flow direction has a great importance on the pressure distribution along the TBM shield. When using 220 kN/m² of pressure for the injected grout, the difference whether there will be flow towards face or tail, is about 70 kN/m² or 0.7 bar at its maximum.

The pressure decrease in the gap between lining and surrounding soil has only been approximated and is chosen to be constant in the later FEM-analysis (for further information about grout consolidation and pressure decrease within the ground-lining gap, one is referred to Talmon et al., 2009 or Thienert, 2010).

Approximated pressure distributions:

Case A:

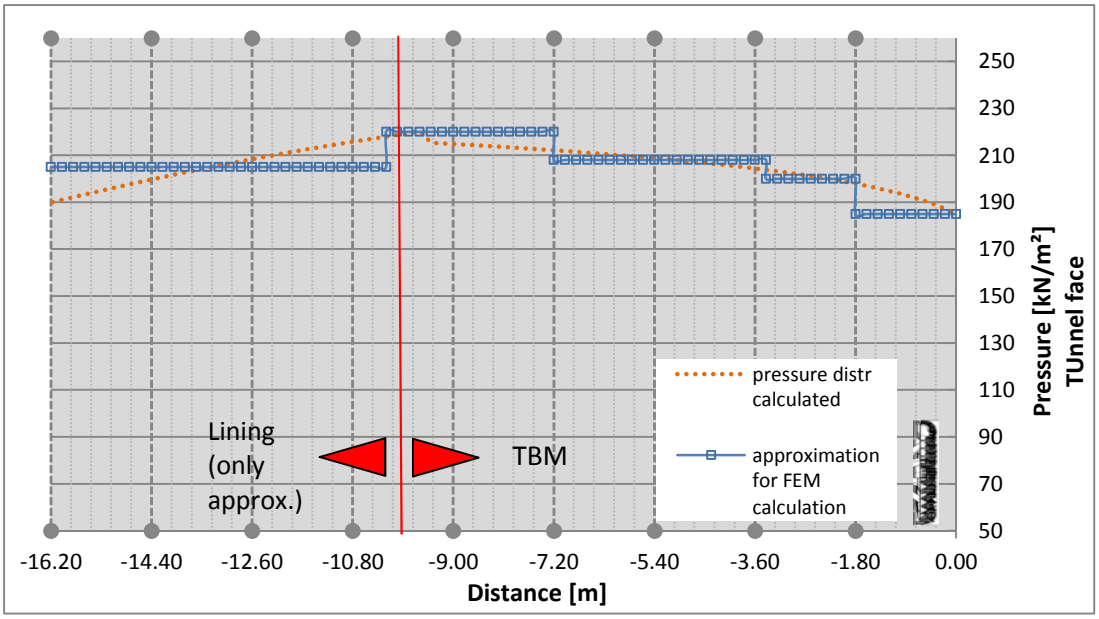

Figure 3-32: Approximated pressure distribution for FEM analysis, Case A

Case B:

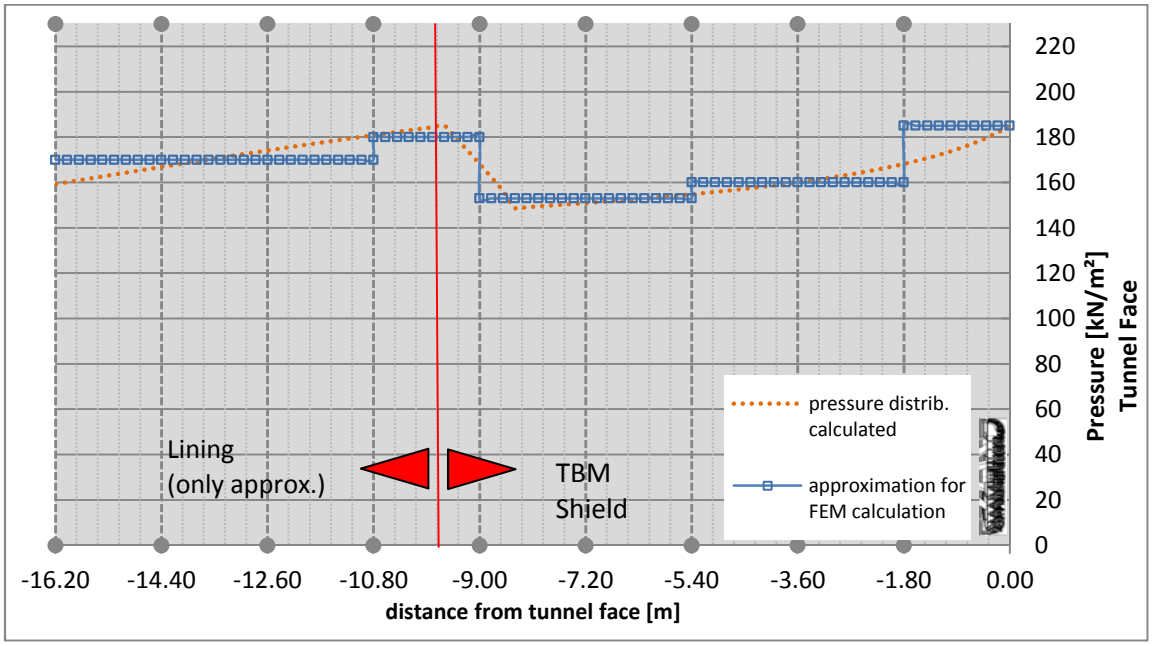

Figure 3-33: Approximated pressure distribution for FEM analysis, Case B

Case A shows the approximated pressure distribution along the TBM shield when using a grout pressure which is higher than the support pressure at the tunnel face. As already mentioned above, the pressure within the gap between lining and cut-surface was roughly approximated and to ease the input for the analysis it is chosen to be constant.

The length for each pressure-change, which are represented in the figures above, depends on the length of one lining ring, which in case of the city tunnel in Leipzig is 1.80 m. The cut-off at

16.2 m was randomly chosen (it actually depends on the consolidation of the fresh injected grout material). For the later 3D analysis 5 lining rings or volume-elements (5 times 1.80 m = 9.0 m) were chosen to represent the influence of the gap in the back of the TBM (see also chapter 5).

Case B indicating that the flow of grout is uncertain and a pressure-decrease occurs from the front to the tail. The lowest peak of the pressure trough is henceforth somewhere along the shield. Again the pressure within the ground-lining gap was chosen to be constant.

3.4.3.2 Cross Section II

The settlements for cross section II have been measured with normal geodetic levellers instead of tube-levellers as there was no building adjacent to it, thus giving less accuracy in the measured data. Figure 3-34 shows the measured settlements including the station of the TBM and the distance to the tunnel face. For this case, the receiving-shaft of the metro station “Markt” is approximately 30 m ahead of this cross section, implying an unnatural boundary condition in front of the face. The closer the machine gets to the concrete wall of the shaft, the more it inhibits the arching effect ahead of the tunnel face.

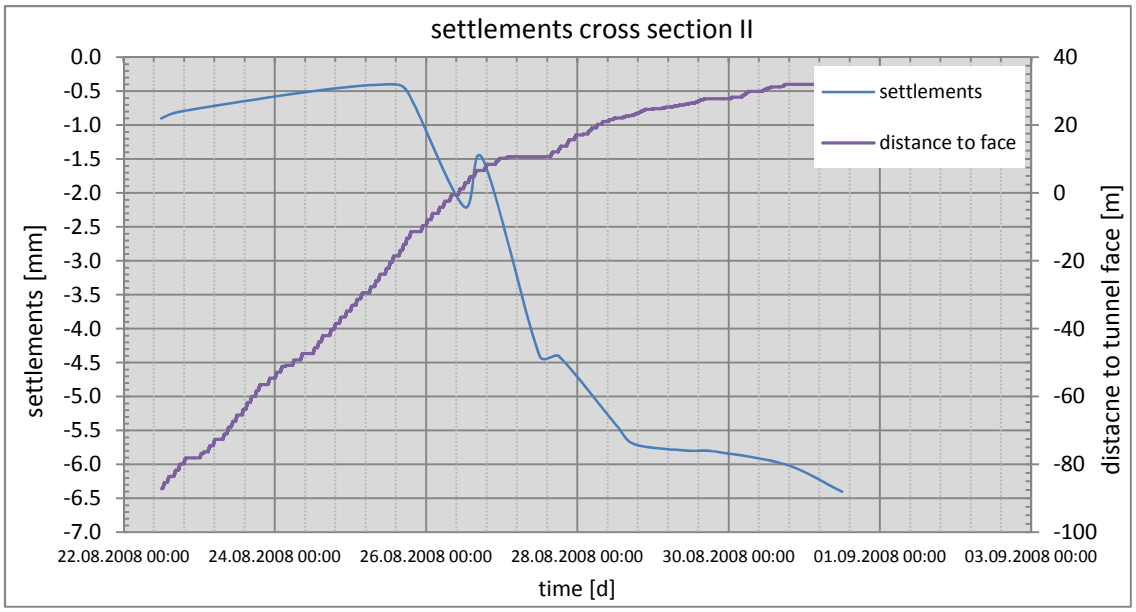

Figure 3-34: Settlement cross section II

Maximum settlement cross section II: ~5.5 mm (surface settlements)

Most of the settlements occur after the TBM passed the monitored cross section, because after undermining this point the distance to the receiving shaft of the metro station is only about 30 m and the face pressure thus needs to be reduced. The grout pressures need to be reduced similarly to prevent uncontrollable outflow of grout into the excavation chamber.

Due to this pressure drop it is even more difficult to evaluate the decisive pressures which are influencing the settlements at cross section II. Thus this cross section was investigated less thoroughly than cross section I and the analysis case study was only examined on surface settlements. Lining forces and lining behaviour have only been elaborated for cross section I.

3.4.3.2.1 Slurry pressure

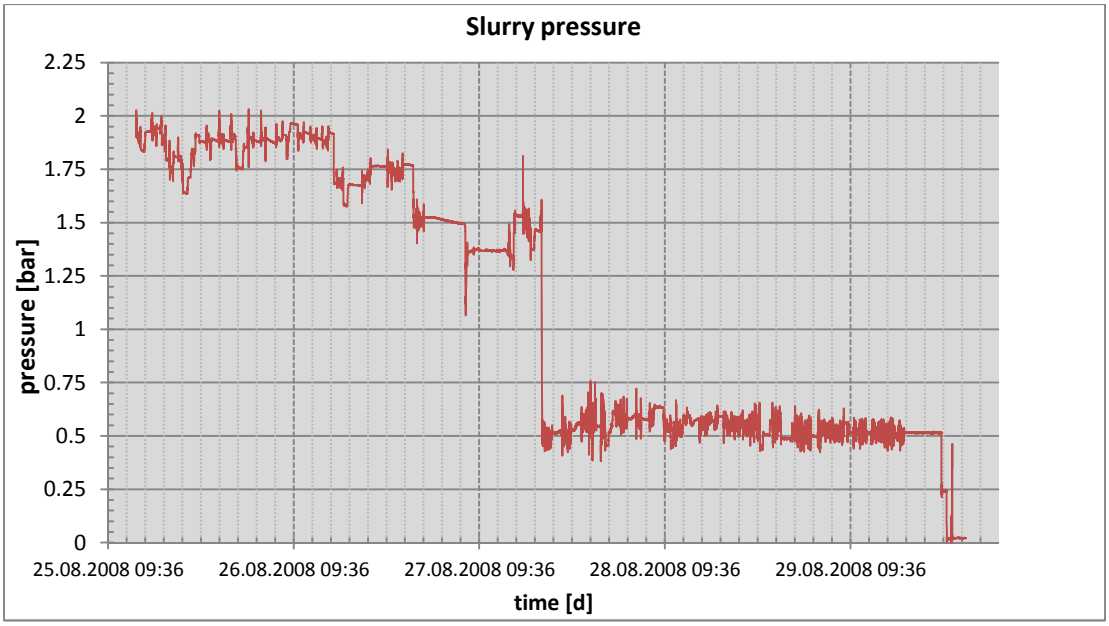

Figure 3-35: Decisive slurry pressures for cross section II

Figure 3-35 shows a drop in pressures on the 27.08, because the machine is approaching the receiving shaft of the metro station.

Average decisive slurry pressure until drop (25.08-27.08): ~1.9 bar

Average decisive slurry pressure after drop (27.08-30.08): ~0.5 bar

3.4.3.2.2 Grout pressure

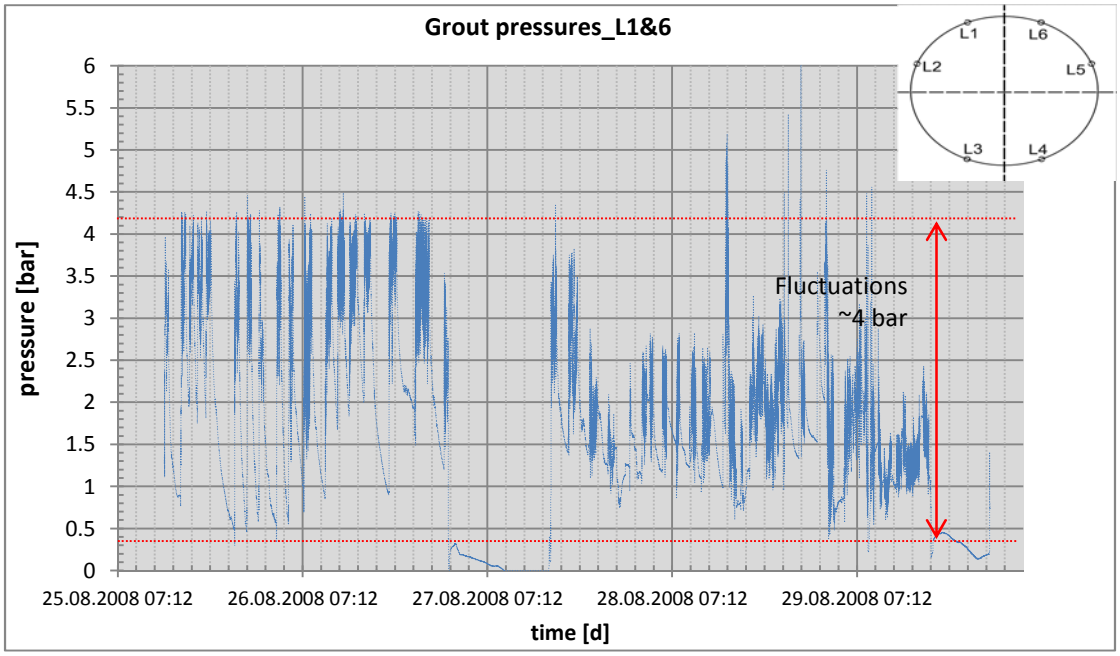

Figure 3-36: Decisive grout pressures for cross section II

Figure 3-36 illustrates the significant pressure fluctuations for the grout injection at Lisene 1 and 6. It is again necessary to consider the difference between TBM advance and ring erection.

The decisive average grout pressure for excavation and ring erection from the 25.08 to the 27.08 (as per figure 3-34) amounts to approximately 2.0 bar. For excavation only, the average value amounts to 3.0 bar and for ring erection about 1.75 bar. After the 27.08, the pressure experiences a decrease and the average value during TBM advance is now ~1.75 bar. During standstill of the machine the average pressure is 1.55 bar.

Again assuming that the grout pressures during ring erection contribute 70% to the settlements and the ones measured during TBM advance 30%, it is possible to elaborate the values for the input for the grout flow assumption along the shield.

	1	2	3
Average grout pr. values cross section II	Excavation [bar]	ring erection [bar]	0.30*(1)+0.7*(2) [bar]
until pressure drop	3,10	1,80	2,20
after pressure drop	1,78	1,57	1,50
until drop end of shield tail (-0.5bar)	2,60	1,30	1,70
after drop end of shield tail (-0.5bar)	1,28	1,07	1,00

Table 6: Average grout pressures values

Decisive grout pressure until pressure drop: ~ 1.5 to 1.8 bar

Decisive grout pressure after pressure drop: ~ 0.9 to 1.1 bar

3.4.3.2.3 Pressure distribution cross section II

Cross section II has only been investigated performing a 2D-Analysis. Thus no grout-flow assumption had to be taken into account. The results of the 2D analysis are shown in chapter 5

4 City tunnel Leipzig (CTL)

4.1 General

The City Tunnel in Leipzig was built to connect the existing Metro station “Bayrischer Haltepunkt” and the main central station within the city centre. It comprises two tunnels including single-line tracks with a diameter of 9.0 m. It undermines almost the entire city centre of Leipzig, including some historically valuable buildings, which made the construction process more difficult and challenging.

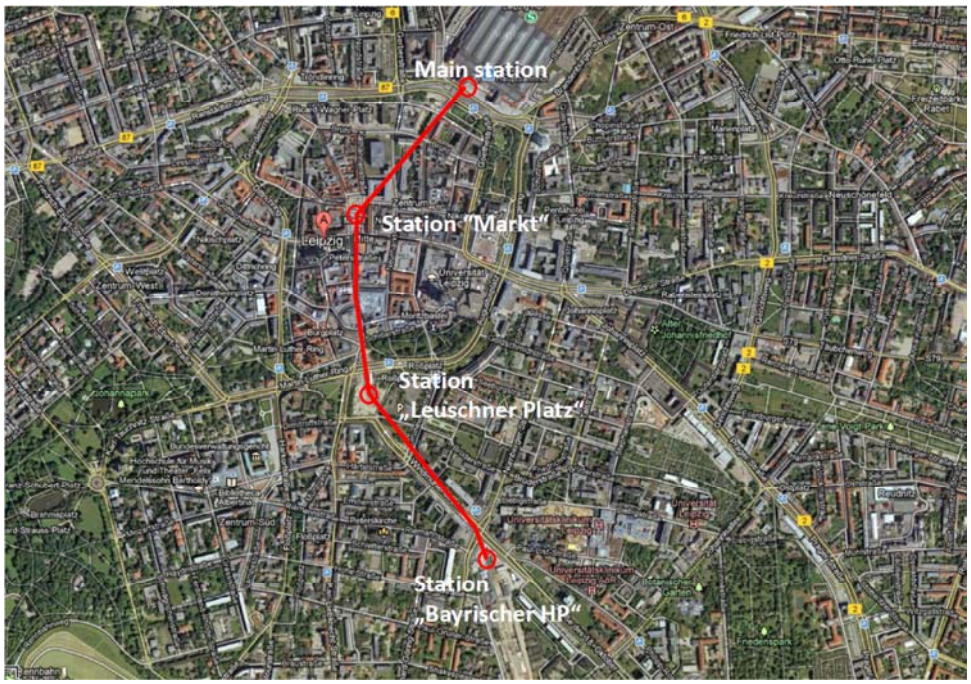

Figure 4-1: Areal view of Leipzig including the alignment of the tunnel (www.google.com/maps, access: 15.06.2012)

4.2 Geology

From a morphological point of view, Leipzig is situated in the northwest of Germany in the so called “Leipziger-lowland-bay”. The lowland bay, with a radial spread of about 50 km was formed due to the rising “Erz”-mountains in the southeast of Germany during tertiary times.

The geological conditions in the area of Leipzig have been strongly influenced from the last glacial periods, the “Saale” ice age and the “Weichsel-Kaltzeit”. The last glacial period did not reach Leipzig, only covering the north of Germany and leaving a lower moraine field in the south, nowadays including the area around Leipzig. After withdrawal of the ice in the north and due to the orogenesis happening all over Europe, sedimentation and fluvial transportation led to the accumulation of gravelly, partly silty sands in the northeast of Germany.

(www.wikipedia.com. access: 21.08.2012)

The ground can be described as partly silty, gravelly fine sands, which are accumulated above layers of silt and silty clays. Due to the presence of swamps millions of years ago, those sand deposits also contain a slight amount of organic material, which was then again overlain by silty sediments.

The tunnel axis, 15-20 m below surface, mostly penetrates through fine and mean sands, partly gravelly sands, in some parts including coal and organic material. Just below ground surface one can encounter layers from earlier ages, like fill, fluvial marls or layers of gravel.

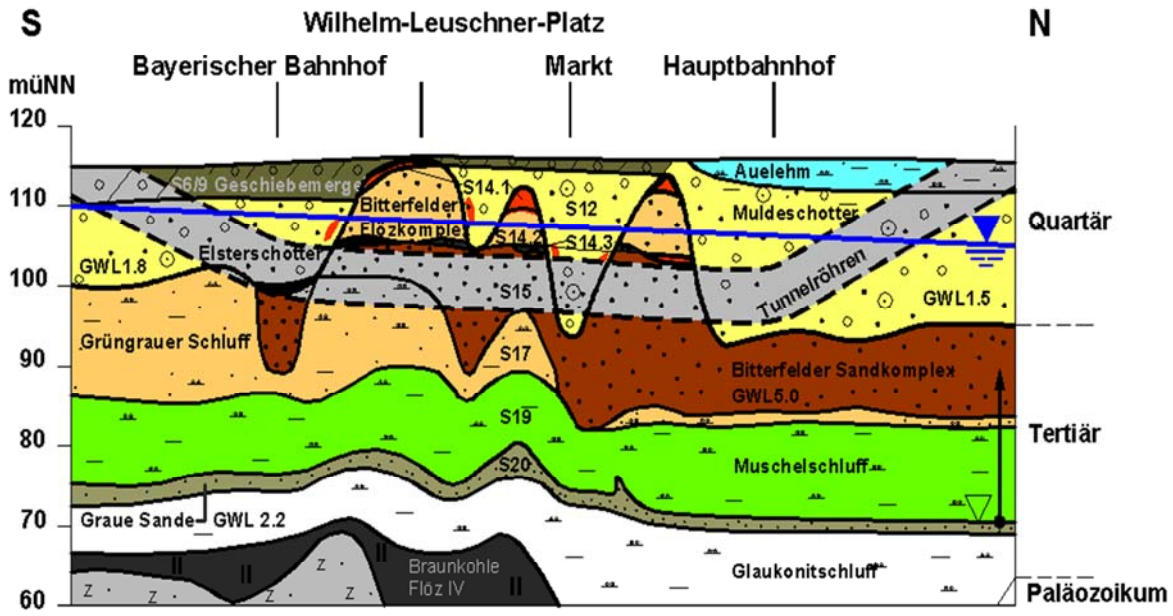

Figure 4-2: Geology Leipzig (Alpine Bau GmbH)

The tunnel indicated in figure 4-2 is shaded in gray and is predominantly mining through fine gravelly sands.

4.3 Investigated cross sections

The chosen cross sections (figure 4-3) are located in-between the metro stations “Leuschner-Platz” and “Markt”. Undermining the very congested “Petersstraße”, the tunnel (yellow, figure 4-3) is passing a very sensitive area. Consequently a large effort needs to be taken to prevent settlements of the adjacent buildings along the street. During the time of construction, the pressures acting around the TBM needed to be monitored more closely and thus adjusted if any kind of slurry-loss or pressure drop occurs. Both sections were analysed using 2D numerical simulation. For the 3D analysis in Plaxis however, only cross section I was investigated.

Before commencing the tunnel works some of the structures close to the tunnel-axis were supported and stabilized using compensation grouting or soil-freezing. In many cases the buildings experienced a small heave due to the pre-grouting in order to compensate the subsequent settlements caused by the tunnelling process.

These pre-grouting measurements, although causing a change in soil stresses, have been neglected at the analysis. However, on the one hand such a pre-imposed heave of the structures causes a change in stress, but on the other hand would lead to an unloading-reloading behaviour of the soil.

The adjacent sewer lines, injection shafts etc. have been also neglected in the FEM analysis.

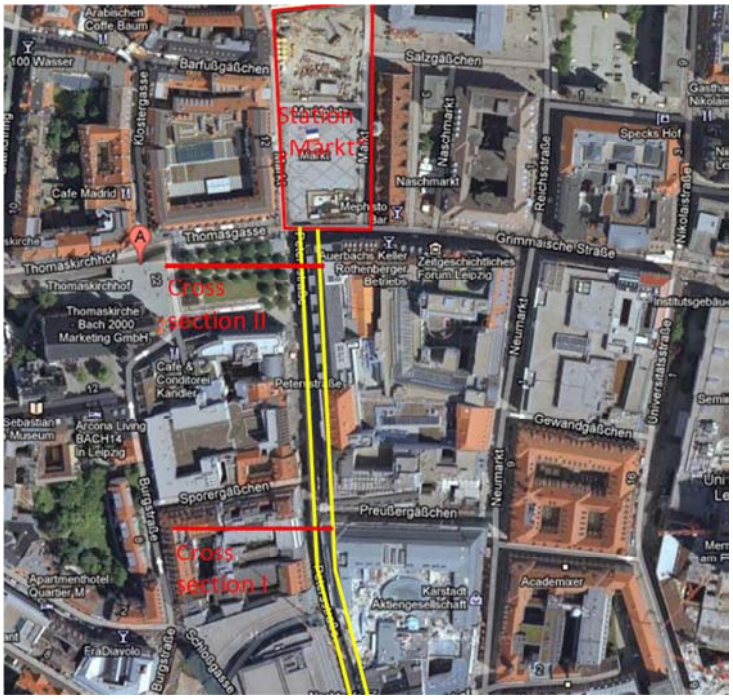

Figure 4-3: Investigated cross sections (www.google.com/maps, access: 15.06.2012)

The soil layer distribution from the surface down was elicited from adjacent bore logs and investigations in intermediate cross sections.

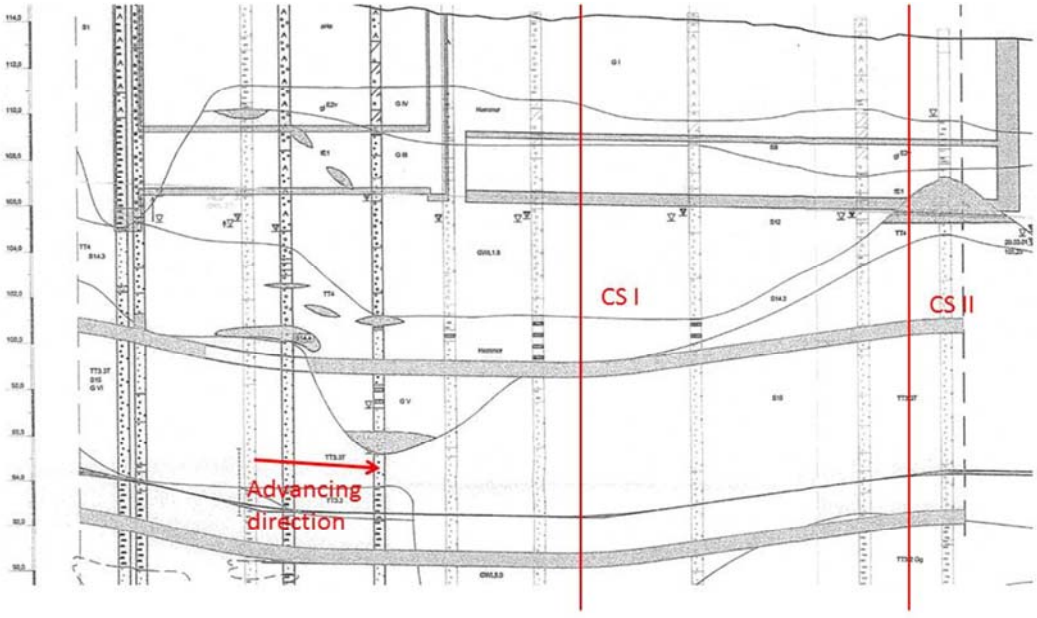

Figure 4-4: Longitudinal view, investigated area

Approximate layer distribution along the investigated area:

0 – ~5 m > Fill

~ 4 – 7 m > Marl: sandy, gravelly Silt

~ 7 – 15 m > Fluvial-Sand: gravelly Sand

~ 12 – 28 m > Bitterfeld-Sand: fine – medium Sand

~ 24 – 31 m > Greenish-Silt: sandy clayey Silt

~ 30 – 40 m > Clam-Silt: highly silty, sandy Clay

There are no exact borders in-between those layers, thus the level of margins are strongly fluctuating. The assumed and approximated soil profiles used for the analysis are outlined in chapter 5.

4.3.1 Soil properties

The ground conditions and soil properties have been evaluated regionally and not only locally for the two cross sections, which resulted in more detailed output for the soil properties.

The evaluation of parameters for later FEM Calculation is based on the geotechnical data and reports provided by company Alpine Bau GmbH.

Schichtnummer/Bezeichnung			Bodengruppe n. DIN 18 196	Bodenklasse n. DIN 18300 Bohrbarkeitsklasse nach DIN 18301	Lagerungsdichte/ Konsistenz	Wichte		Scherfestigkeit			Verformungsmodul	Durchlässigkeit
Geotechnische Schicht	im stratigraphischen Normalprofil					cal. γ	cal. γ'	cal. q_u	cal. c'	cal. φ'	cal. E_s	cal. k_f
						[kN/m³]	[kN/m³]	[kN/m²]	[kN/m²]	[°]	[MN/m²]	[m/s]
I	S 1	Auffüllung	A, [SU*, SU, SE, GU, G]	3, z.T. 4 LN, LB, S 3	weich – halbfest	18,0	10,0	-	0	30,0	1 bis 8	-
III	S 12	Flussschotter	SE, SI, GW, GI (ST*, SU*)	3 LN, S 3	mitteldicht – dicht	19,0	11,0	0	0	36,0	bis 105,0 m üNN 80 <105,0 m üNN 100	$8 \cdot 10^{-4}$ bis $1 \cdot 10^{-3}$
IV	S 9	Geschiebemergel	SU*, ST, TL	4 bis 6 LB, LN, S 3	steif – halbfest	21,0	12,0	200	16	30,0	25	ca. $1 \cdot 10^{-8}$
VI	S 14.2 S 15	Bunte Sande Bitterfelder Sande	SE, SU (SI, GI)	3 LN	mitteldicht – dicht	18,0	10,0	0	0	34,0	150	$2 \cdot 10^{-4}$ bis $5 \cdot 10^{-3}$
V_K	S 14.3	Braunkohlenschluff	SU*-TM, (OU-UM)	5 LB, LO	steif	17,0	7,0	40	5	18,0	5	$1 \cdot 10^{-8}$ bis $1 \cdot 10^{-10}$
VII	S 17	Grüngrauer Schluff	UL, UM, TL, TM	4 LB	steif – halbfest	20,0	11,0	100	15	26,0	45 [1]	$5 \cdot 10^{-8}$ bis $5 \cdot 10^{-9}$
IX	S 19	Muschelschluff	TL-TA, UL, SU*	4 bis 5 LB	steif – halbfest	20,0	11,0	220	22	24,0	bis 85,0 m üNN 55 [1] <85,0 m üNN 60 [1]	IX_o $2 \cdot 10^{-10}$ IX_u $5 \cdot 10^{-9}$ IX_o $5 \cdot 10^{-11}$
X	S20 S 21	Grauer Sand Glaukonitschluff	TL, TM SU*	4 LB	weich – halbfest mitteldicht	21,0	12,0	80	10	27,0	60 [1]	$1 \cdot 10^{-7}$ bis $5 \cdot 10^{-9}$

Figure 4-5: Soil parameters given in the geotechnical report

Based on the data given in the geotechnical report and the cross/longitudinal sections for all the four metro stations, it was possible to evaluate the existing stiffness parameters for all the decisive soil layers. An abstract from the technical report is shown in figure 4-5.

Each soil layer has been assigned to a geotechnical and geological soil number. Using roman letters the decisive soil layers will be later always noted as:

- (I) Fill
- (IV) Marl
- (III) Fluvial-Sand
- (VI) Bitterfeld-Sand
- (VII) Greenish-Silt
- (IX) Clam-Silt
- (V) Coal

The data has been collected for all the 4 metro stations including intermediate cross-sections in-between. Based on the soil-layer distribution with related water levels, effective stresses have been calculated and assigned to the pre-evaluated stiffness parameters.

Calculating the effective vertical stresses (σ_v') in each station and intermediate cross section, those values could be opposed to the 1-dimensional or oedometric soil stiffness (E_{oed}) given in the geotechnical report (figure 5-6).

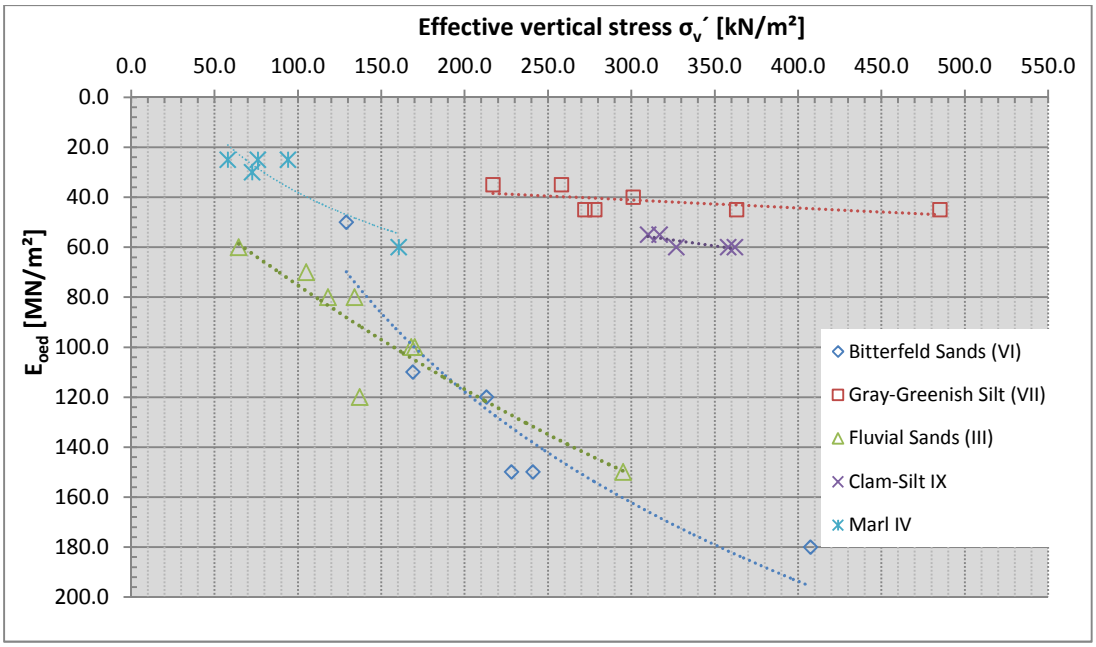

Figure 4-6: Effective stress versus oedometric soil stiffness, collected soil parameters

Because of the stress dependent stiffness of soil, the values could be further used for calculating the reference stiffness of the high order constitutive models. Thus it was necessary to decide which constitutive models should be used for later calculation. For this thesis PLAXIS was chosen for all the geotechnical analysis. The most developed models implemented in the FEM program are the Hardening Soil (HS) and the Hardening-Soil-Small model (HSS), as well as the standard Mohr-Coulomb model (MC).

Soil Parameters											
Layer No.	Layer Description	Consistency	Density		Shear-Strength			Permability	Stiffness		
			γsat [kN/m³]	γd[kN/m³]	c´ [kPa]	φ [°]	K0=1-sinφ	k [m/s]	Depth [m] from Surface	σv´ [kPa]	Eoed [Mpa]
I	Fill	Sa: loose-medium dense Cl: soft-stiff	18	18	0	30	0,500	-	- -	- -	8
III	Fluvial Sand	mediumdense-dense	19	16	0	36	0,412	8*10^-4 - 1*10^-5	4-12 12 - 24	60 - 200 200 - 315	60 - 110 110 - 150
IV	Marl	stiff-semi stiff	21	18	16	30	0,500	1*10^-8	2 - 10	65 - 160	35 - 60
Vk	Coal		17	17	5	18	0,691	1*10^-8 - 1*10^-10	10-20	-	5
VI	Bitterfeld Sand	mediumdense-dense	19-20	16	0	34	0,441	2*10^-4 - 5*10^-5	5 - 17 17 - 24 24 - 34	125 - 210 210 - 330 330 - 435	50 - 120 120 - 170 170 - 180
VII	Greenish gray Silt	stiff-semi stiff	20	16	15	26	0,562	5*10^-8 - 5*10^-9	20 - 30 30 - 40	210- 300 300 - 510	35 - 45 45
IX	Clam-Silt	stiff-semi stiff	20	16	22	24	0,593	5*10^-9 - 5*10^-11	25-50	310-400	55-60

Figure 4-7: Collected regional soil parameters

After collecting all the data from the reports and evaluating the stiffness with respect to the effective stresses of soil, the parameters for the decisive layers could be summarized, which are shown in figure 4-7.

4.3.2 Evaluation of parameters for the Hardening Soil & HS-Small model

The more advanced parameters needed for this model, are not given in any report nor in any kind of test result for this project therefore it is necessary to calculate or estimate those values.

The determination will be shown below on the example of the soil type “Fluvial Sand”.

For further information see also Brinkgreve et al. (2011) or PLAXIS Manual (2012)

4.3.2.1 Example evaluation for Eoed, E50, Eur & G0ref on basis of “Fluvial Sand”:

Parameters needed for HS/HSS model:

φ (phi)	angle of internal friction (effective)
c´	cohesion (effective)
ψ (psi)	angle of dilatancy (default = φ-30)
v_{ur} (nu)	unloading-realoding (ur) Poisson´s ratio
m	power for stress level dependency of stiffness
E_{oed}^{ref}	tangent stiffness for primary oedometer loading
E_{50}^{ref}	secant stiffness in standard triaxial test
E_{ur}^{ref}	unloading reloading stiffness (default value $E_{ur}^{ref} = 3*E_{50}^{ref}$)
p_{ref}	reference stress (default value = 100 kPa)

The geotechnical definition of “Fluvial-Sand” in this case is:

“Middle and coarse gravel, fine to middle sandy with local silt deposits;
from early ice age (Weichseleiszeit)” (Geotechnical report by Alpine Bau GmbH)

Shear strength parameter and oedometric stiffness modulus listed below, are given in figure 4-7:

Layer No.	Layer Description	Consistency	Density		Shear-Strength			Permability	Stiffness		
			ysat [kN/m³]	γd[kN/m³]	c´ [kPa]	φ [°]	K0=1-sinφ	k [m/s]	Depth [m] from Surface	σv´ [kPa]	Eoed [Mpa]
III	Fluvial Sand	mediumdense-dense	19	16	0	36	0,412	8*10^-4 - 1*10^-5	4-12 12 - 24	60 - 200 200 - 315	60 - 110 110 - 150

Figure 4-8: Fluvial-Sand, parameters

Correlated stress-stiffness:

$\sigma_v´$ =~ 200 kPa >> E_{oed} =~ 110-115 MPa

$\sigma_v´$ =~ 315 kPa >> E_{oed} =~ 150 MPa

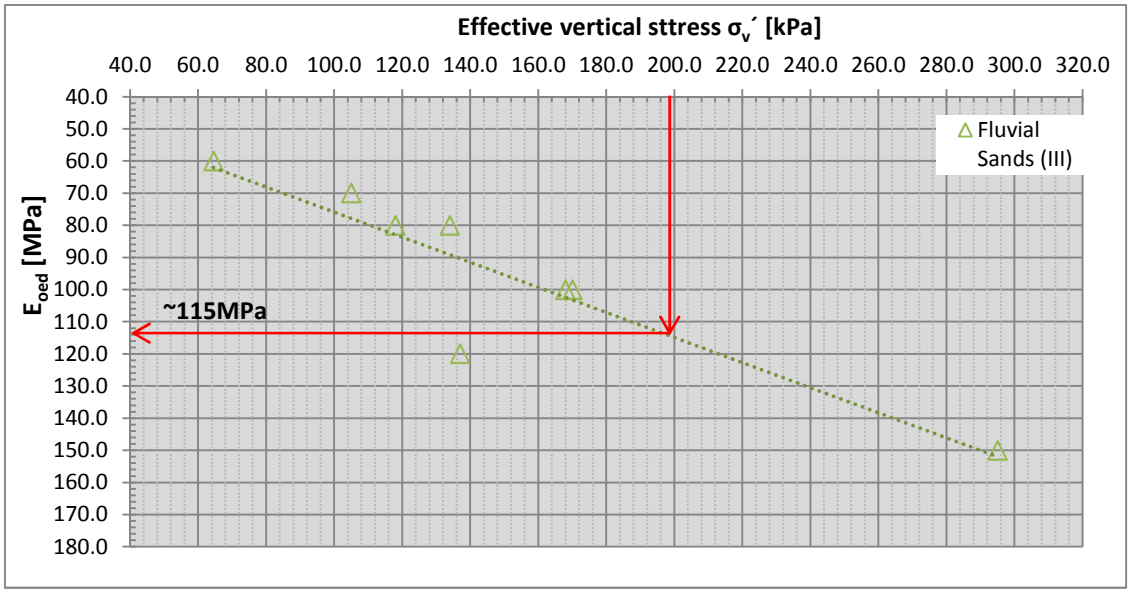

Figure 4-9: Fluvial-Sand, effective vertical stress with respect to the oedometric modulus

The stress-dependent stiffness was deducted from figure 4-9, choosing a stress level and the corresponding stiffness value. The dotted line in figure 4-9 is only a fitted curve, which is supposed to outline the accumulated values and displays an approximate line further values could lie on.

E_{oed}^{ref} for Fluvial-Sand:

$$E_{oed} = E_{oed}^{ref} * \left(\frac{c' * \cos\varphi + \sin\varphi * \sigma_v'}{c' * \cos\varphi + \sin\varphi * p_{ref}} \right)^m$$

Because the cohesion (c´) is 0, the formula is simplified to,

$$E_{oed} = E_{oed}^{ref} * \left(\frac{\sigma_v'}{p_{ref}} \right)^m$$

E_{oed} = 110 MPa

σ_v' = 200 kPa

m = 0,6 (for Sand usually m=0,5)

p_{ref} = 100 kPa (preconsolidation stress; p_{ref}=100kpa)

Converting the equation above to E_{oed}^{ref}, results in:

- E_{oed}^{ref} = 72,6 MPa

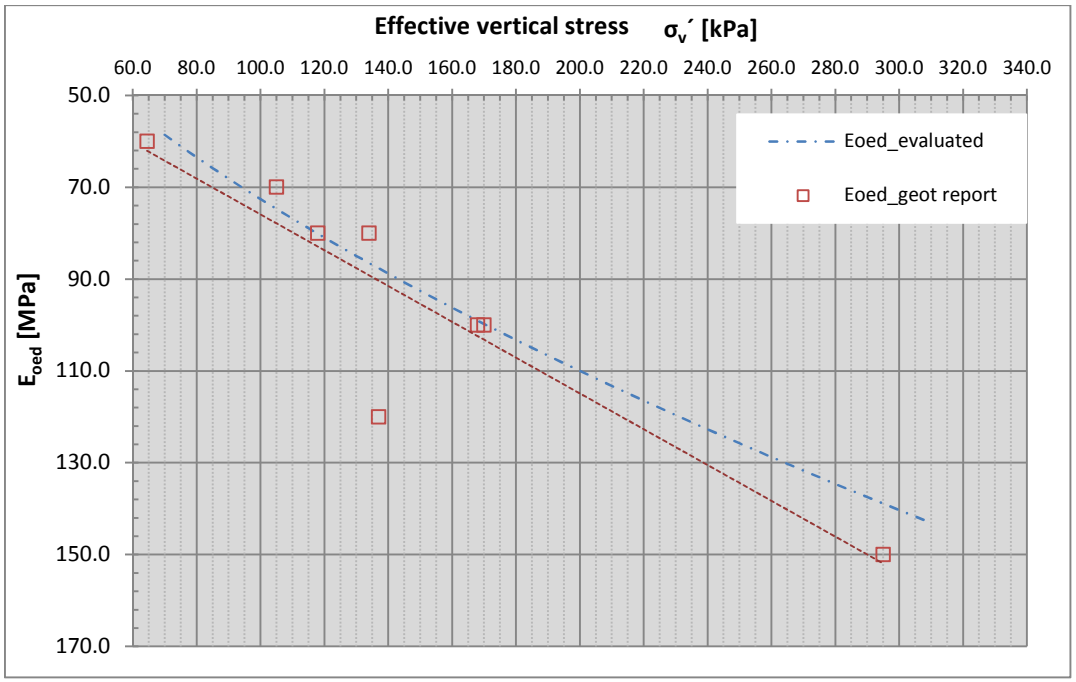

Figure 4-10: Oedometric modulus with respect to the effective vertical stress for Fluvial Sand

E_{50}^{ref} for Fluvial-Sand:

The E50 value is determined by the horizontal stress.

Again the cohesion is zero and the equation can be simplified to:

$$E_{50} = E_{50}^{ref} * \left(\frac{\sigma_h'}{p_{ref}} \right)^m$$

$$\Rightarrow E_{50}^{ref} = E_{oed}^{ref}$$

- $E_{50}^{ref} = E_{oed}^{ref} = 72{,}6$ MPa

E_{ur}^{ref} for Fluvial Sand:

E_{ur}^{ref} default value = 3 * E_{50}^{ref}.

E_{ur}^{ref} = 3 * 72,6 MPa = 217,8 MPa

$v_{ur} = 0.2$

Small strain stiffness:

See also Brinkgreve et al. (2011) or PLAXIS Manual (2012)

The small strain stiffness defines the shear modulus of soil at very small strains.

Parameters needed for the small strain stiffness:

G_0^{ref}……reference shear modulus at very small strains

$y_{0.7}$……..shear strain ration where $G/G_0 = 0.7$

$$G_0^{ref} = (2.5 \; to \; 10) G_{ur}^{ref}$$
$$\gamma_{0.7} = (1 \; to \; 2) * 10^{-4}$$

where

$$G_{ur}^{ref} = \frac{E_{ur}^{ref}}{2 * (1 + \nu_{ur})}$$

(Hardin&Black, 1969) & (Benz, 2007)

Parameters for small strain stiffness used for FEM calculation:

$$G_0^{ref} = 4 * G_{ur}^{ref}$$

$$\gamma_{0.7} = 1.5 * 10^{-4}$$

with

$$G_{ur}^{ref} = \frac{E_{ur}^{ref}}{2 * (1 + \nu_{ur})}$$

$$\nu_{ur} = 0.2$$

$$E_{ur}^{ref} \text{ .....see evaluation } E_{ur}^{ref}$$

4.3.2.2 Parameters for the HS/HSS model

HS/HSS Parameter	γsat	φ	c´	Eoed_ref	E50_ref	Eur_ref	m	ψ	v_ur	K0_NC	γ0.7	Go_ref
	[kN/m³]	[°]	[kPa]	[MPa]	[MPa]	[MPa]	[-]	[°]	[-]	[-]	[%]	[MPa]
Fill	18	30	0	13	13	40	0,5	0	0,2	0,500	1,5*10-4	67
Marl	21	30	16	37	74	222	1	0	0,2	0,500	1,5*10-4	370
Fluvial Sand	19	36	0	73	73	220	0,6	6	0,2	0,412	1,5*10-4	367
Coal	17	18	5	5	5	15	1	0	0,2	0,691	1,5*10-4	25
Bitterfeld Sand	19	34	0	83	83	250	0,6	4	0,2	0,441	1,5*10-4	417
Greenish Silt	20	26	15	20	40	120	0,75	0	0,2	0,562	1,5*10-4	200
Clam Silt	20	24	22	26	52	156	0,75	0	0,2	0,593	1,5*10-4	260

Figure 4-11: HS/HSS parameter

4.3.2.3 Mohr-Coulomb parameters

For the Mohr-Coulomb parameters see chapter 5 at the individual cross sections.

5 2D Analysis

The Analysis is based on the data from the city tunnel in Leipzig which was evaluated in the previous chapter. More precisely, the data for the calculations are evaluated on the basis of 2 cross sections in-between the stations of “Leuschner Platz” and “Markt”. Since the calculation input parameters strongly depend on the constitutive model being used, a first decision needs to be made which models to choose (see also 4.3.1).

5.1 Constitutive models

5.1.1 Mohr-Coulomb (MC)

Parameters needed for the Mohr-Coulomb model:

- ϕ' …friction angel
- c' …cohesion
- E' …Young´s modulus
- $\gamma_{sat/unsat}$ …saturated and unsaturated density of the soil
- v …Poisson ratio
- ψ …dilatancy angle
- k_s …for undrained modelling and consolidation

The Mohr Coulomb Criterion is based on linear-elastic, perfectly plastic stress-strain relations. Besides fully elastic reversible strains, there are also plastic irreversible strains while using Mohr-Coulomb.

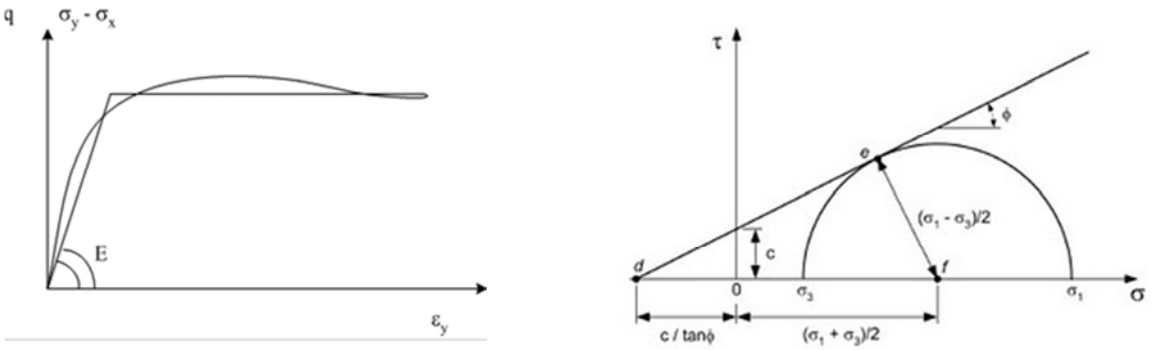

Figure 5-1: Mohr Coulomb failure criterion

5.1.2 Hardening-Soil & Hardening-Soil-Small model (HSS/HS-model)

The Hardening Soil or Hardening Soil Small model is formulated with a hyperbolic stress-strain relationship, which determines the dependency of deviatoric loading to irreversible plastic strains, for stress states below the failure criteria (Brinkgreve, et al., 2011).

The parameter derivation is thoroughly described in chapter 4 (see chapter 4.3.2).

5.2 Cross section I

For further information on the cross sections and for description of the city tunnel Leipzig, see also chapter 4.

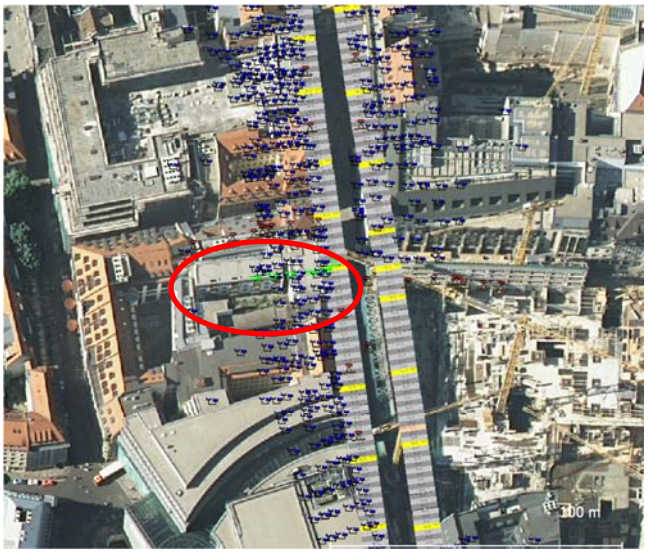

Figure 5-2: Location of cross section I with indicated tube leveller

The chosen cross section, located at the congested “Petersstraße”, is shown in figure 5-2. Using tube-leveller, all the buildings have been monitored and supervised during the construction of the tunnel. The red highlighted area shows the building and the tube leveller in this cross section. For all the calculations however, a green-field situation has been assumed, neglecting the buildings and thus the surcharge load acting on the ground.

5.2.1 Soil profile

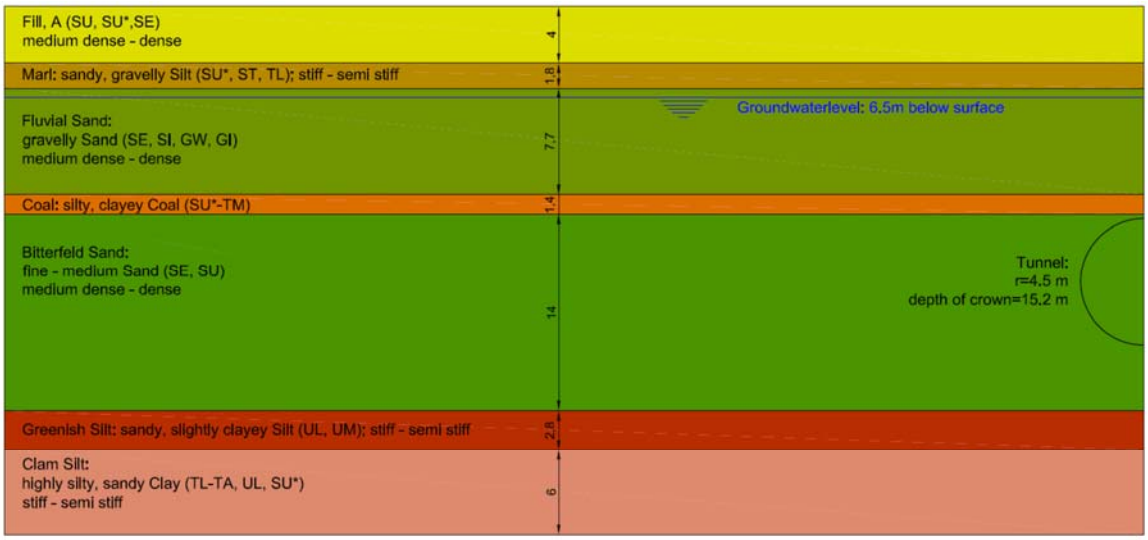

Figure 5-3: Soil profile cross section I

The soil profile illustrated above was elaborated on the basis of the geotechnical report, the longitudinal- and the cross-sections along the tunnel axis (see also chapter 4). As already mentioned in chapter 4, the tunnel mainly penetrates through fine, dense sands (Bitterfeld-Sands). Underneath those layers of sand, at a depth of about 28m from ground level, one will encounter sandy to silty clays (Greenish-Silt and Clam-Silt), which do contain some organic material.

For estimating an appropriate soil profile and layer distribution, the 2 closest cross sections were chosen from the geotechnical report. The profile in-between was assumed to be linearly adjusted, thus giving stratification as shown in Figure 5-3. The layer of coal just above the tunnel crown is not distributed over the total length in actual conditions, but for modelling convenience the layer was chosen to be constant and assumed to be existent all the way across the model. The groundwater head is situated 6.5 m below the ground surface, which is 8.7 m above the tunnel crown.

The height of the 2D and also the 3D numerical model is determined by the influence of the boundary conditions. Since the vertical displacements at the bottom boundary are inhibited, the height of the model below the invert of the tunnel needs to be sufficient to omit the influence of the boundary. Möller (2006) suggested 2 times the diameter of the tunnel for height of the model below the invert. The thickness of the layer Clam-Silt (figure 5-3), just displays a random value and does not go along with the height used for the 2D numerical analysis. For the analysis the height of the model was chosen to be 40.0 m, implying that the tunnel-invert lies at 24.2 m, the model thickness below amounts to 15.8 m, which is 1.75 times the diameter of the tunnel.

Figure 5-4 illustrates the 2D model including the generated mesh, the height of the model below the tunnel invert and the width.

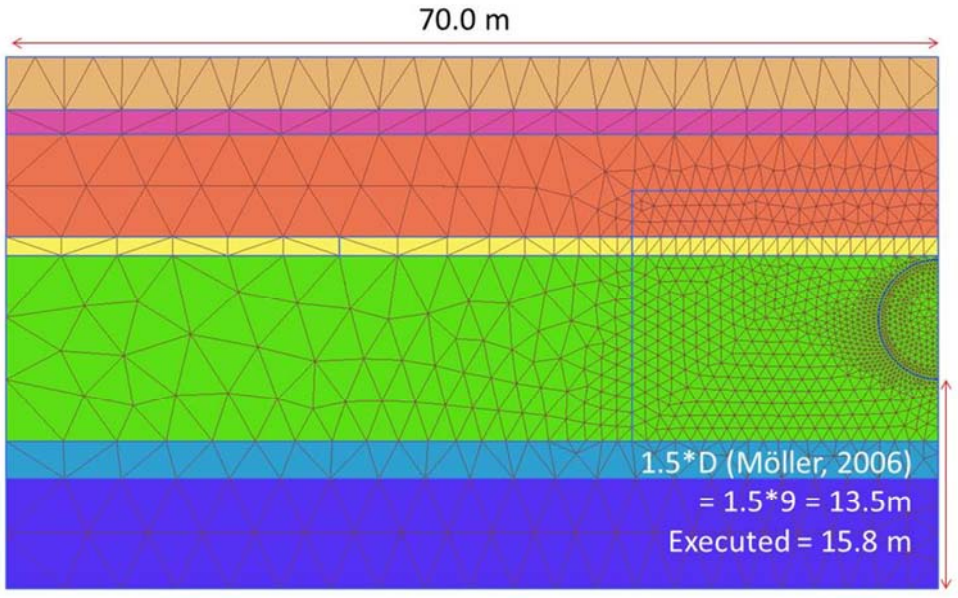

Figure 5-4: 2D model size and mesh distribution

5.2.2 Parameters

Regional soil parameters elaborated from the geotechnical report are highlighted in Figure 4-7. On basis of those regional parameters, the soil properties for the individual cross sections have been established. (see also chapter 4 and tables below)

The parameters for this specified cross section are listed below:

Mohr-Coulomb parameters:

MC Parameter	γ	φ	c	E_{oed}	ν	K_0	E_{ur}^{ref}*
	[kN/m³]	[°]	[kPa]	[MPa]	[-]	[-]	[MPa]
Fill	18	30	0	8	0,3	0,500	24
Marl	21	30	16	36	0,3	0,500	234
Fluvial Sand	19	36	0	93	0,3	0,412	218
Coal	17	18	5	5	0,4	0,691	15
Bitterfeld Sand	19	34	0	147	0,3	0,441	240
Greenish Silt	20	26	15	43	0,3	0,562	120
Clam Silt	20	24	22	57	0,3	0,593	156
*Eur only for Layers underneath Tunnel							

Figure 5-5: Mohr-Coulomb model parameters cross section I

The soil stiffness parameters for Mohr-Coulomb are different for each cross-section because the model does not take stress dependent stiffness into account. Whereas the HSS/HS model takes the stress-dependency into account, thus parameters can be used for all cross sections.

HSS/HS parameters:

HS/HSS Parameter	γ	φ	c	E_{oed}^{ref}	E_{50}^{ref}	E_{ur}^{ref}	m	ψ	ν_{ur}	K_0^{NC}	$\gamma_{0.7}$	G_0^{ref}
	[kN/m³]	[°]	[kPa]	[MPa]	[MPa]	[MPa]	[-]	[°]	[-]	[-]	[%]	[MPa]
Fill	18	30	0	13	13	40	0,5	0	0,2	0,500	1,5*10-4	67
Marl	21	30	16	37	74	222	1	0	0,2	0,500	1,5*10-4	370
Fluvial Sand	19	36	0	73	73	220	0,6	6	0,2	0,412	1,5*10-4	367
Coal	17	18	5	5	5	15	1	0	0,2	0,691	1,5*10-4	25
Bitterfeld Sand	19	34	0	83	83	250	0,6	4	0,2	0,441	1,5*10-4	417
Greenish Silt	20	26	15	20	40	120	0,75	0	0,2	0,562	1,5*10-4	200
Clam Silt	20	24	22	26	52	156	0,75	0	0,2	0,593	1,5*10-4	260

Figure 5-6: HSS/HS model parameters

Figure 5-7 illustrates the oedometric stiffness with respect to the model depth from ground surface for the Mohr-Coulomb and the Hardening-Soil models. As can be seen from figure 5-7, the HS and the HSS model take a stress dependent stiffness into account. For the chart below the oedometric stiffness was opposed for both inputs.

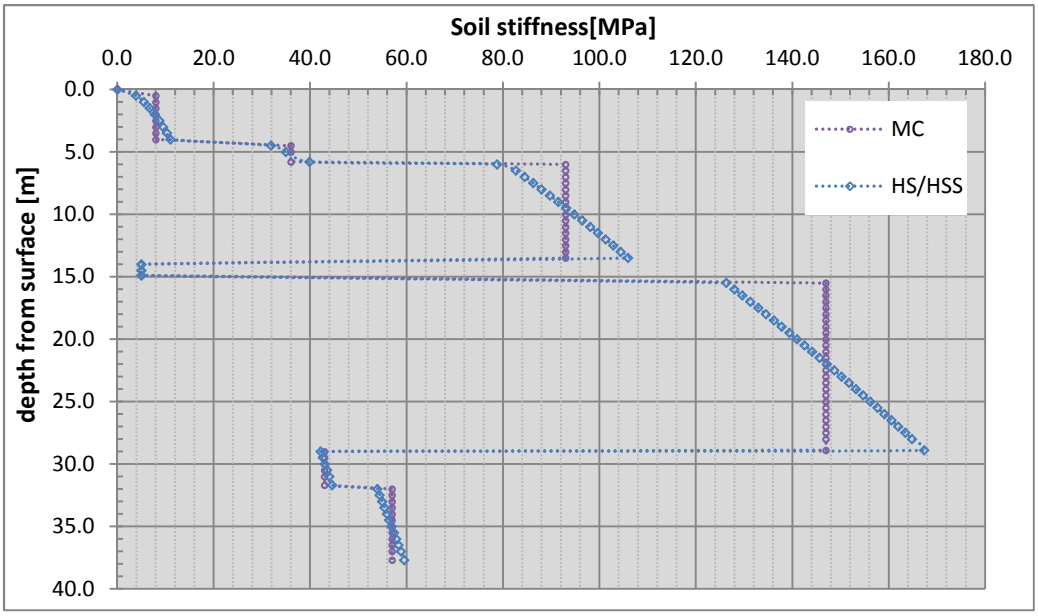

Figure 5-7: Soil stiffness with respect to depth, cross section I

5.2.3 Results

In 2D analyses 3D effects have to be taken into account in an approximate manner. This can be either achieved by means of a pressure or displacement approach. This is implemented by a stress reduction where the initial stress conditions are reduced to an appropriate support pressure or by means of a given tunnel contraction resulting in a defined amount of ground loss. In this thesis a slightly modified approach, called “Grout-pressure” method (Moeller, 2006) has been used.

Hereby the support pressure is simulated by using a pressure-controlled boundary. After the initial phase the tunnel is subjected to a defined amount of pressure using “user-defined” pore pressures (Figure 5-8). For 2D analysis this method represents an easy approach to simulate fluid supported tunnelling machines.

Maximum measured settlement at cross section I (see Figure 3-26)

~4.75 mm (displacement of the building-foundation, thus the value is measured in approx. 9m depth)

Analysis:

HSS-model, using "Grout pressure method" (Moeller, 2006)

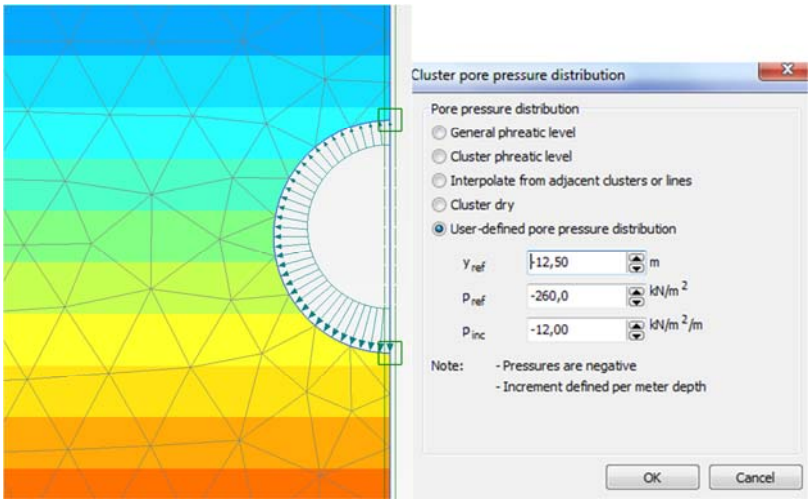

Figure 5-8: Grout pressure method, user defined pore pressure

On the one hand the elaborated settlement troughs in the charts below show the displacements at the ground surface, but on the other hand it also shows the trough in a depth of 9.0 m as well, because the tube levellers are fixed on the building which thus monitor the settlement of the foundation, which is in approximately 9.0 m depth (z=-9m) from surface.

The influence of adjacent buildings and the consequential surcharge have been neglected. The data of the tube leveller closest to the tunnel axis is displayed in figure 3-26, showing the settlement and the distance to the tunnel face in relation with time. For the 2D analysis it is only possible to compare the results with the measured maximal settlement value, because only predefined points (buildings) were monitored during tunnel excavation, thus giving a settlement relation with time which displays the settlement in correlation with the distance to the tunnel face and time. (see also chapter 3)

The pressures used in the analysis are described and elaborated in chapter 3.4.3. As already mentioned, due to the strokes of the pump for conveying the fluids all the way to the tunnel face, fluctuations will occur in the amount of ± 0.1 to 0.2 bar. This has been taken into account in the analysis, running the calculations with different pressure values. The gradient of the pressure with depth was chosen to be 11 kN/m²/m.

Looking at the results of the calculation using the HSS model (Figure 5-9), one can see a range between 2.2 mm and 6.0 mm for a difference in pressures of 40 kN/m² or 0.4 bar. As mentioned before, fluctuations occur for both fluids, the slurry which is supporting the tunnel face and the injected grout. Thus a first 2D approximation using different pressure values can be quite useful to determine whether those values are realistic and is able to cope with the actual data or not.

Hardening-Soil-Small model (HSS):

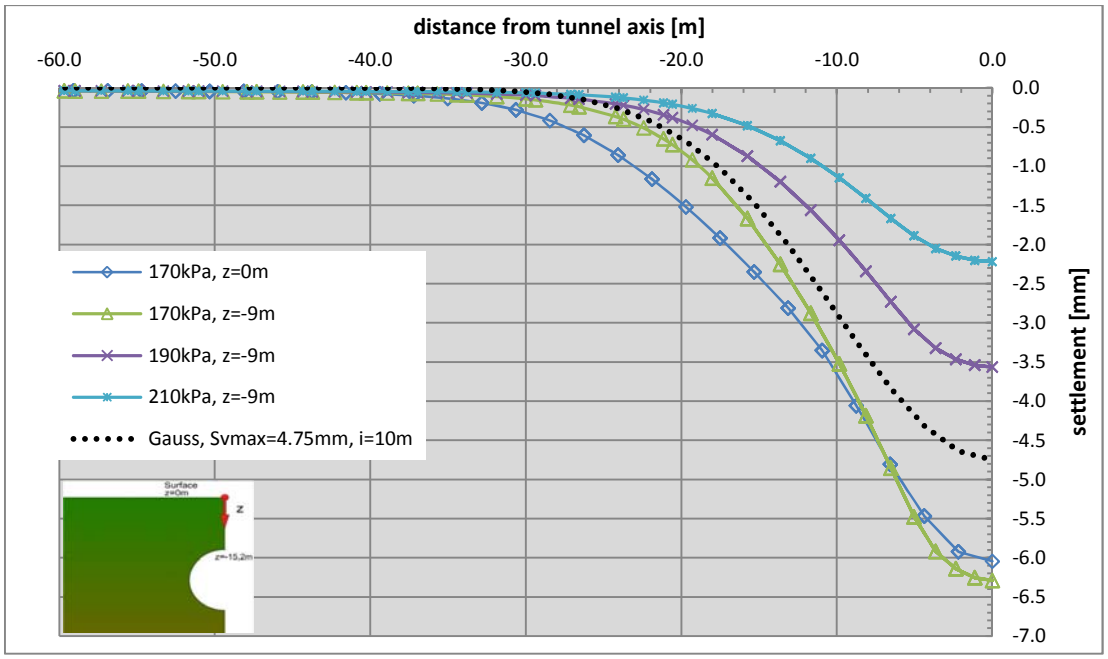

Figure 5-9: 2D HSS model, grout pressure method

Figure 5-9 illustrates that the settlement trough on the surface (z=0m) is less steep than the one in a certain depth and apparently the maximum value does not change very much. This can also be observed for the HS model. Furthermore the dotted black line in the chart shows the measured maximum settlement at cross section I approximated by an empirical approach using 10 m for the point of inflection. The shape of the trough created by the Hardening-Soil-Small model evidently fits well to the one from the empirical approach.

The decisive grout pressure for cross section I is 180 kN/m^2 ± 10 kN/m^2. As shown in figure 5-9, the calculations using those pressures are evidently able to approach the actual measured settlement more accurately than the analysis using a higher pressure. The outcome is, that the evaluated pressures go along with the realities.

HSS model, using "Stress-reduction method":

The stress reduction method was only used for cross section I, to show the difference to the alternative grout pressure method approach. The stress reduction method incorporates the 3rd missing dimension into 2D analysis by reducing the initial geostatic stresses.

Therefore M_{stage} is set as the following value:

M_{Stage} = 1-ß

With ß (beta) simply being the unloading factor for the stress reduction method.

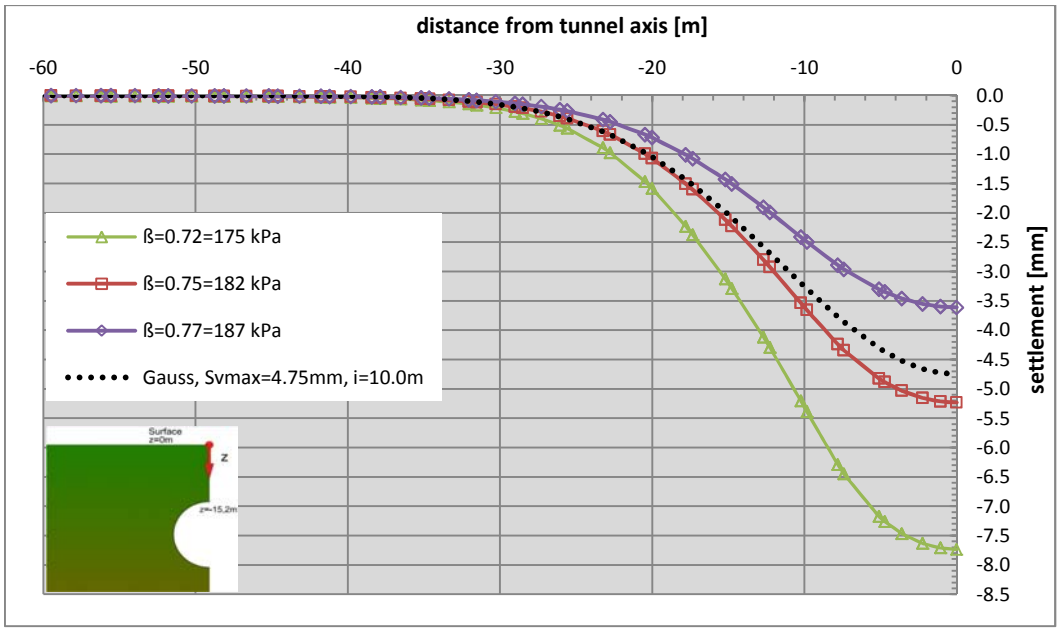

Figure 5-10: 2D HSS model, stress reduction method

The difference in settlements comparing the grout pressure and the stress reduction method is insignificantly small in this case.

Mohr-Coulomb, grout pressure method:

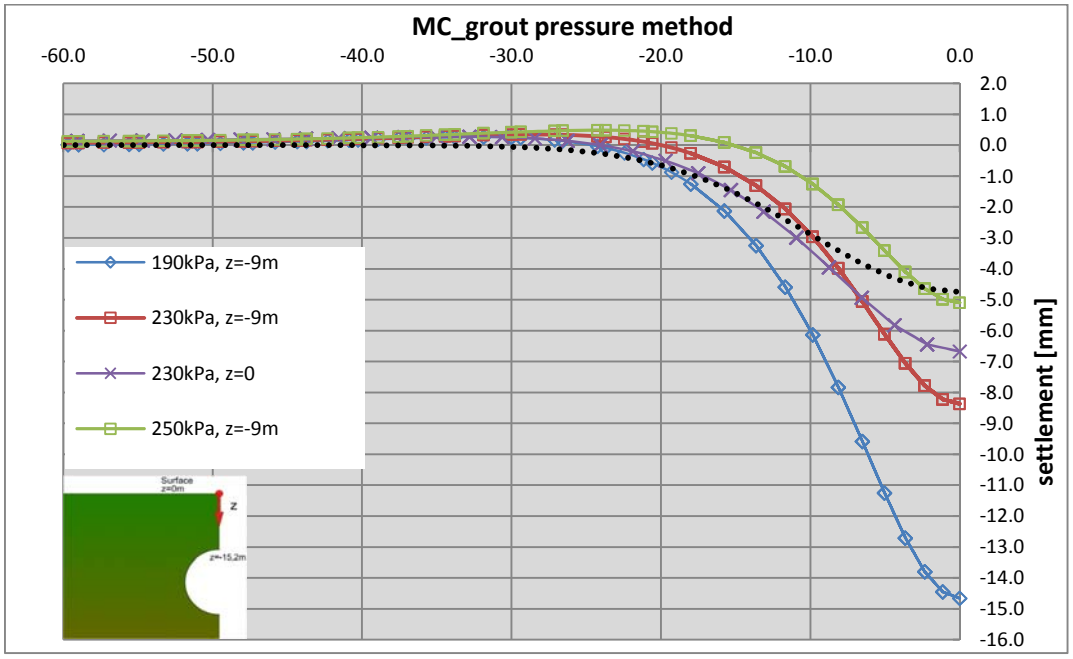

Figure 5-11: 2D MC-model, grout pressure method

Using Mohr-Coulomb as a constitutive model, the settlements for the same pressure are much higher. Compared to the HSS-model, the displacement for 190 kPa of stress boundary is 14.5 mm when using the MC model. This is an increase of more than 400 %.

Comparison HSS/HS/MC-model (grout pressure method):

Figure 5-12 compares the settlements of all three constitutive models in a depth of 9.0 m, using the same pressure condition.

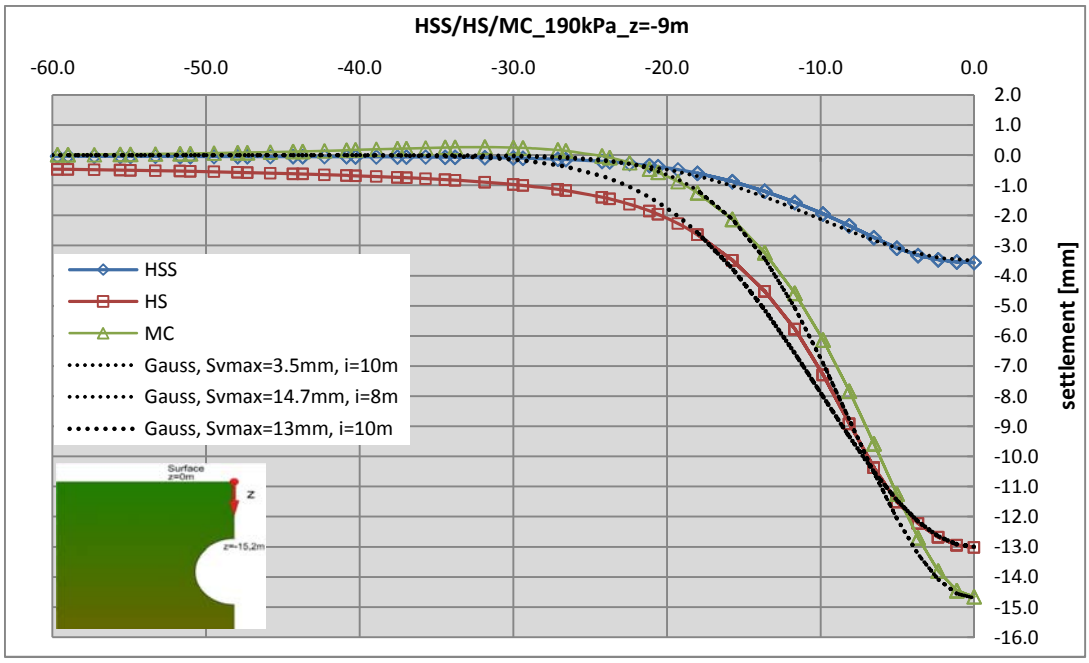

Figure 5-12: 2D comparison of HSS/HS and MC model, Pg=190 kPa

Figure 5-12 contrasts 3 different kinds of constitutive models, the Hardening-Soil, the Hardening-Soil-Small and the Mohr Coulomb model. All 3 calculations were executed with 190 kPa pressure at the crown. Simultaneously three empirical troughs have been plotted using respectively the maximum settlement of the HSS, the HS and the MC model. As one can see in figure 5-12, the shape of the HSS trough is almost identically to the shape of the empirical one. The volume loss, in case of the HSS model, with a maximum settlement of 3.5 mm amounts to 0.13%, whereas for the HS model the volume loss is 0.46% and for the MC model 0.52%

Evidently visible in figure 5-12 is that the small strain stiffness has a large effect on the settlements of a shallow tunnel excavated in soil.

model/pressure	190 kPa		230 kPa	
z=-9	settlement [mm]	Volume-loss [%]	settlement [mm]	Volume-loss [%]
HSS	3.6	0.13	1.5	0.05
HS	13.0	0.46	7.7	0.27
MC	14.7	0.52	8.4	0.30

Table 7: Settlements & volume loss cross section I (z=-9m)

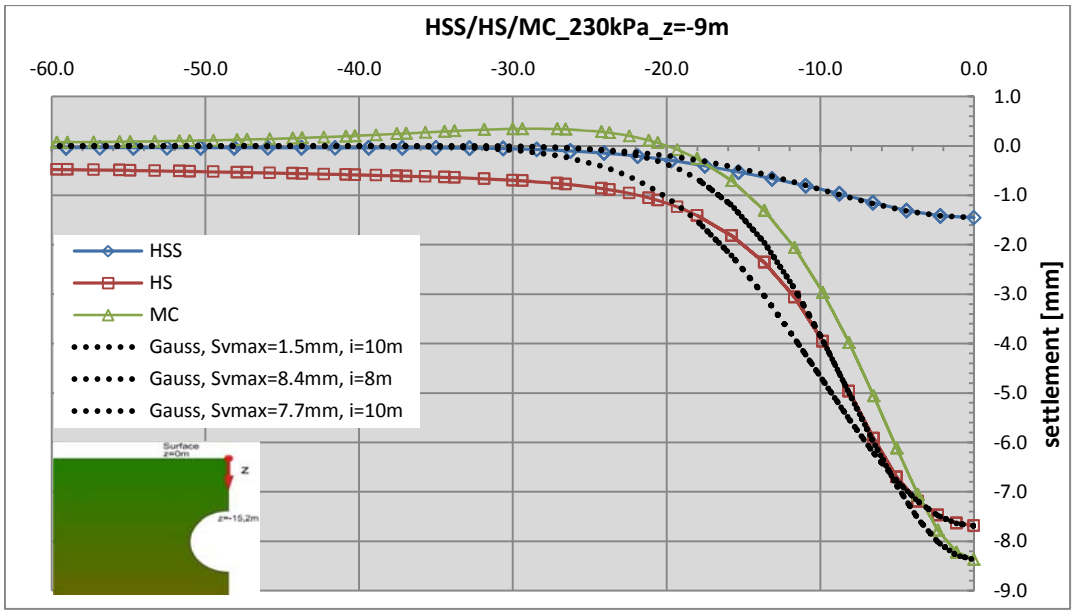

Figure 5-13: 2D comparison of HSS/HS and MC model, Pg=230 kPa

To achieve the same settlement with the HS and MC model a much higher pressure is needed. It is visible that the MC model creates uplift approximately 20 m away from the centreline which is due to the inefficiency of this constitutive model.

Influence of depth using the HS and MC-model:

As one can see in figure 5-14, there is an influence of depth and constitutive model on the settlement trough. On the one hand Mohr-Coulomb predicts less settlement with a steeper curve on the ground surface compared to HS. In 9 m depth on the other hand, the Hardening Soil model results in a lower value. Furthermore the difference of settlements on the surface to the one in 9m depth when using the HS-model, is apparently almost non-existent.

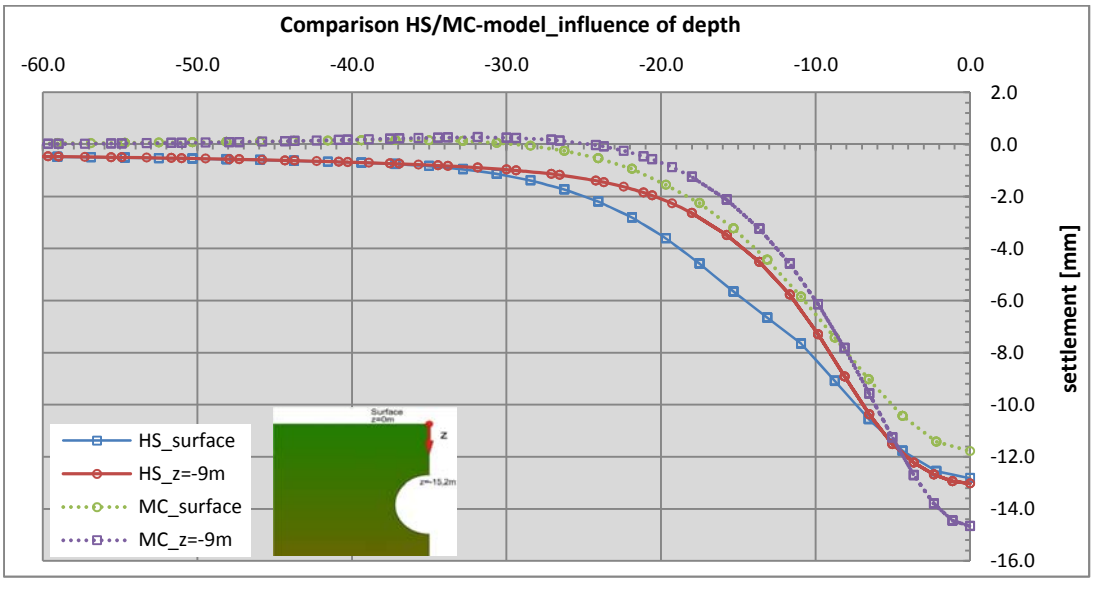

Figure 5-14: Influence of constitutive model and depth on the settlement trough

Plotting the vertical settlements with respect to the depth of the model (Figure 5-15) at the tunnel axis (x=0), it is clearly visible that the increase of settlements from the surface down to the tunnel crown is very low. The HS-model predicts 1.0 mm of settlement increase and the MC-model 3.5 mm.

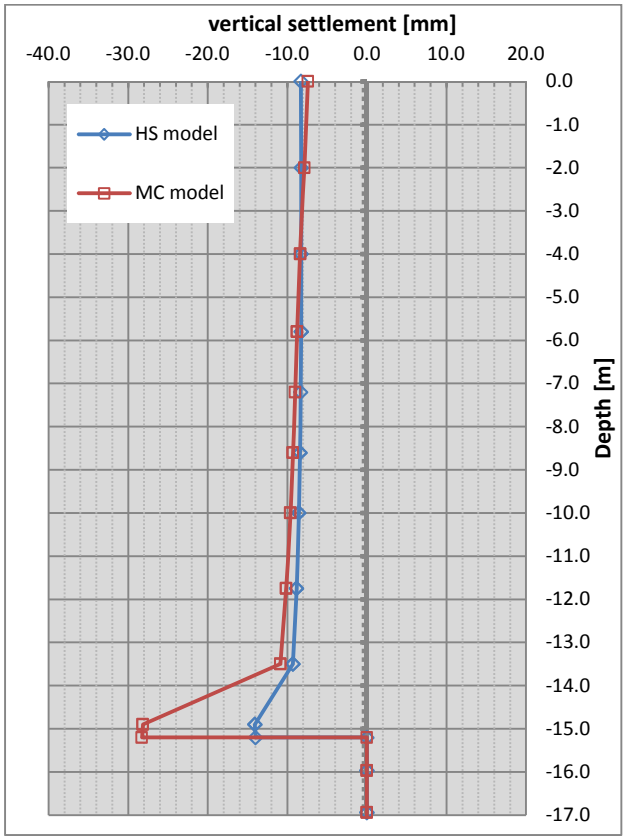

Figure 5-15: Vertical settlements with respect to the depth at the tunnel axis

5.3 Cross Section II

Cross section II is only analysed using 2D numerical methods. This cross section is situated very close to the metro station „Markt“. As one can see in Figure 5-16, there is no influencing structure to the left of the tunnel axis, which means the settlements were only measured using a normal geodetic leveller instead of tube-levellers fixed on the building. Thus giving less accurate results which was already mentioned in 3.4.3.2.

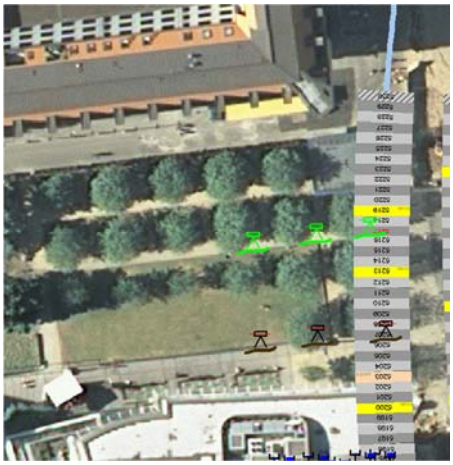

Figure 5-16: Location cross section II

5.3.1 Parameters

Mohr-Coulomb parameters:

MC Parameter	γ	φ	c	E_{oed}	ν	K_0	E_{ur}^{ref}*
	[kN/m³]	[°]	[kPa]	[MPa]	[-]	[-]	[MPa]
Fill	18	30	0	8	0,3	0,500	24
Marl	21	30	16	40	0,3	0,500	234
Fluvial Sand	19	36	0	88	0,3	0,412	218
Bitterfeld Sand	19	34	0	133	0,3	0,441	240
Greenish Silt	20	26	15	40	0,3	0,562	120
Clam Silt	20	24	22	42	0,3	0,593	156
*Eur only for Layers beneath Tunnel							

Figure 5-17: MC-parameters cross section II

The parameter for the HS and HSS model remain the same as in cross section I. (see chapter 5.2.2)

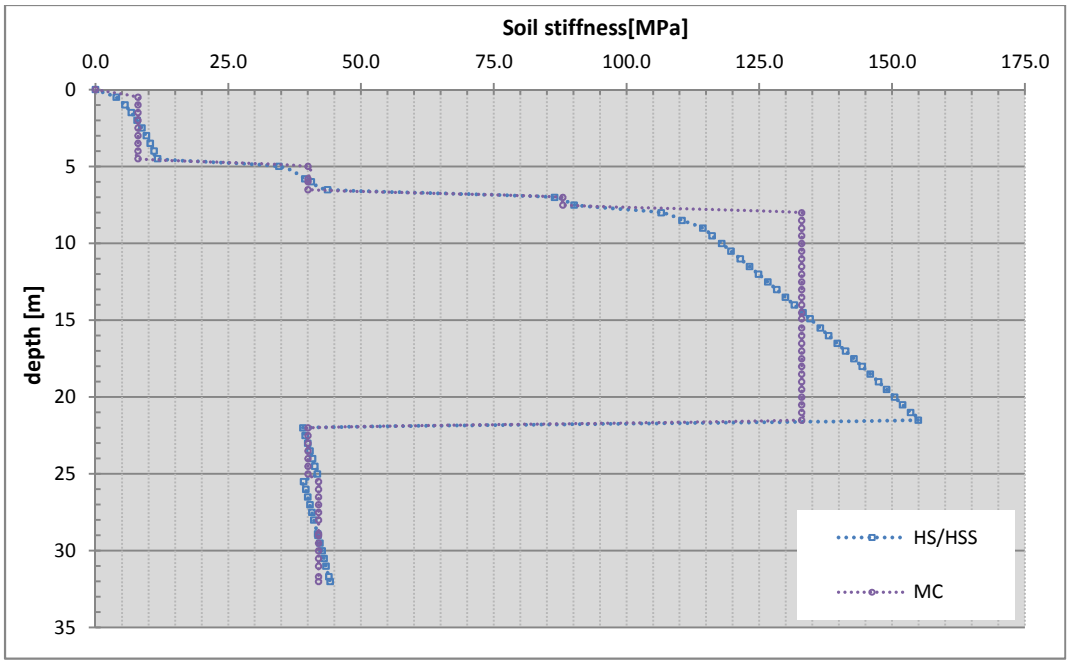

Figure 5-18: Soil stiffness with respect to depth, cross section II

In figure 5-18 again the oedometric stiffness has been opposed for the MC, the HS and the HSS model. Using the evaluated oedometric stiffness for the Mohr-Coulomb model (figure 5-17) and the calculated oedometric stiffness for the HS and HSS model, which is based on E_{oed}^{ref} and σ_1' (see also 4.3.2.1)

5.3.2 Soil profile

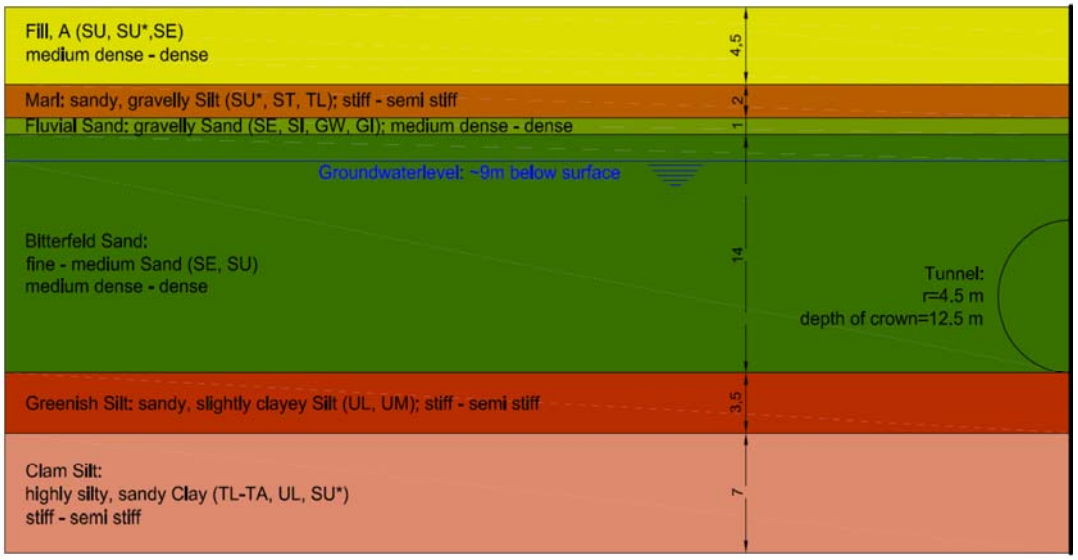

Figure 5-19: Soil profile cross section II

The layer distribution does not differ very much to cross section I, only the „Marl“ and „Fluvial Sand“ layers are less thick, but the tunnel itself remains again just in the layer of „Bitterfeld Sands“. Depth of the tunnel crown is 12.5 m.

5.3.3 Results

Hardening-Soil-Small model:

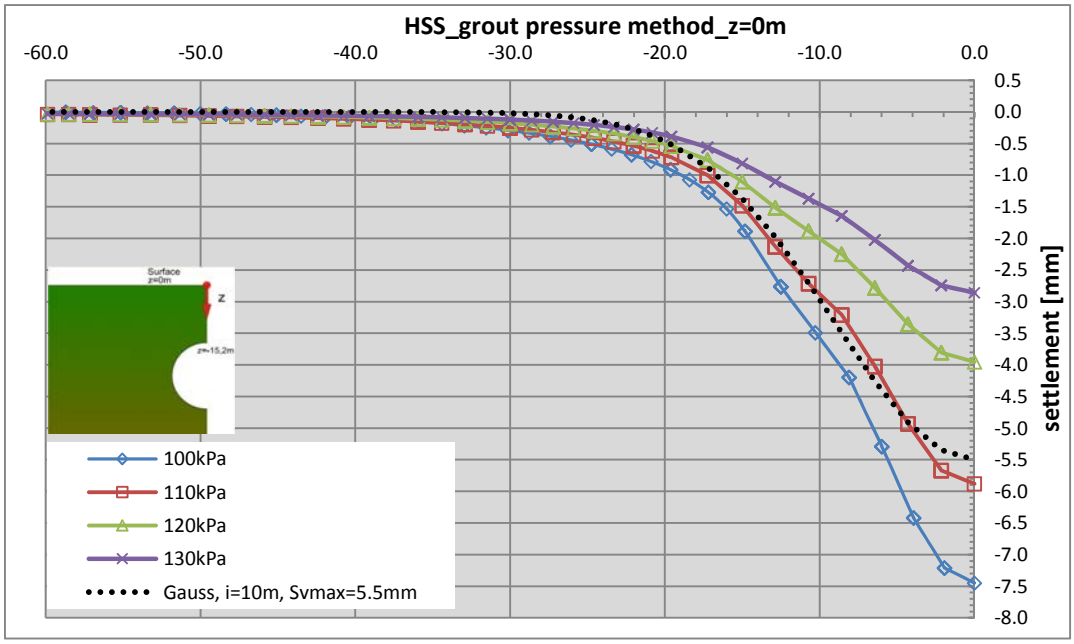

Figure 5-20: 2D HSS, grout pressure method, cross section II

The settlement trough using 110 kN/m² of pressure fits best to the measured settlement value of approximately 5.5 mm. Comparing with the actual grout pressures monitored at cross section I, which are in a range of 110 kN/m² to 130 kN/m², the 2D approach is close to the actual conditions. On the other hand the Mohr-Coulomb model predicts 3 times as much settlement using the same pressure. Furthermore, using a higher pressure for the MC-model, again a small heave appears to be present in 20 to 30m distance from the tunnel face.

Mohr Coulomb-model:

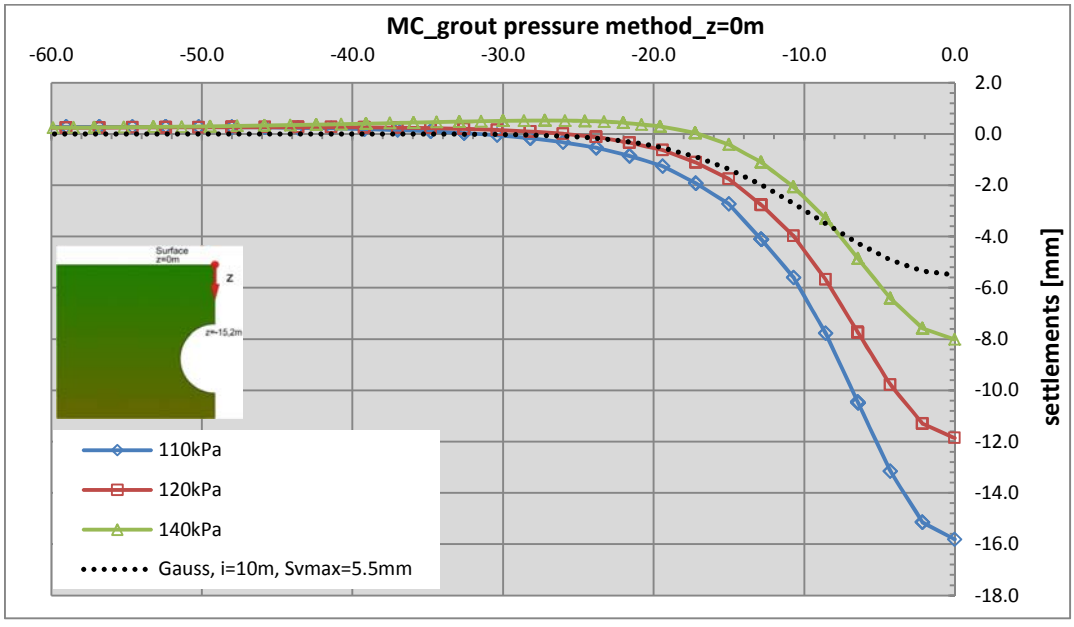

Figure 5-21: 2D MC model, grout pressure method, cross section II

Comparison HSS/HS & MC model:

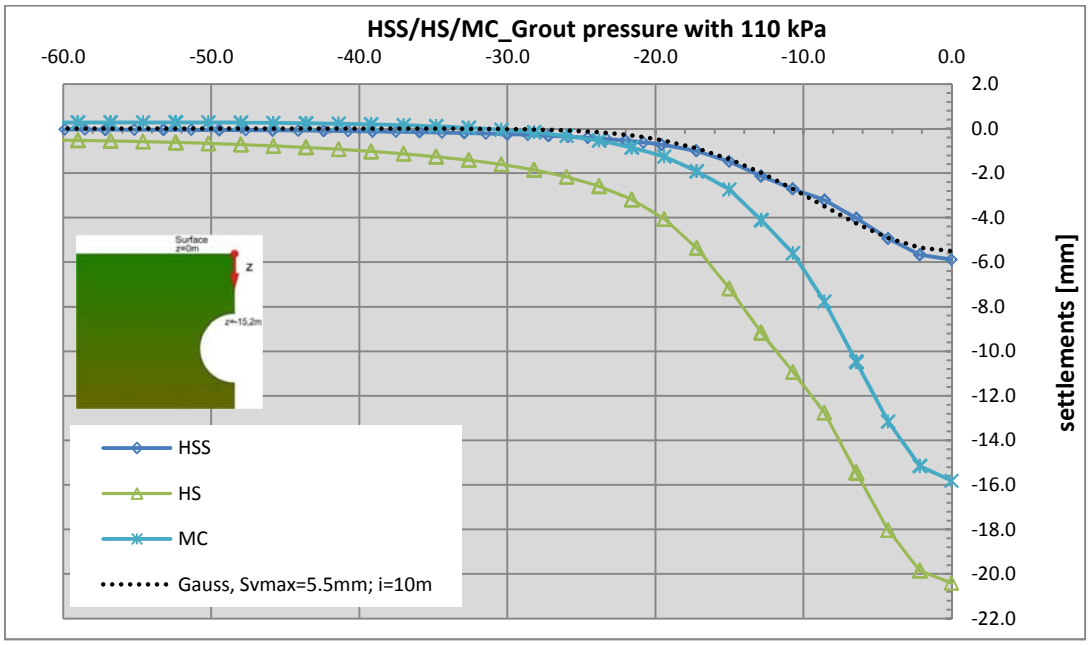

Figure 5-22: 2D comparison HSS/HS and MC model, Pg=110 kPa

Contrasting all 3 constitutive models, the figure above illustrates that only the Hardening-Soil-Small model is able to approach the empirical settlement trough and thus the monitored maximum settlement at cross section II.

Furthermore Figure 5-22 5-22 shows that the Hardening-Soil model predicts more settlement than the Mohr-Coulomb model, which is different compared to cross section I. This is due to the fact that the increment of settlements with depth is larger at the MC model than at the HS model (Figure 5-15). Looking at cross section I, the difference in settlements at the surface to settlements in 9 m depth is about 2.0 mm or 25% for the Mohr-Coulomb model and only 0.2 mm or 2% for the HS model.

The previous charts and figure 5-23 implies that only the Hardening-Soil model with small strain stiffness appears to be applicable for this kind of situation and for simulating the influence of a pressure imposed boundary condition due to a fluid supported tunnelling machine.

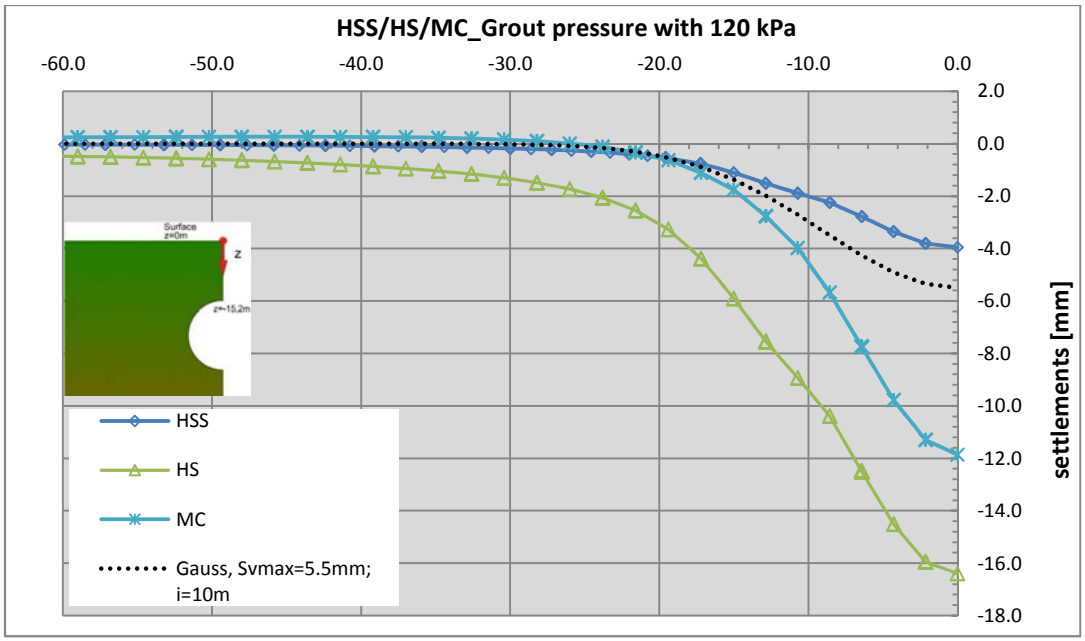

Figure 5-23: 2D comparison HSS/HS and MC model, Pg=120 kPa

Volume loss values for cross section II:

model/pressure	110 kPa		120 kPa	
z=-9	settlement [mm]	Volume-loss [%]	settlement [mm]	Volume-loss [%]
HSS	5.8	0.15	3.9	0.10
HS	20.4	0.51	16.4	0.41
MC	15.8	0.40	11.9	0.30
Gauss	5.5	0.22	5.5	0.22

Table 8: Volume loss cross section II

Conclusions for 2D approach:

The 2D approach is a good tool for a preliminary prediction of settlements. Using the “grout pressure method” it is possible to simulate fluid supported tunnelling machines and the imposed pressure from grout and slurry onto the soil, thus resulting in certainly realistic settlement values. The choice of the constitutive model has a large impact on the results. Whereas the Hardening Soil Small model results in feasible settlements when using realistic pressures, the Mohr-Coulomb and the Hardening Soil model give much higher settlements using the same pressure.

6 3D-Analysis

The constitutive models used for 3D calculations are the same as for the 2D analysis. Thus the parameters and soil properties remain the same.

For the 3D analysis the model had to be simplified in order to keep the computational effort within acceptable limits for this thesis. The priority in the thesis was, to investigate the influence of the tunnel boring machine and corresponding pressures on surface, sub-surface settlements and lining forces, as well as the effect of constitutive models and construction staging on the results.

6.1 Model Geometry

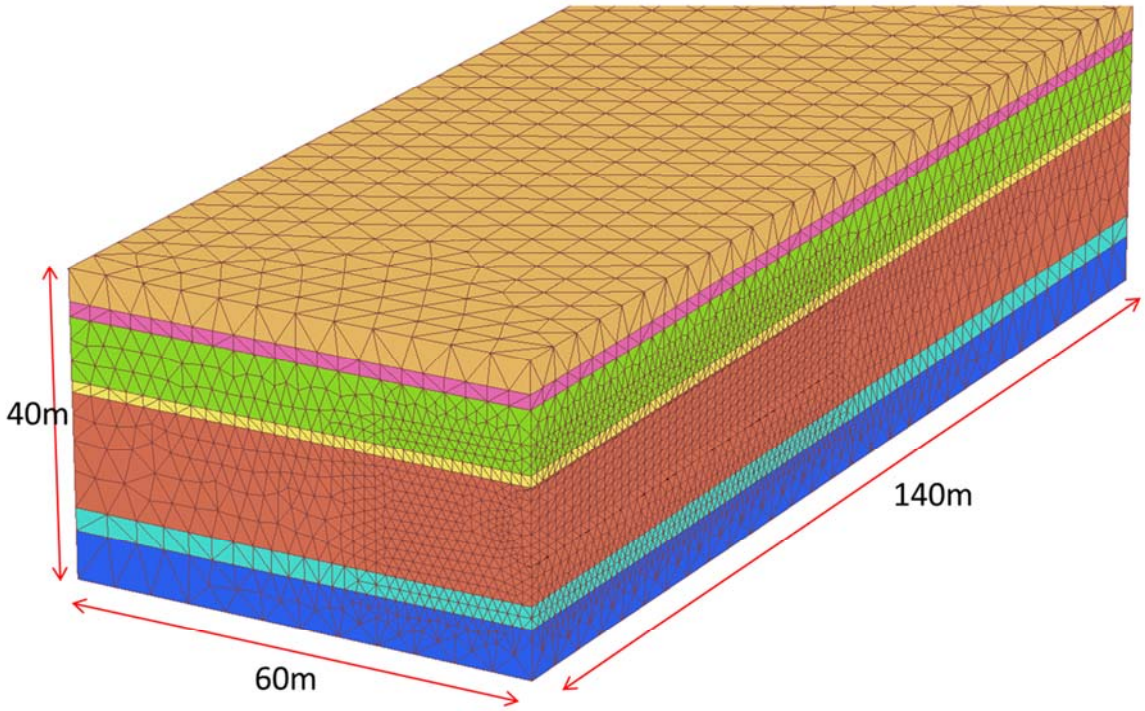

Figure 6-1: Model geometry in 3D

The model geometry is based on the soil distribution and on the influence of the boundary conditions. To omit the boundary influence the model width should be about 8*D (D=Diameter of the tunnel) and the depth below the tunnel invert about 1.5*D. The length depends on the construction stages as well as the length of slices for 1 excavation step. For this case, 140 m were chosen for the length of the model. (see also Möller, 2006)

Since the chosen cross section is located at the Petersstraße in Leipzig, which is a very congested street with one building adjacent to another, there would be a surcharge acting on the ground changing the initial conditions. To avoid modelling the structural parts, it is possible to assume that the soil weight is approximately the same as the load of the buildings which are about 7-8 storeys high.

A load of 20 kN/m² per storey leads to a total amount of approximately 160 kN/m², compared to the soil weight which is about 19 kN/m³ x 9 m, which results in a total of 170 kN/m². Consequent-

ly, the assumption that the soil weight will simulate the adjacent buildings is valid and thus simplify the model .

6.2 Modelling sequence

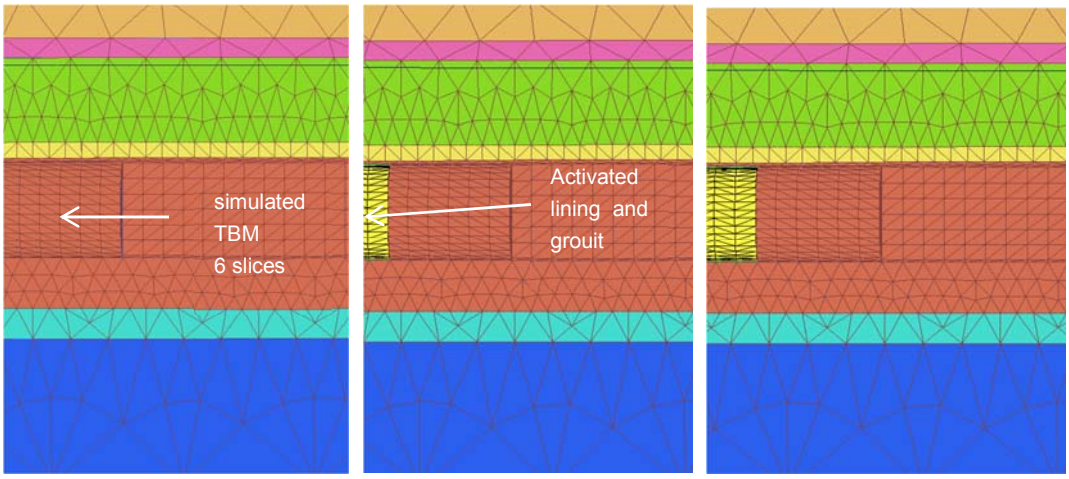

Figure 6-2: Step-by-step modelling procedure

As indicated in figure 6-2 a step-by-step approach is used, deactivating 1 slice with a length of 1.8m (length of the lining) at the face and simultaneously activating lining and the surrounding grout in the rear. The slurry at the face is simulated with an axial pressure increasing with depth. The same applies for the shield and the annular gap at the lining, which is simulated with a corresponding pressure.

Hence a pressure-controlled boundary applies for the TBM and the gap in the back, which is most certainly realistic for modern Hydro- or Slurry-shields. (see also Möller, 2006)

Step-by-step approach using FEM:

For implementing the step-by-step approach into FEM geometry based boundary conditions needed to be established. The length of each step is supposed to equal the length of 1 lining ring and thus the length of 1 TBM-advance (l=1.8 m). To imply the TBM, a total amount of 6 slices are deactivated and a user defined pore pressure, assuming a pressure-controlled boundary is switched on.

At each excavation step the lining and the surrounding grout are switched on in the back of the TBM. Furthermore, a user defined pore pressure is activated simulating the pressure occurring within the soil-lining gap, which should induce realistic lining forces.

The weight of the back-up equipment and the TBM have been neglected.

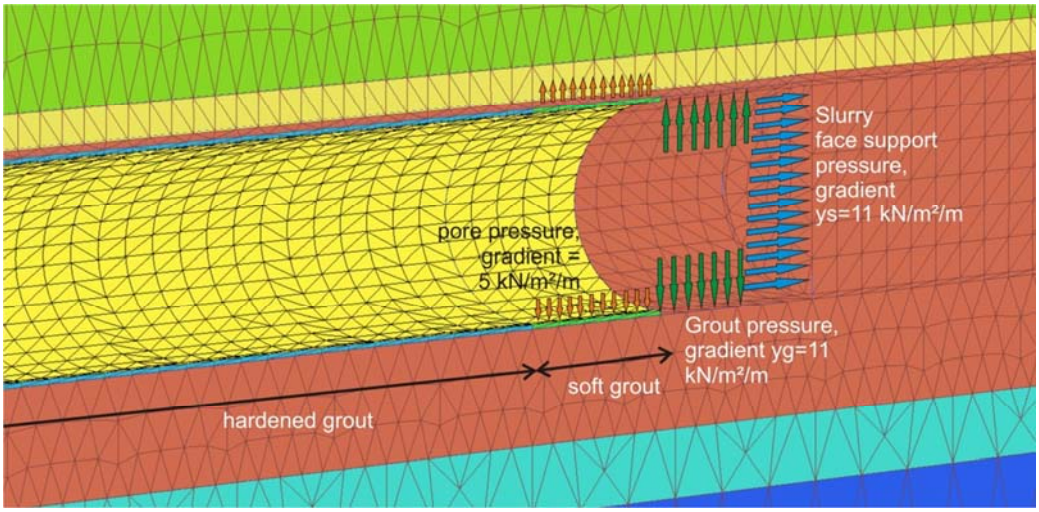

Figure 6-3: Pressure controlled boundary conditions for the FEM implementation

Figure 6-3 shows the user-defined pressures activated at the numerical analysis and the number of slices simulating the TBM and the fresh injected grout in the back.

6.3 Parameters

The soil parameters are the same as in the 2D analysis. The analysis itself has been performed assuming drained conditions only.

6.3.1 Lining parameters

The tunnel lining for machine driven tunnels is usually constructed with pre-fabricated concrete segments. Those segments will be connected and form 1 lining ring. The segmental rings are then connected with each other through bolts and thus form the final tunnel lining. There are different kinds of segmental geometries and connection bolts which all have advantages and disadvantages, but those are not further discussed in this thesis.

Number of segments used for 1 ring:

The number of segments for 1 ring is depending on the diameter of the tunnel.

2 – 5m: 4 to 5 segments + 1 key segment

5 – 8m: 5 to 6 segments + 1 key

More than 8 m: 6 to 8 segments + 1 key

(Gruebl, 2009)

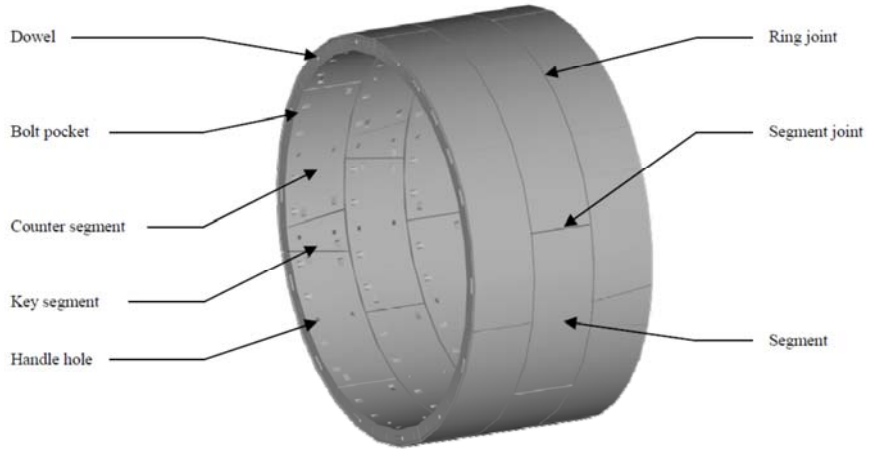

Figure 6-4: Segmental lining definitions, (Luttikholt, 2007)

Since the assembled lining does not show isotropic behaviour, it is necessary to consider anisotropy. This will be accounted through reduction factors for the final lining stiffness. The lining segments are connected in radial and the coupled rings in axial-direction, consequently a reduction for both directions needs to be applied.

Reduction in radial direction:

Muir Wood (1975) suggested the following equation for reducing the moment of inertia of the overall lining due to the jointed segments:

$$I_{red} = Ij + I * \left(\frac{4}{N}\right)^2$$

I_{red} reduced moment of inertia of the overall lining (in radial direction)

I_j second moment of inertia of the joint (negligible)

I second moment of inertia of the segment

N number of joints, (>4)

If the ring consists of less than 4 segments, Wood proposed that the lining stiffness is not being influenced and thus not being further reduced. This might not be fully valid but the reduction using less than 4 segments would be insignificantly small.

This equation is only valid for the reduction in radial direction, in axial direction the length of the tunnel and thus the number of joints would be too high, thus the factor $(4/N)^2$ would almost converge to zero.

Reduction in axial direction:

When constructing a long tunnel in soft soil, the lining-tube of the tunnel behaves similar to a cantilever beam additionally supported through a subgrade reaction simulated with springs (Figure 6-5).If the lining would be a homogeneous material without joints, the young´s modulus in axial direction would be identical to the one in radial direction. Yet for tunnelling in soft soil segmental prefabricated linings are used, which are connected through bolted joints and thus not show isotropic material behaviour. As already mentioned, the number of joints in radial direction depends on the radius. For the tunnel in Leipzig 7 segments plus 1 key segment were used. Whereas the number of joints in axial direction depends on the length of the tunnel and width of the segments, but it will evidently be much higher than in radial direction. Consequently a reduction factor needs to be introduced differently than the one mentioned by Wood, 1975.

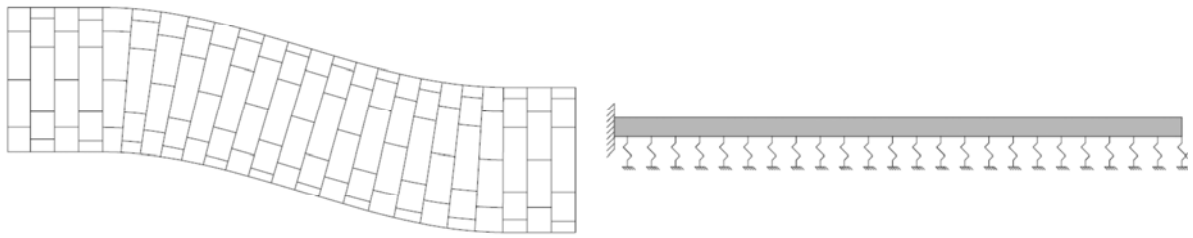

Figure 6-5: Beam behaviour tunnel lining, (Luttikholt, 2007)

Empel et al. (2000) suggested that the stiffness in axial direction depends on the material being used for the flexible plates which are supposed to transfer the thrust-jacking forces due to the TBM advance into the concrete lining. Those plates are either made out of plywood of hard rubber (Kaubit). (Figure 6-6)

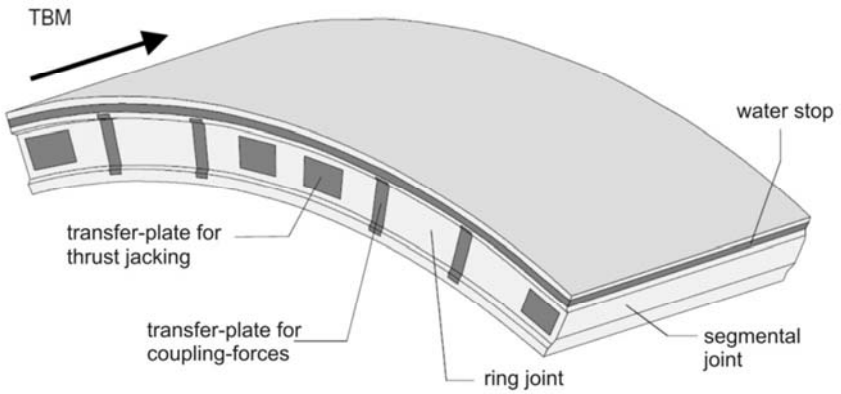

Figure 6-6: Prefabricated concrete segment with transfer plates (Winselmann, et al., 2000)

Empel et al. (2000) suggested following stiffness reduction for the young's modulus in axial direction:

- When using Kaubit: $E_{axi} = 0.9*E_c$
- When using Plywood: $E_{axi} = 0.3*E_c$

With:

E_c…..Young´s modulus of concrete

E_{axi}…Young´s modulus in axial direction of the jointed tunnel lining

Implementation into PLAXIS:

PLAXIS is using linear plate elements which are flexural rigid connected with each other. PLAXIS is furthermore using a local coordinate system for those elements defined by axes in the directions 1,2 and 3 (Figure 6-7).

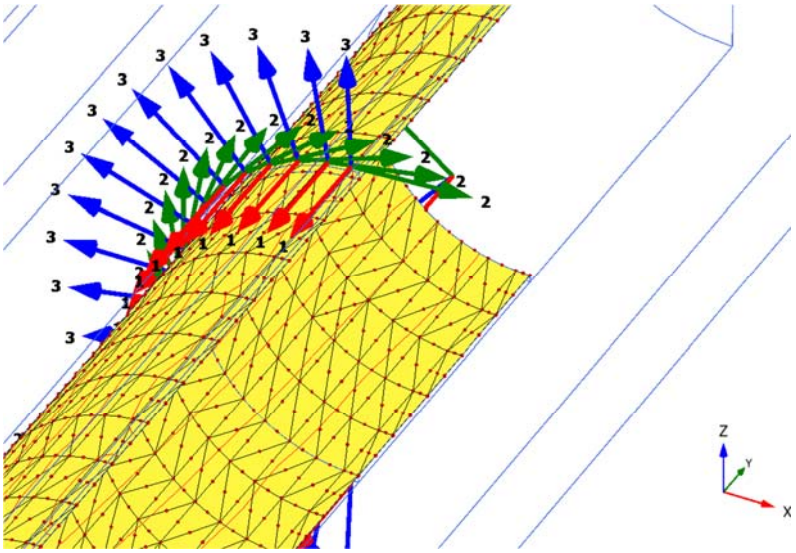

Figure 6-7: Local axis for plate elements

Input parameters in PLAXIS:

E_1	Young´s modulus in direction 1 (axial direction) [kN/m²]
E_2	Young´s modulus in direction 2 (radial direction) [kN/m²]
d	Thickness of the plate [m]
v	Poisson´s ratio [-]
y	Unit weight of plate [kN/m³]

With:

$$E_1 = \frac{12 * E * I_1}{d^3} \qquad E_2 = \frac{12 * E * I_2}{d^3}$$

According to the Plaxis material model manual, 2012.

Before calculating E_1 and E_2 for the FEM analysis it is necessary to look up the actual lining and concrete properties of the segments being used.

Concrete-properties for the lining at the city tunnel Leipzig:

Concrete grade C50/60

$f_{ck,cyl}$ = 50 N/mm²…….cylinder compression strength

$f_{cm} = f_{ck,cyl} + 8$ =58 N/mm²…….design value of compression strength

E_{c0m} = 9500*($f_{ck,cyl}$+8)^1/3… …mean tangent modulus of concrete

$E_{cm} = E_{c0m}$ * (0,8+0,2*f_{cm}/88). ..mean secant modulus of concrete

E_{cm} = 9500*(58)^1/3 * (0.8+0.2*58/88) = 34 273 N/mm²

d = 0.40 m

v = 0.15 (Poisson´s ratio)

With the secant young´s modulus of concrete, the equation for E_2 and the reduction factor for the second moment of inertia, it is possible to derive a reduced thickness (d) for the lining:

$$I_2 = I * \left(\frac{4}{N}\right)^2$$

$$\frac{d^3{}_{new} * b}{12} = \frac{b * d^3}{12} * \left(\frac{4}{N}\right)^2$$

$$d^3{}_{new} = d^3 * \left(\frac{4}{N}\right)^2 = 0.4^3 * \left(\frac{4}{8}\right)^2$$

$$d_{new} = 0.275m$$

$$E_2 = E_{cm}$$
$$E_1 = 0.8 * E_{cm}$$

Empel et al., 2000, suggested a 10% reduction of the Young´s modulus when using Kaubit as a joint material, in this thesis a 20% reduction was used assuming a more conservative approach.

Anisotropic lining parameters:

Lining parameters		
unit weight	25	kN/m³
E1	27 440	N/mm²
E2	34 300	N/mm²
d	0.275	m
v	0.15	-

Table 9: Lining parameters

6.3.2 Grout parameters

The grout parameters had to be separated into properties for the fresh injected grout and the "old" hardened grout far after the TBM has passed.

Imposing a certain user-defined pore pressure on the fresh grout, the oedometric stiffness should not be too low as there will be heave in the invert of the tunnel, which is caused by the high pressures of the injected material.

Thienert (2010) suggested the fresh consolidated grout to behave similar as the surrounding soil.

Properties of fresh consolidated grout (Thienert, 2010):

E_{oed} =~ 10 000 to 20 000 kN/m²

E_{ur}^{ref} =~ 30 000 to 75 000 kN/m²

(Those values were deducted from a standard triaxial test, by Thienert)

For the analysis a grout stiffness of 1000 kN/m² has been chosen to simulate not only the consolidated grout but also the fresh injected material.

The above-mentioned heave of the invert of the tunnel lining is due to high pressures of the injected grout at the openings on the bottom of the TBM. Since the input in the analysis relies on a reference point, a pressure gradient will be chosen to determine the increase of pressure with depth and thus the uplift force acting on the lining. If the gradient is chosen too high, the lining will experience uplift, which causes excessive bending of the tunnel in longitudinal direction.

6.3.2.1 Uplift, grout pressure gradient

Assuming that the lining ring is fully surrounded with grout, there has to be an equilibrium state between the vertical downward and the uplift forces. Figure 6-8 shows the forces acting on the system of a bedded lining ring.

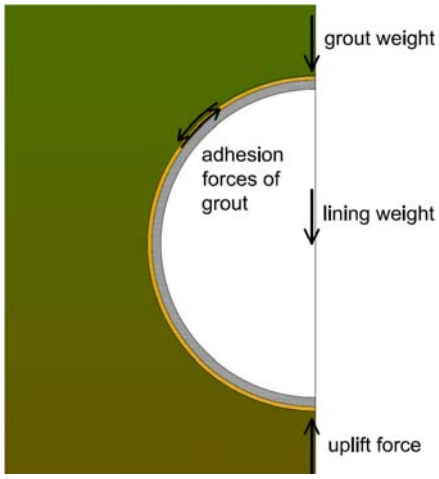

Figure 6-8: Uplift force

$\Sigma F_v = F_g + F_l + F_a$

F_g…..self-load of grout for 1m length (γ=21 kN/m³)

F_l……self-load of the lining for 1m length (γ=25 kN/m³)

F_a…..adhesion forces of grout acting on the lining (T_y=~1.0 kN/m²)

F_l = ~ 260 kN

F_g = ~ 60 kN

Tangential adhesion forces:

T_y….yield strength of grout (assuming T_y=1.0 kN/m²)

r = 4.5 m

b = 1.0 m

F_a = 2*r*π*b*2*Ty = 2*4.5*π*1.0*2*1.0 = 56.5 kN

Total vertical downward force:

F_v = 260 + 60 + 57 = 377 kN

Uplift force, Fu:

$$F_u = r^2 * \pi * b * \gamma g$$

With γ_g being the pressure gradient.

Equilibrium:

$$F_u = F_v$$
$$377 = r^2 * \pi * b * \gamma_g$$
$$\gamma_g = \frac{377}{4.5^2 * \pi * 1{,}0}$$
$$\gamma_g = 5.9\, kN / m^2 / m$$

The calculation above shows that the gradient for the grout pressure is supposed to be lower than the gradient used for the face support pressure.

A higher gradient would cause uplift and heave of the lining invert, which not only exerts difficulties in FEM analysis but especially during construction and ring erection. Consequently the pressure gradient for grout needs to be thoroughly controlled on site.

6.3.2.2 Case-study grout pressure gradient

As mentioned before, the pressure gradient could cause certain uplift if chosen too high. A small case-study has been conducted on the impact of the gradient and thus on the displacement of the lining. Further the influence of the grout stiffness on lining deformations was investigated likewise.

For the case-study higher mesh coarseness was chosen and only 1 soil layer was assigned using HSS as a constitutive model.

Soil properties used for the case - study:

E_{oed}^{ref} = 80 000 kN/m²

E_{ur}^{ref} = 240 000 kN/m²

φ = 34°

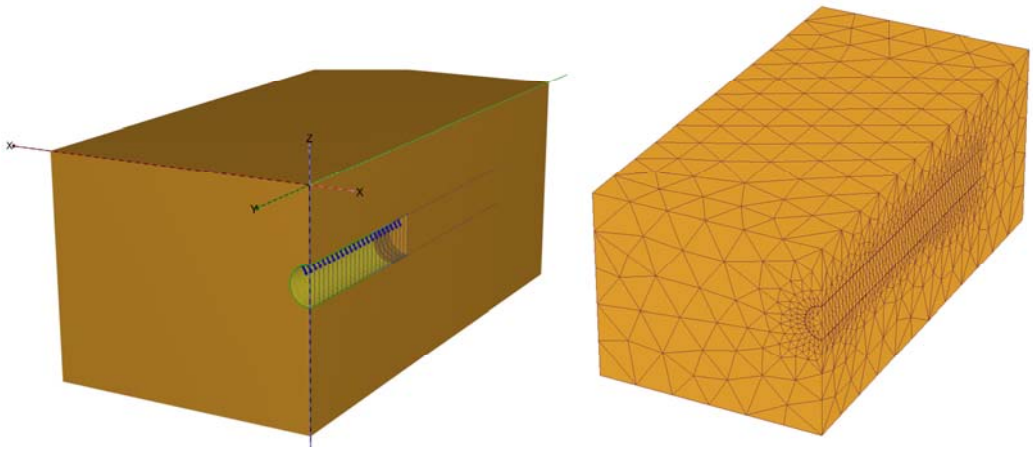

Figure 6-9: 3D model case study grout pressure gradient

Variation in grout stiffness:

E_g=50 kN/m², γ_g =11 kN/m³/m

E_g= 1000 kN/m²; γ_g =11 kN/m³/m

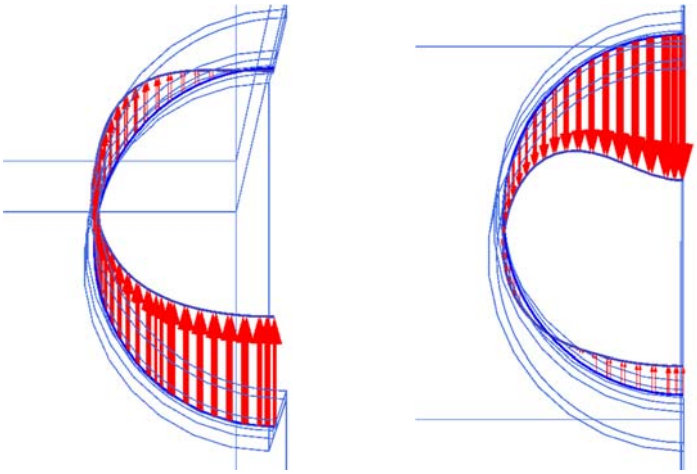

Figure 6-10: Displacement lining, variation of grout stiffness (scaled up 500 times)

E_g…..young´s modulus of grout

Figure 6-10 shows that the deformation of the lining, when using a high gradient, is highly dependent on the grout stiffness. The analysis using 50 kN/m² grout stiffness shows significant uplift of the lining invert, whereas when using a 20 times stiffer grout material the crown experiences the most crucial displacement.

Variation in the pressure gradient:

E_g=50 kN/m²; γ_g =11 kN/m³/m E_g=50 kN/m²; γ_g =5 kN/m³/m

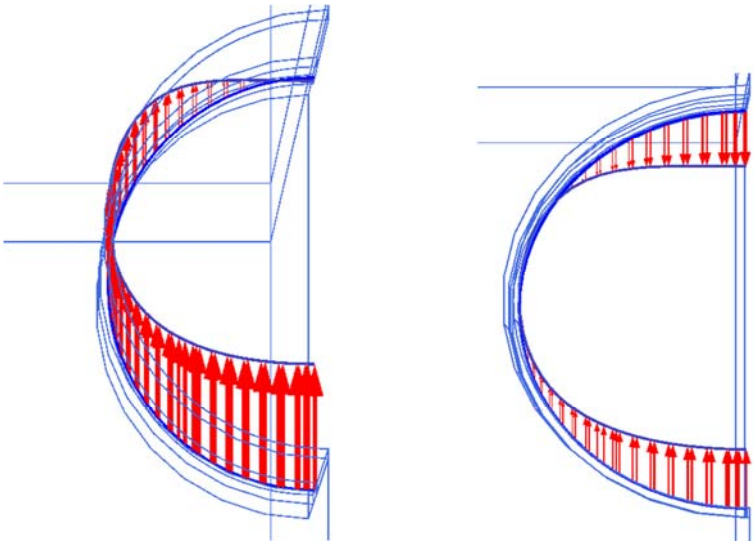

Figure 6-11: Displacement lining, variation of grout pressure gradient (scaled up 500 times)

The change from 5 to 11 kN/m³/m in the grout pressure gradient shows the significant influence of the uplift force acting on the lining. (Figure 6-11)

Longitudinal effect:

The longitudinal bending of the lining also shows clearly the difference when using different values for the grout stiffness.

E_g=50 kN/m²

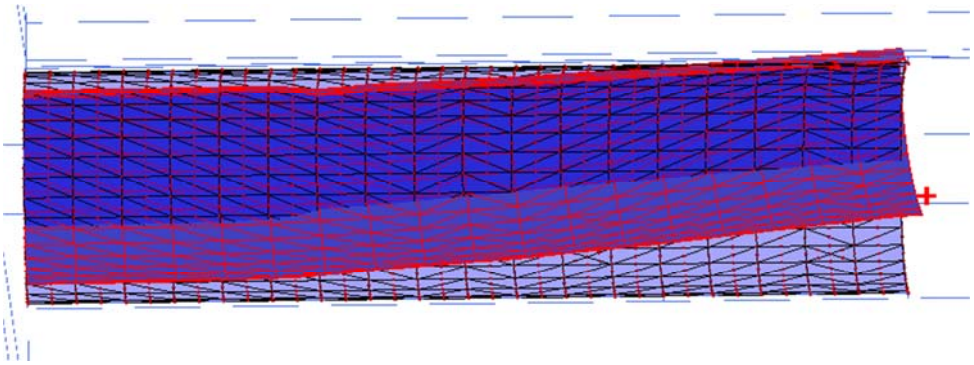

Figure 6-12: Longitudinal displacement lining, E_g=50 kN/m² (scaled up 500 times)

E_g=1000 kN/m²

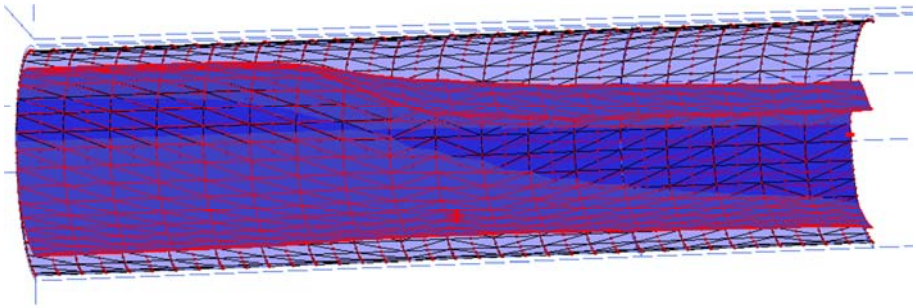

Figure 6-13: Longitudinal displacement lining, E_g=1000 kN/m² (scaled up 500 times)

Grout parameters:

The Grout was assumed to behave linear-elastic:

Parameter grout	Grout young (undrainded)	Grout old (drained)	
Density, y	21	21	kN/m³
Youngs modulus, E	1000	500 000	kN/m²
Poisson ratio, u	0.495	0.15	-
gradient, yg	5	-	kN/m³/m

Table 10: Parameters grout young/old

The gradient was chosen to be somewhat lower than the calculated one, to make sure there is no excessive uplift of the lining in axial direction. Thus a value of 5 kN/m²/m was chosen for the gradient. Furthermore the undrained grout was assumed to surround the lining at 5 slices after the simulated TBM. Subsequently the grout was expected to behave hardened and drained (Figure 6-15).

6.4 Results

The derivation of the pressure distribution (Figure 6-14) for the numerical analysis is presented in chapter 3.4.3.2.3.

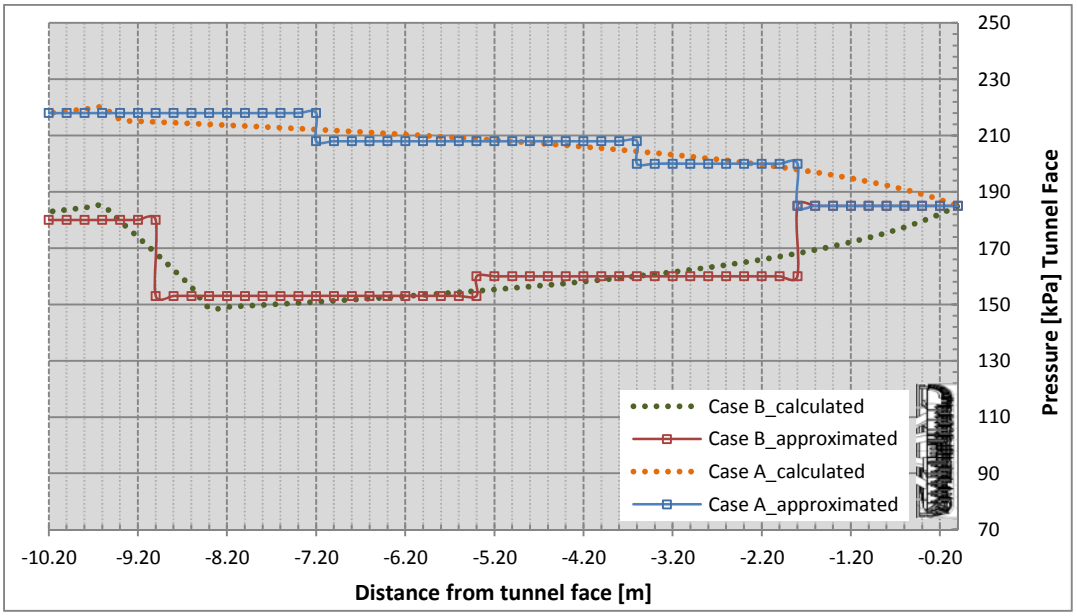

Figure 6-14: Pressure distribution along TBM shield, Case A & B (see also chapter 2)

The figure above illustrates both pressure cases which are thoroughly described and evaluated in chapter 3.4.3.1 and which are also shown in figure 3-32 and 3-33. The dotted lines show the calculated pressure distribution for each case and the red and blue marked ones the approximation for the FEM analysis.

The overall mean grout pressure for Case A amounts to ~210 kN/m² and 165 kN/m² for Case B. Figure 6-15 indicates the implemented pressure cases in the FEM analysis. All calculations were performed in drained conditions.

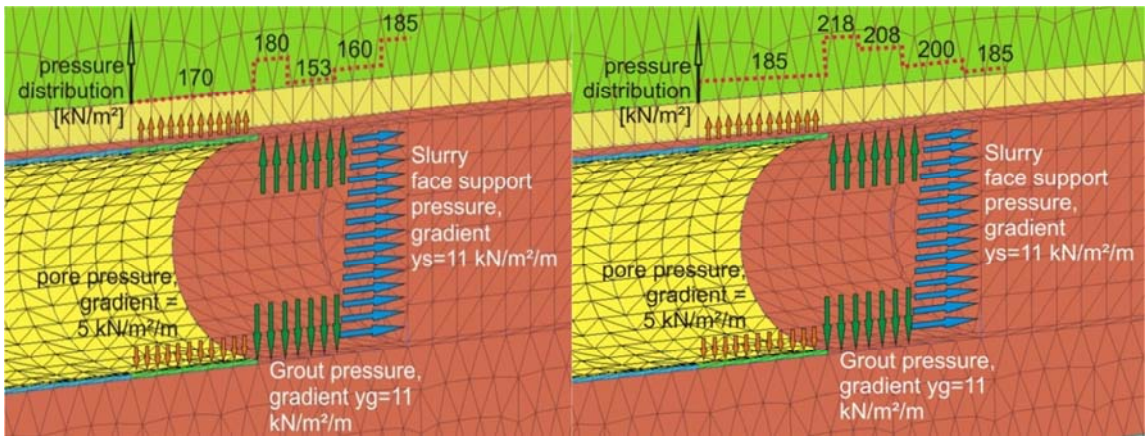

Figure 6-15: Pressure distribution Case A&B implemented in FEM

Figure 6-16 shows the notation for settlement troughs.

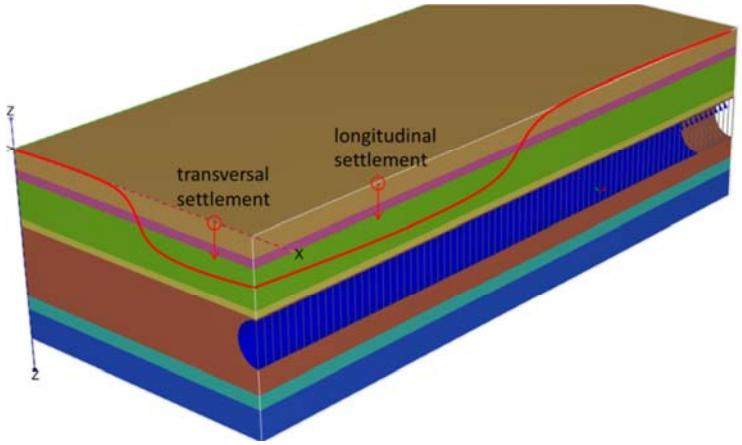

Figure 6-16: Notation for settlement troughs

6.4.1 Vertical settlements

Longitudinal settlements, HSS model:

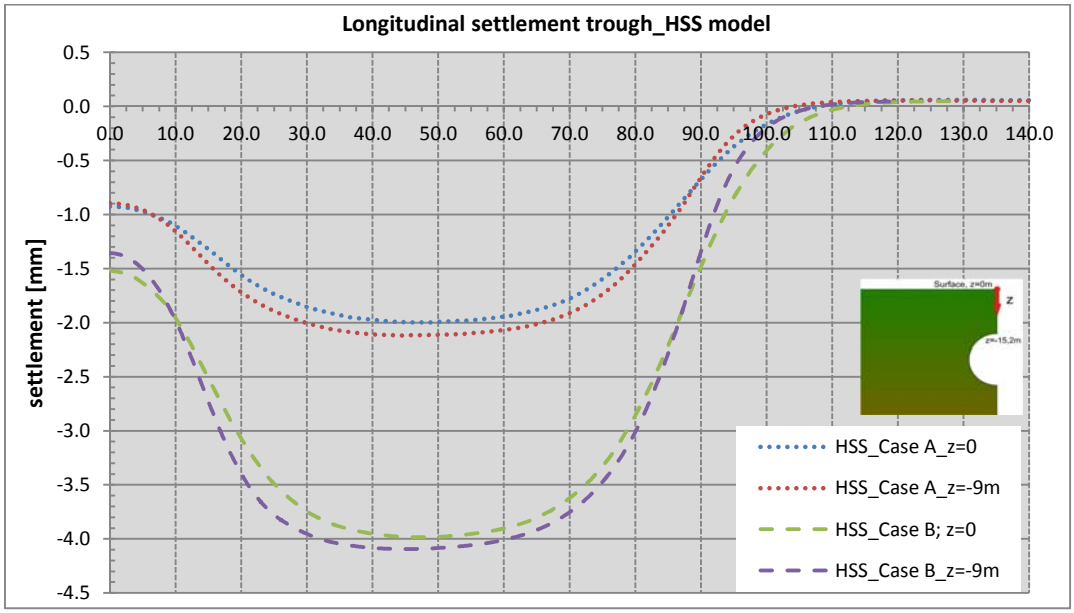

Figure 6-17: Longitudinal settlement trough HSS-model, cross section I

According to figure 6-17, the analysis using pressure case B seems best to express the real conditions as it fits best to the measured maximum value for cross section I of 4.75 mm. Again similar to the 2D analysis no distinct difference of settlements in 9.0 m depth can be seen.

Comparison HSS/HS and MC model:

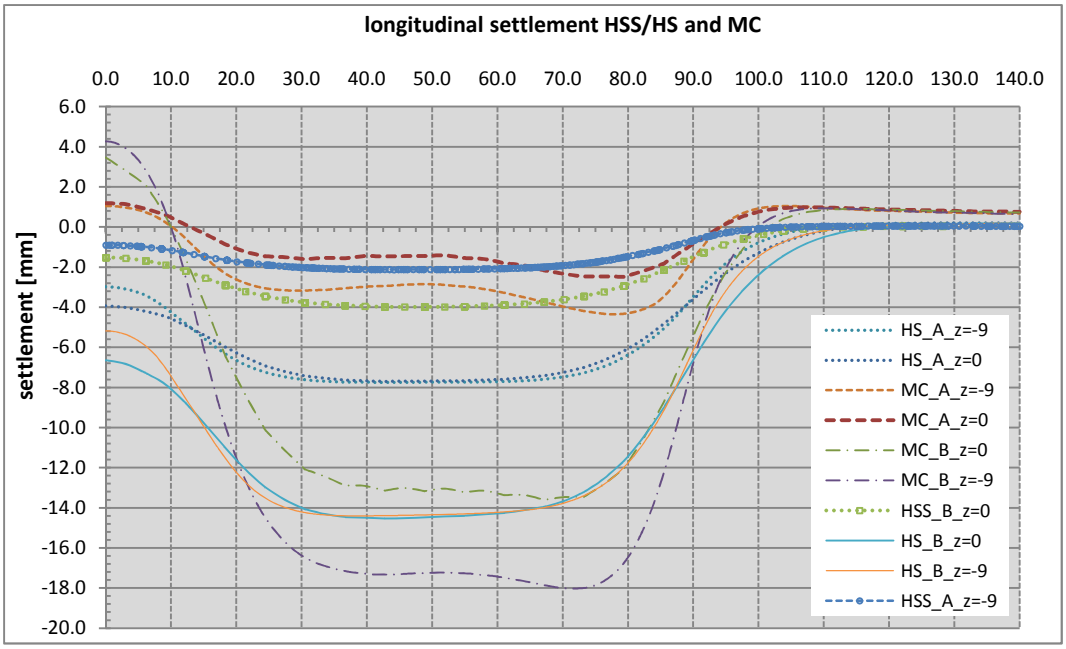

Figure 6-18: Longitudinal settlement trough HSS/HS and MC-model, cross section I

Figure 6-18 clearly indicates the difference among the various constitutive models. Using the same pressure controlled boundary conditions, the HSS model results in 75% less settlement compared to the HS-model.

If looking at the MC trough in detail, one can see that in the centre of the model an upward directed bulge exists, thus meaning that settlements increase after the tunnel face has passed a fixed point. No obvious reason can be found for that phenomenon, but the same reason why the Mohr-Coulomb model predicts heave in a certain distance adjacent to the tunnel axis, has to be responsible for the bulge in longitudinal direction. The unloading due to the excavation of the cavity and the constant stiffness with depth at the MC-model might cause this excessive heave in longitudinal and transversal direction. (Figure 6-19)

Mohr-Coulomb settlement trough; Case A:

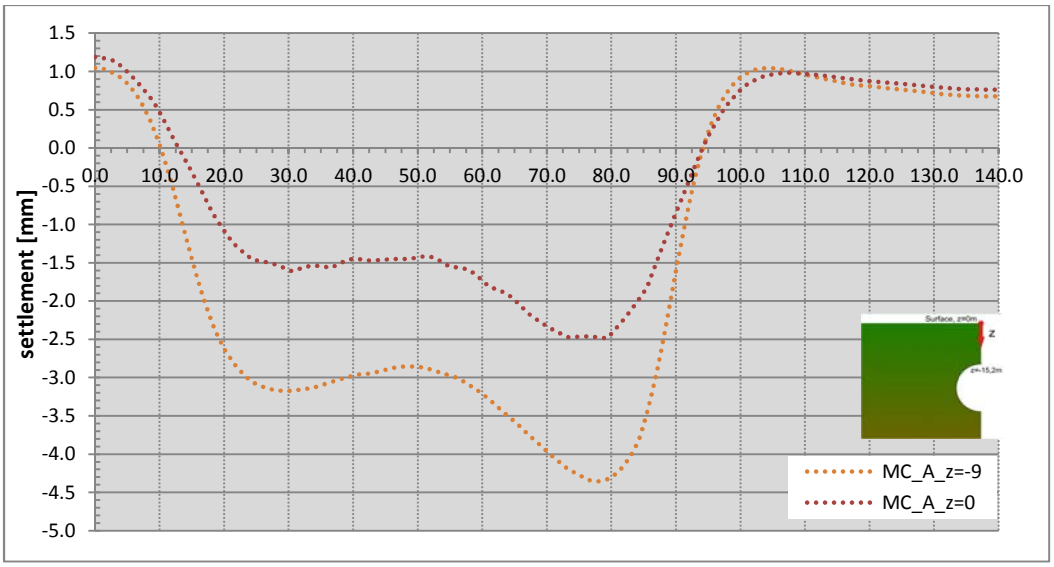

Figure 6-19: MC-model, heave at longitudinal trough

This phenomenon is also experienced when using pressure case B. Figure 6-20 shows the development of the settlement trough for the MC-model in longitudinal direction. At phase 50 the tunnel face is located at 90.0 metres away from the model boundary.

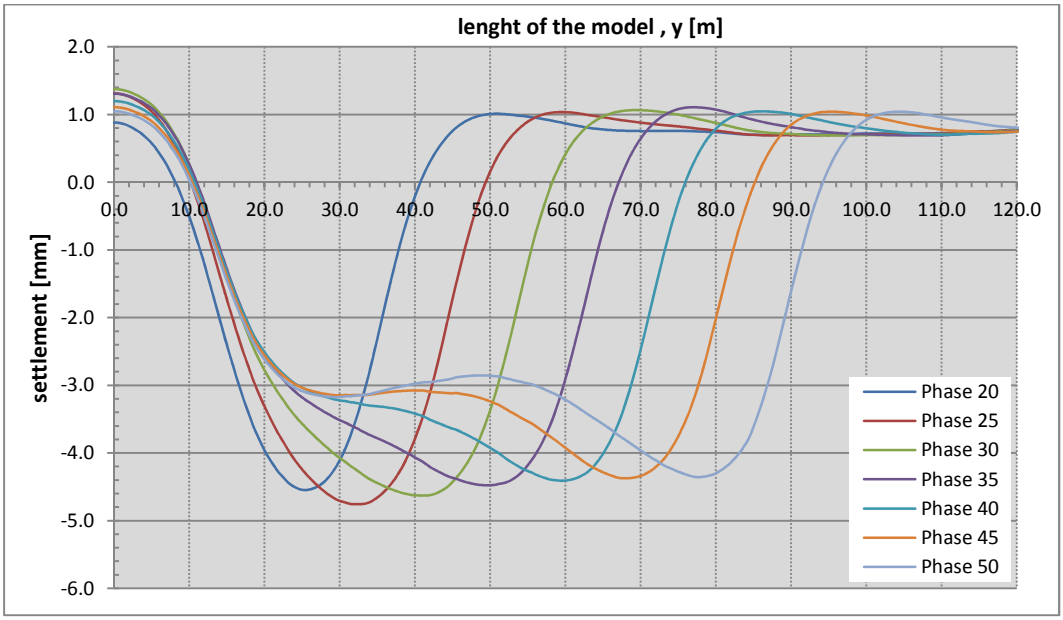

Figure 6-20: MC-model, settlement versus modelling phases

Obviously not reaching steady-state conditions, the Mohr-Coulomb model seems not to be applicable for analysing this type of problems

Settlements versus distance to tunnel face/shield tail:

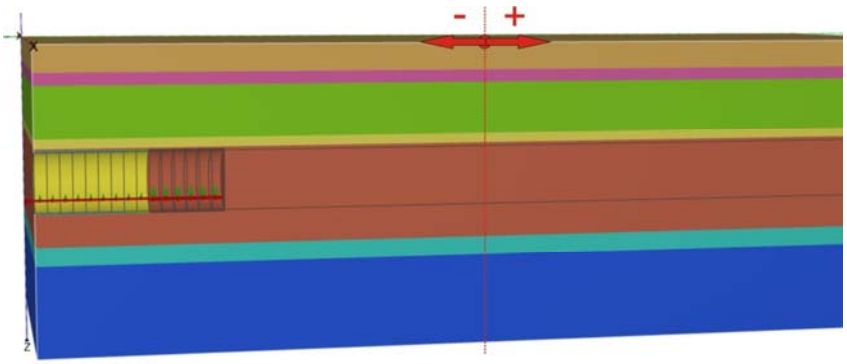

Figure 6-21: Rule for settlement versus distance to tunnel face/shield

Furthermore the settlements have been plotted with respect to the distance of the tunnel face and the shield-tail, to investigate the amount of displacements occurring before and after passing a certain point. For the following charts the distance to the shield-tail versus settlements has been plotted, since the aim is to elaborate the influence of the fluid-imposed pressures around the TBM and the henceforth induced settlements.

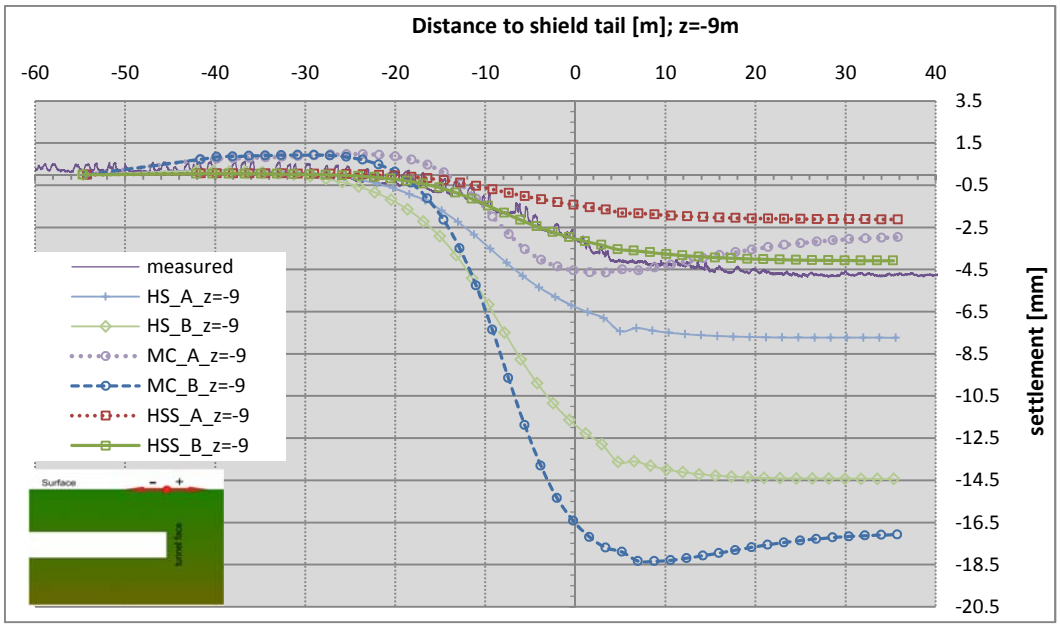

Figure 6-22: Settlement versus distance to shield-tail, all models, cross section I

The Mohr-Coulomb model is apparently the most sensitive model regarding changes in the pressures conditions, whereas the Hardening Soil Small-model gives the most realistic and accurate results related to the shape and the value of the settlement trough.

The chart below shows only the settlements due to the MC and HS-model. Those two constitutive models can only approach the measured trough by implementing pressure case A. Yet both are not able to approximate the shape of the settlement trough. Mohr-Coulomb giving excessive heave, which furthermore leads to a very steep trough and the Hardening-Soil model, overestimates the settlements before the tail is passing the point.

HS and MC-model, case A:

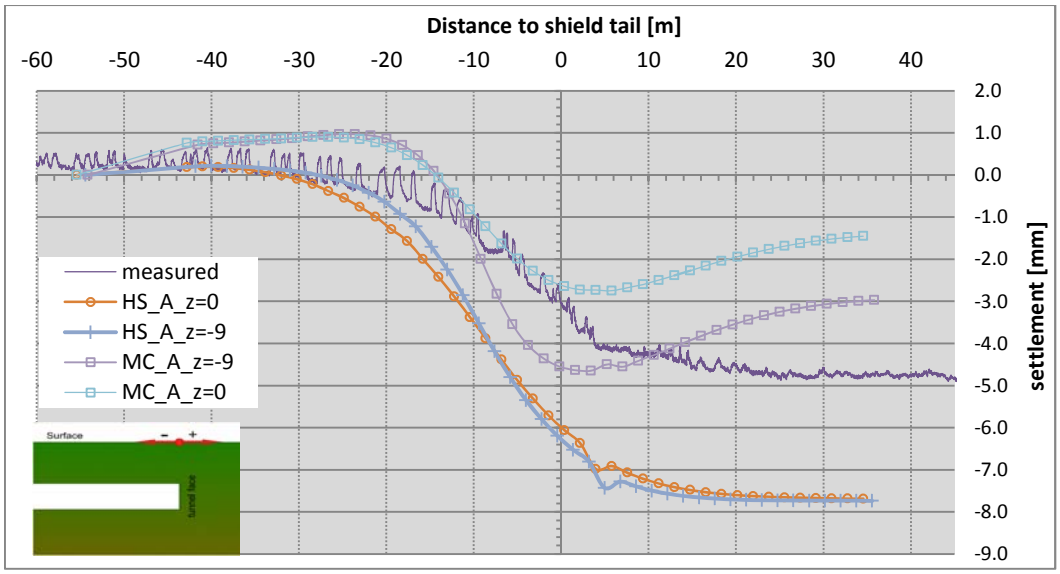

Figure 6-23: Settlement versus distance to shield tail, HS and MC model, cross section I

The calculation was performed using the pressure models which are described in chapter 3. A value of 0.5 bar was chosen to be subtracted from the actual measured pressures (see chapter 3.4.3), resulting in the distribution simulated by case B. Yet this distribution does not fully converge with the monitored settlements, thus leading to the conclusion that the value of 0.5 bar might be too low. As a recommended factor 0.6 to 0.7 bar can be chosen, which will result in a slightly higher maximum settlement.

Using a factor of 0.6 bar to be subtracted from the original pressures, the grout pressure at the TBM tail would be approximately 160 kN/m² and the average pressure along the shield also about 155 kN/m² compared to 165 kN/m² at the present pressure case B.

HSS-model only:

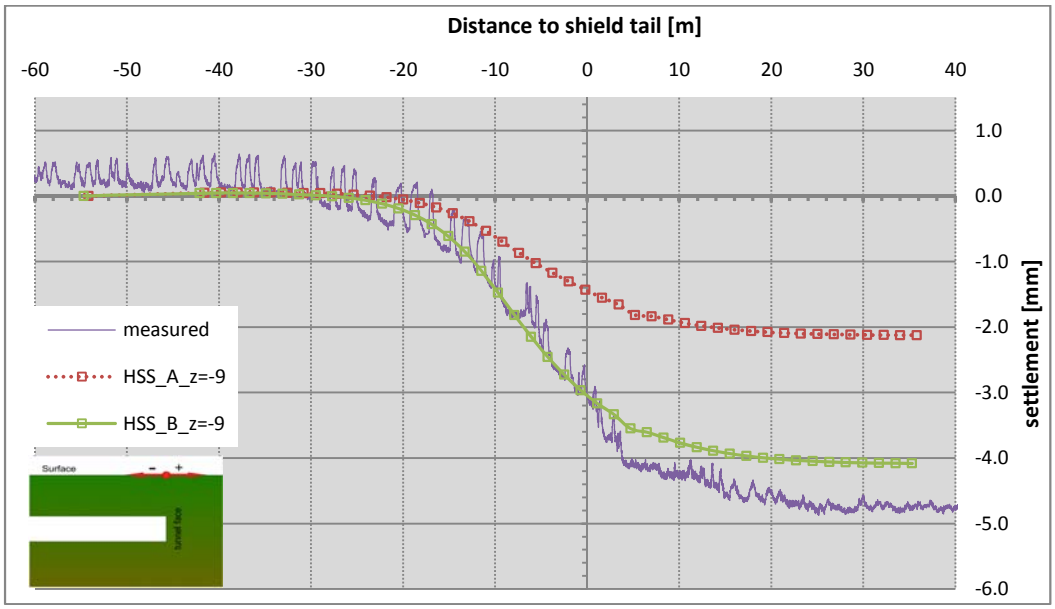

Figure 6-24: Settlements versus distance to shield-tail, HSS model only

Percentage of settlements before and after TBM-shield is passing:

The amount of settlements has been divided by a percentage occurring before and after the TBM shield tail is passing a certain point.

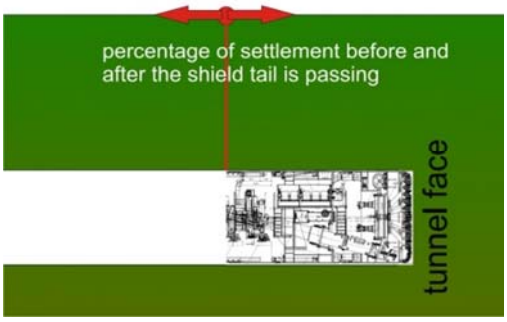

Figure 6-25: Settlement versus distance to shield tail illustration

It was necessary to divide the settlements into the amount before and after the TBM shield is passing, because due to this separation it is evident to see that about 2/3 of the settlements occur until the shield tail of the TBM has passed a certain point. After the tail passed, the remaining 25-30% of settlements are due to the consolidation of grout, soil and the displacement of the lining.

model/percentage	before tail is passing	after
HSS	65-70%	30-35%
HS	80-85%	15-20%
MC	90-95%	5-10%
Actual at the CTL	67%	23%

Table 11: Settlement percentage before & after shield tail is passing

Percentage of settlements before and after TBM-face is passing:

model/percentage	before face is passing	after
HSS	30-35%	65-70%
HS	45-50%	50-55%
MC	35-40%	60-65%
Actual at the CTL	26%	74%

Table 12: Settlement percentage before & after TBM face is passing

The outcome of table 10 and 11 is that about 30-35% (HSS-model) of settlements occurs before the face has passed the focused point. Approximately 35% occur due to directly undermining the location with the TBM and further 25% due to grout/lining-displacement and consolidation.

Thus the TBM and all the adjacent work procedures have a strong influence on ground settlements. Only the HSS model can meet those requirements and can go along with the actual conditions. The HS and the MC model overestimate the settlements before the machine passed the point of focus. When using Mohr-Coulomb decay in settlements is experienced after the shield tail has passed.

6.4.2 Transversal vertical settlement trough

The transversal settlement trough for the HSS and the HS model was elicited in 50 m distance from the model boundary.

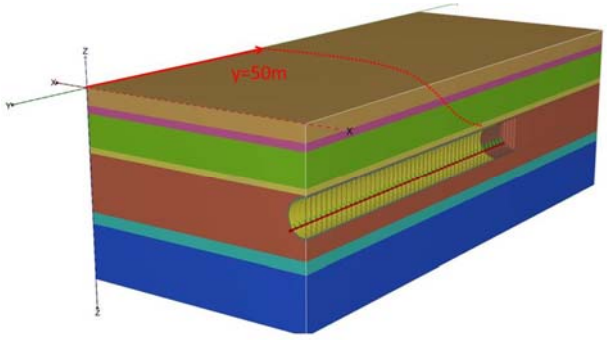

Figure 6-26: Transversal settlement trough

Transversal settlement trough HSS/HS and MC (HSS case A is not illustrated in this chart because the settlements are somewhat small and not easy to verify on this plot):

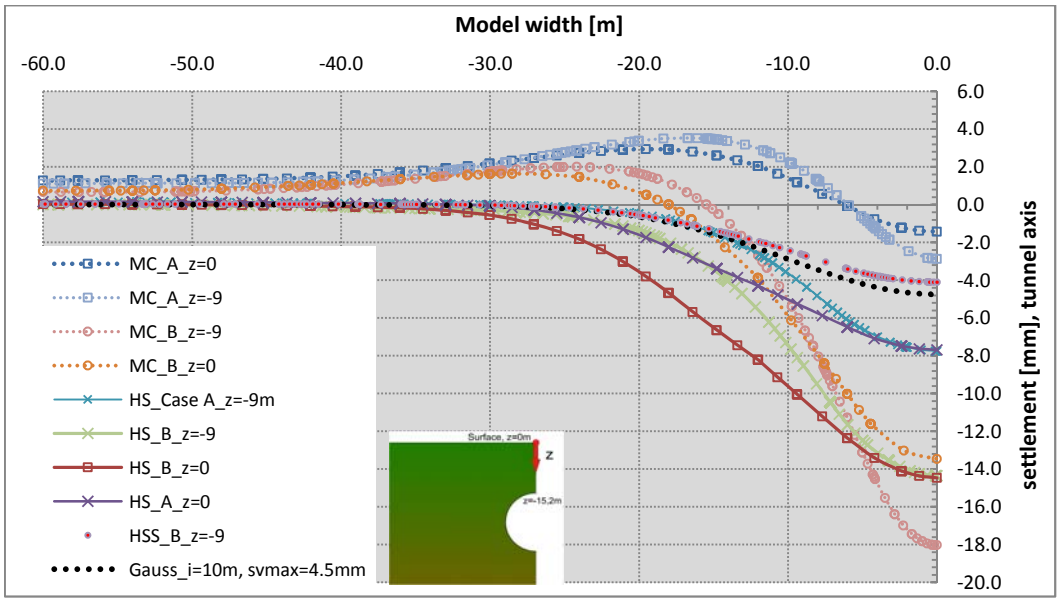

Figure 6-27: Transversal settlement trough, cross section I, all models

Comparing all three constitutive models it is clearly visible that especially the MC and HS-model when using pressure model B, do not fit to the measured values and the Gaussian analytical ap-

proach. From MC-case A to MC-case B there is a range of 17.0 mm, thus outlining the sensitive behaviour of Mohr-Coulomb to different unloading and loading pressures.

Figure 6-27 additionally shows, that the settlement trough produced by the HSS model using a lower grout pressure (Case B) in 9 m depth, fits best to the Gaussian approach and thus to the trough in reality. The surface settlements generate a wider trough, which does not fit as well as the one in a greater depth. Using a higher pressure, the maximum settlement is too low.

Excluding the outranging results, the spread of settlements can be narrowed to about 7.0 mm.

Looking at the figure 6-27 it is clearly visible that neither the MC nor the HS constitutive model can approach the measured settlements of about 4.5 mm. Only the Mohr-Coulomb using a higher pressure reaches the mentioned value but is generating excessive heave 15 m away from the tunnel axis. Similar to the 2D analysis, the HS and the HSS-model again do not predict a significant increment of settlements with depth at the tunnel axis.

HSS/HS and MC_case A:

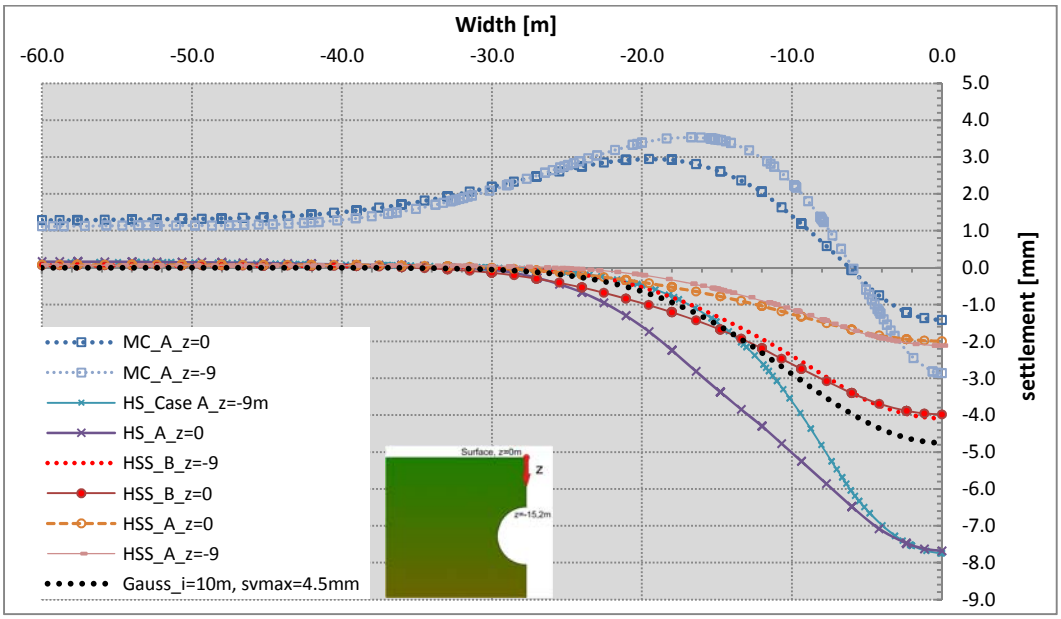

Figure 6-28: Transversal settlement trough, cross section I

HSS -model only:

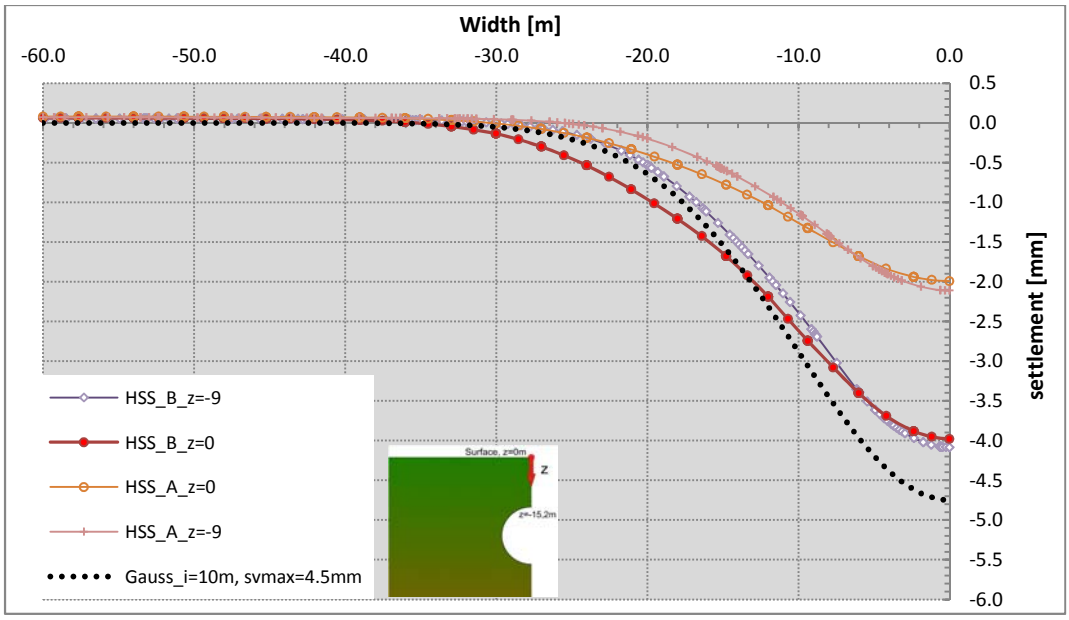

Figure 6-29: Transversal settlement trough, cross section I, HSS only

In figure 6-29 only the HSS model has been plotted, showing that pressure case B fits best to the empirical approach of Gauss with an inflection point of 10.0 m and with Svmax being 4.75 mm.

Volume loss for each constitutive model:

The volume loss has been evaluated for the transversal settlement troughs and does not constitute the real 3 dimensional volume loss which occurs in real conditions.

c.model/pressure case	Case A i=12.0m	Case B i=8.8m
HSS	~0.1%	~0.14%

Table 13: Volume loss, HSS

c.model/pressure case	z=0m i=~12.0m	z=-9m i=8.0m
HS....Case A	0.37%	0.25%
HS.....Case B	0.68%	0.44%

Table 14: Volume loss, HS

c.model/pressure case	z=0m i=6.0m	z=-9m
MC....Case A	0.03%	i=4.3m 0.05%
MC....Case B	0.32%	i=7.4m 0.53%

Table 15: Volume loss, MC

6.4.3 Lining forces & displacement

The chosen cross sections for the lining forces are shown in the figure below (Figure 6-30). One section is immediately after lining installation (“fresh grout”) and the second one is approximately 40 m behind the tunnel face (“old grout”).

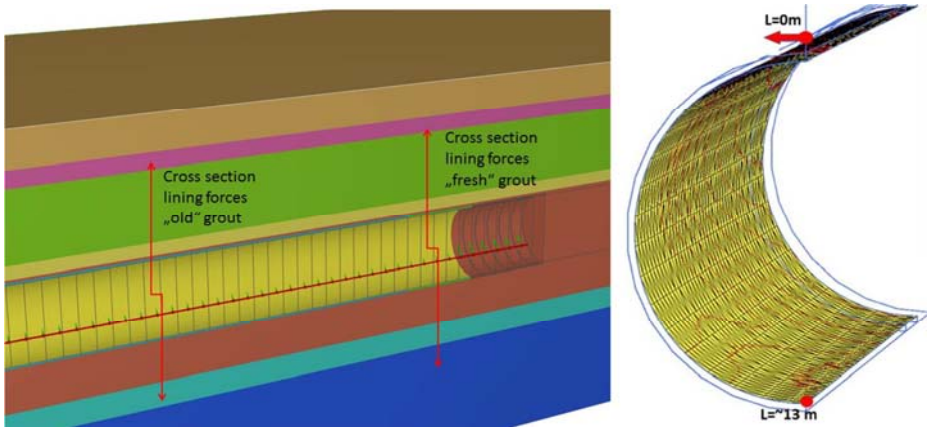

Figure 6-30: Specified cross sections and rule for lining forces

The local axis used in PLAXIS 3D for the structural lining is shown in figure 6-31. In the following elaborations, the axial forces and the bending moment for the second axis (N2 and M2) have been plotted against the circumferential length. 2 denotes the axis in tangential direction of the lining and 1 the axis in axial direction.

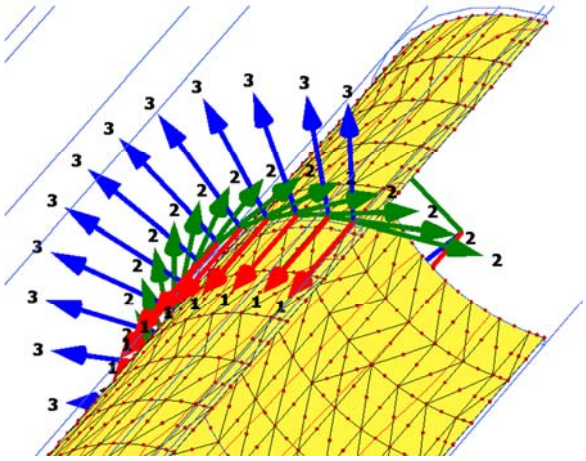

Figure 6-31: Local axis of the structural lining in PLAXIS 3D

Comparison pressure model case A & B:

Bending moment:

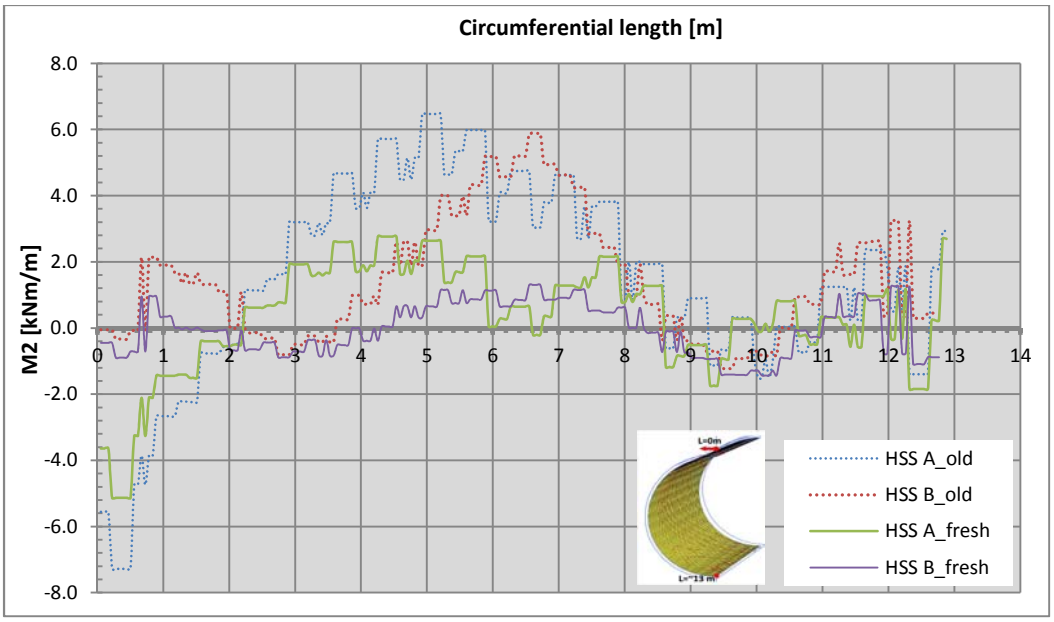

Figure 6-32: Bending moment comparison case A and B

The horizontal axis in the charts always displays the circumferential length, starting at the crown of the tunnel lining (l=0m).

“Fresh” and “old” describes the location of the lining, which is expressed in figure 6-28.

Axial force (N):

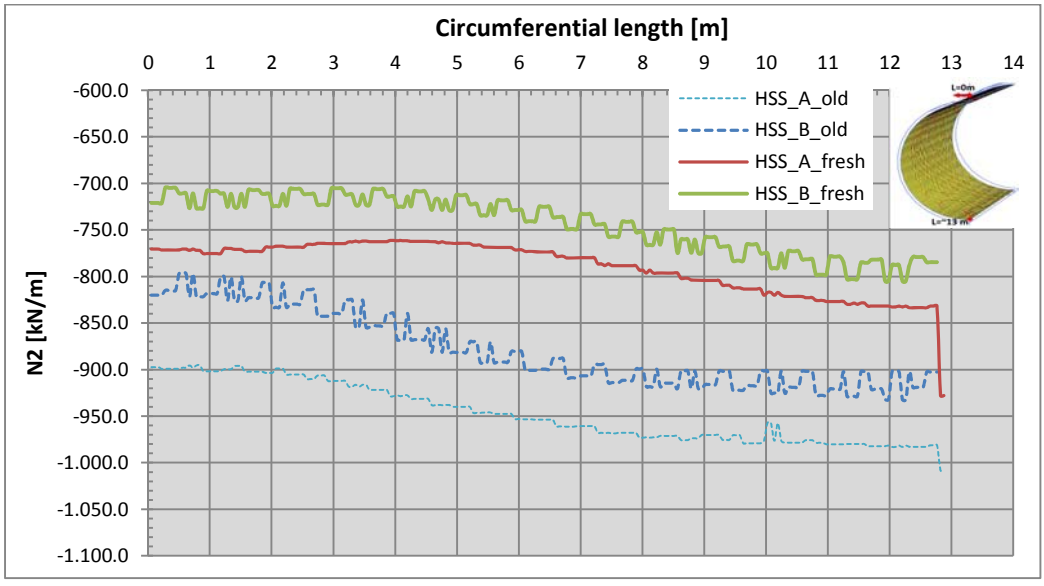

Figure 6-33: Axial force comparison case A and B

The outcome from figure 6-32 and figure 6-33 is that the lining forces short after ring erection are slightly lower than the forces in the lining rings far back in the tunnel. Furthermore, using the same constitutive model, but imposing different pressures within the ground-lining gap, leads to different lining forces. Pressure case B (lower pressure) leads to lower lining forces. Thus one

can see that the construction sequence as well as the imposed pressure in case of a Hydro-shield-TBM is having a significant influence on later lining forces.

Comparison MC/HS and HSS:

Bending moment:

The charts below are based on the lining forces in the cross section “old grout” and on pressure case B.

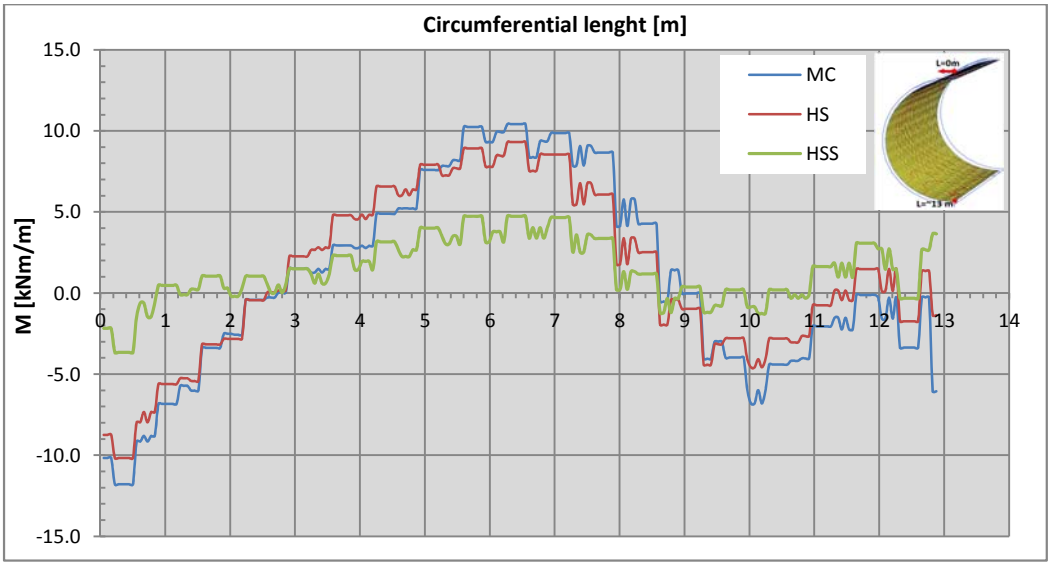

Figure 6-34: Bending moment comparison MC/HS and HSS model

Axial force:

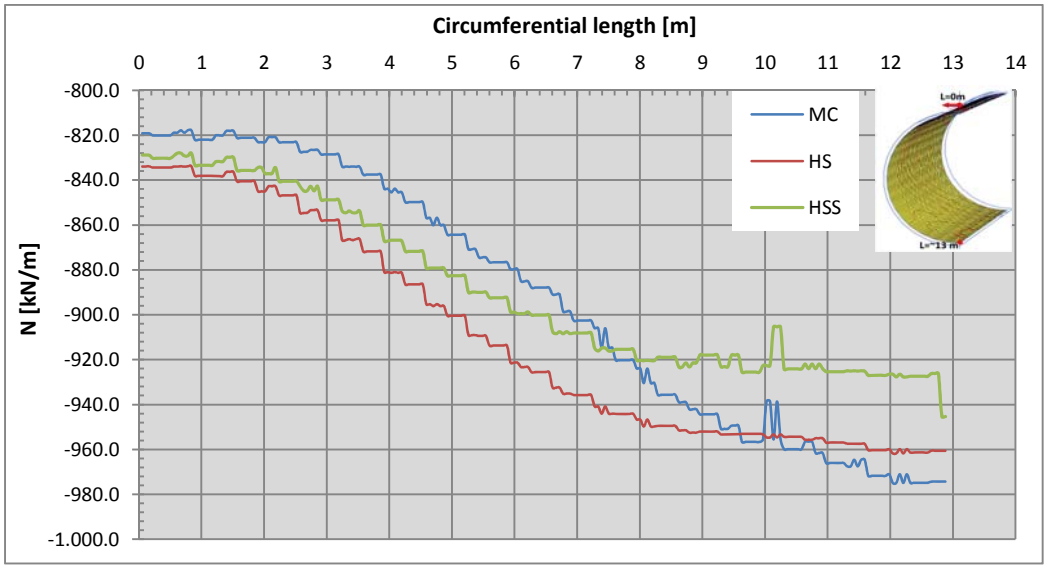

Figure 6-35: Axial force comparison MC/HS and HSS model

Following from the two previous charts, Mohr-Coulomb results in the highest lining forces, whereas the Hardening Soil Small model marks the lowest bending moment and axial force.

Lining Displacement:

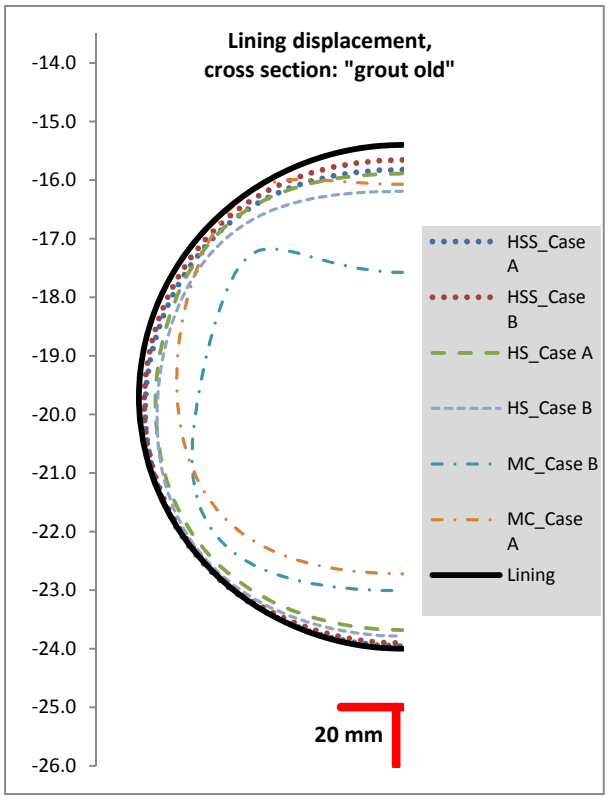

Figure 6-36: Lining displacement, all models

The longitudinal location of the lining displacement was chosen to be nearly in the half of the model, with a distance of 45 m to the tunnel face and 34.2 m to the end of the shield-tail. On basis of the lining displacement, it is obvious to see that the Mohr-Coulomb model again predicts the highest values and results in excessive deformation of the lining. This highlights the fact even more, that the MC-model is not very well applicable analysing this kind of geotechnical structure.

model/ vertical displacement	displacement crown [mm]	displacement invert [mm]
MC	-43.5	19.7
HS	-15.8	4.2
HSS	-8.4	8.4

Table 16: Lining displacement, case B

6.4.4 Comparison anisotropic versus isotropic lining behaviour

The comparison of anisotropic and isotropic lining behaviour was carried out using the HSS model and pressure case A.

Lining displacement:

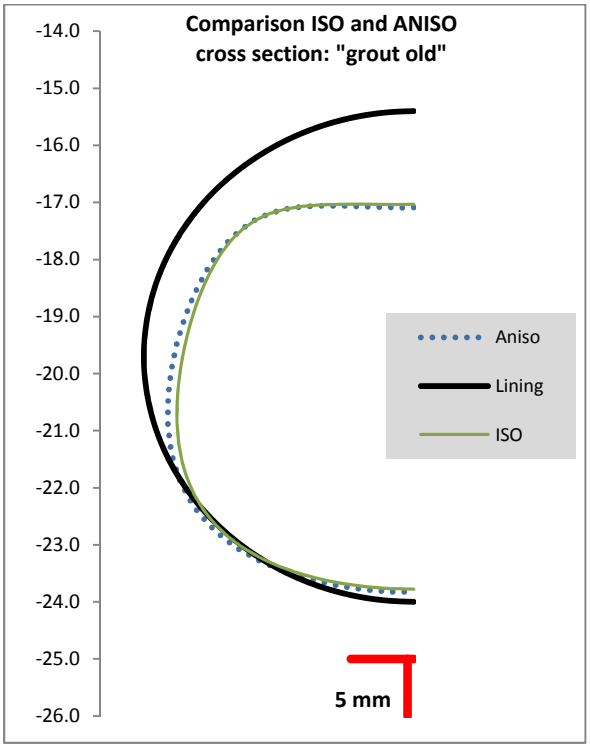

Figure 6-37: Lining displacement anisotropic and isotropic behaviour

The displacement of the isotropic and the anisotropic lining are basically the same. Merely a small difference can be deducted from figure 6-34.

Lining forces:

- Axial:

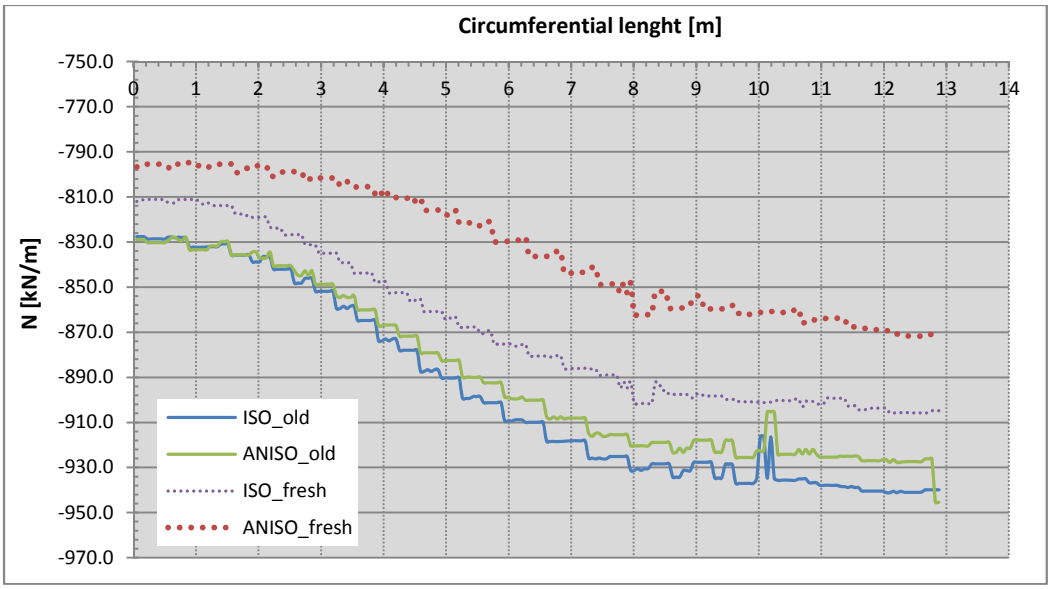

Figure 6-38: Axial force, comparing iso- and anisotropic lining properties

- Bending moment:

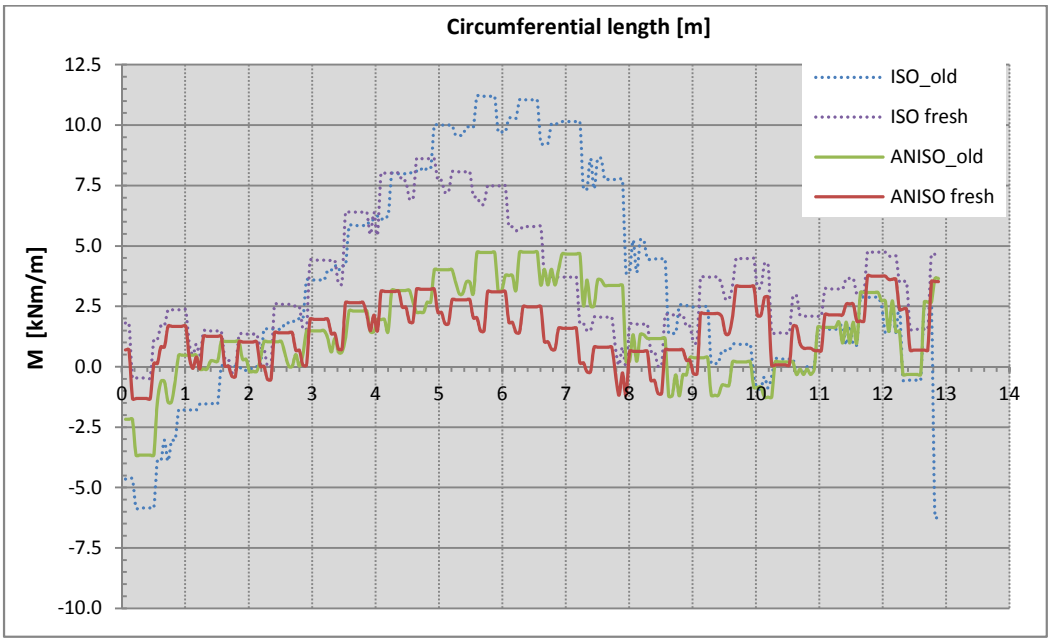

Figure 6-39: Bending moment, comparing iso- and anisotropic lining properties

Anisotropic and Isotropic longitudinal bending of the lining:

At the anisotropic case, the lining shows a heave or an upward directed movement directly behind the TBM in axial direction. This is due to the reduced E_1 in the analysis and the imposed pressure at 5 adjacent lining rings subsequently to the simulated tunnel boring machine. But the figure below illustrates that although the anisotropic case predicts heave, there is no significant difference between the isotropic and the anisotropic lining behaviour in axial direction.

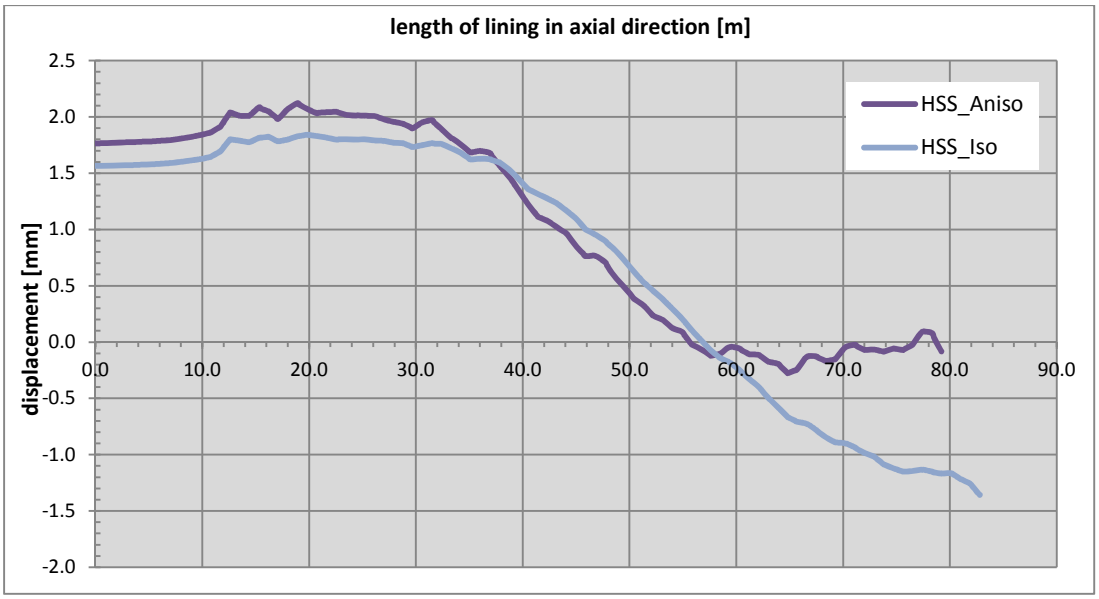

Figure 6-40: Axial displacement of the lining, comparing iso- and anisotropic conditions

7 Summary

At first an investigation on different kinds of tunnelling machines had been conducted, evaluating the possibilities and the influence of a TBM when using it in soil or loose rock.

With the collected parameters from the geotechnical report of the city tunnel in Leipzig, an evaluation was carried out determining the soil properties for the Hardening-Soil and the Hardening-Soil-Small model. Using the oedometric stiffness specified in the report and the effective stresses calculated for each cross section, it was possible to further calculate the reference stiffness for the oedometric modulus, the secant modulus of the triaxial test and the reference stiffness for unloading-reloading conditions. Subsequently the pressures recorded by the Hydroshield-TBM were evaluated and summarized for the individual sections. The grout pressures needed to be reduced, because the gauge measuring these pressures is not installed at the actual outlet at the end of the shield tail. Thus the grout pressures experience a decrease from the monitoring point until the discharge into the gap between lining and cut-surface of the soil.

Furthermore the values were separated into pressures during excavation and pressures during ring-erection, which was necessary to investigate the influence, on the one hand while the TMB advances and on the other hand while the TBM stops.

Using the evaluated parameters and pressure values a 2D analysis was performed first, analysing only surface and sub-surface settlements. Lining forces and displacements had been neglected because a simplified version of the grout pressure method was applied which does not take the lining into account. The 2D analysis showed that it is an easy method which does obtain quite accurate results and thus being an applicable approach for a preliminary estimation.

The concluding 3D calculation was performed using the same parameters, only the grout and lining properties had to be additionally taken into account. Consequently a case-study was conducted elaborating the grout properties and the influence of grout pressures on the lining displacement. Since the lining consists of prefabricated assembled concrete segments, the stiffness properties in radial and axial direction are somewhat different. Reduction factors mentioned by Wood (1975) and Empel (2000) were used for lowering the Young´s modulus in both directions. Calculations were performed using different constitutive models and it could be shown that only the Hardening-Soil model with small strain stiffness was able to approach the settlement trough measured on site. Furthermore only the HSS model was able to do so when using grout pressures which were actually measured at the TBM.

8 Conclusion and recommendations

The following pages will briefly describe the conclusions which could be drawn from the evaluation and modelling process for shield-driven (mainly fluid-supported) tunnels. Further some recommendations for a preliminary analysis will be mentioned, giving hints on the encountered difficulties while writing this thesis:

Conclusion:

As a short and brief conclusion for the whole thesis one could say that it is possible to roughly approximate the method of fluid-supported tunnelling in numerical simulations. Although, that's why the first sentence mentioned the process to be "rougly", it still does not consider the tunnel boring machine as a mechanical device itself, thus it is still bound to a lot of uncertainties. In case of fluid-supported tunnelling there are additionally uncertainties due to the imposed pressures of the injected grout, which are not directly measured at the discharge opening. In general on can say that a 2D approach is still somewhat more convenient and time saving, but does neglect the stress transfer around the tunnel face in axial direction which plays and important role in shield driven tunnels in soil. A 3D analysis might approach the conditions in reality quite accurately but is still a very time consuming tool to use.

Recommendations:

- Dimensions of the model:

  The dimension and the size of the model are mentioned in **chapter 5.2.1** and **6.1 (Figure 6-1)**, but for further information one is referred to **Möller (2006).** For the length of the 3D model, this thesis would recommend about **120.0 to 140.0m**, which is due to the influence of the model boundary. The influence of the boundary conditions, when implementing a "whished-in-place" phase in the beginning, is about 20.0 to 30.0 m. (see also Möller, 2006). At the 3D calculations in chapter 6, the tunnel simulation was stopped when the face reached 90.0m from the model boundary, thus not the full model length was needed for the analysis.

- Simulation and modelling of the effect of the injected grout:

  As **chapter 6.3.2** shows, the value of the grout pressure gradient with depth, has a strong influence on the behaviour of the tunnel lining. Although it might not change the surface settlements too much, it causes uplift and thus excessive bending of the lining in axial direction. This can be omitted if the grout-pressure for the annular gap of the first lining rings adjacent to the simulated TBM (Figure 6-3) is switched off. Another option would be, not to simulate the gap between lining and soil. The gradient has a strong influence on the actual construction process too, because a large uplift might cause an excessive dislocation of the rings itself. To mitigate this effect it is necessary to keep the pressures for Lisene 4 and 6 (bottom openings) as low as possible.

  For the grout-material properties, the thesis suggests a low stiffness for the fresh grout (~1000 to 10 000 kPa) and a stiffness of about 500 000 kPa for the "old" grout. For further information on grout properties and grout behaviour one is referred to **Thienert (2010)**

- Measured grout pressure values, reduction factor:

  As thoroughly discussed in **chapter 3.4**, the grout pressures are measured at the beginning of the shield-tail, which means, the grout experiences a further decrease in pressure until the actual discharge at the injection opening. Site staff and experience values suggest **0.8 bar** as a reduction factor. For a rough estimation of this value, the thesis suggests the equation mentioned in **chapter 3.4.3.1.2.** This chapter also shows that a value of 0.8 bar is slightly too high and suggests a reduction of **0.5 to 0.7 bar.** Furthermore, the influence of TBM advance and ring erection has been investigated, showing that most of the settlements occur due to TBM standstill. Consequently a simple correlation was adopted saying that 30% of the pressures during TBM advance and 70% during ring erection are responsible for the determining settlements. This specifies an average value of pressures which can be used for further analysis.

- Influence of grout-flow along TBM shield:

  The grout flow theory is a 2 dimensional empirical approach trying to describe the behaviour of fluids acting around the TBM. In reality the flow is highly 3 dimensional and probably too comprehensive to be characterised using empirical methods. But it is a useful application to roughly estimate the behaviour of grout and slurry along the TBM shield. As one can see in **chapter 3.4.2**, an assumption needed to be made whether the fluids tend to flow towards the face or towards the tail which depends on the values of pressures itself. The subsequent analysis revealed that this assumption has a great impact on the pressures acting along the TBM and thus furthermore on the final settlements.

  Usually the grout pressure is supposed to be higher than the slurry pressure. This leads automatically to the assumption of grout flow towards the face. When evaluating the pressures for the analysis, it was evident to see that this is not the standard case. Furthermore, what happens if the grout and the slurry pressure are equal? Thus for analysing settlements it is more conservative to say, that the flow is unknown but a pressure decrease occurs from the tunnel face to the shield tail. The analysis in chapter 5 and 6 shows, that the flow assumption towards the face does not go along with real conditions. The difference in pressure whether there will be flow towards face or tail is about 40 kN/m² or 0.4 bar and the difference in settlements appear to be twice as much for the assumption towards tail.

  For more information on grout flow or grout consolidation see also **Bezuijen (2009) or Talmon et al., 2009.**

- Influence of the constitutive model:

  As one can see in the analysis results in **chapter 5 and 6**, the constitutive model has a great influence on surface and sub-surface settlements.

  Altogether it is possible to say that the Mohr-Coulomb model is not applicable for such kind of geotechnical analysis. The Hardening-Soil is applicable but resulting in higher settlements compared to the HS-small model. In thesis it could be shown that the model including small strain stiffness gets closest to the measured result and also to the shape of the settlement trough. Since the parameters needed for the Hardening-Soil models are usually not given in any kind of report, it is quite complex to get to the properties which

can be used for the further input. **Chapter 4.3.2** describes the evaluation of parameters from a geotechnical report for the properties needed in the HS and HSS model.

As a conclusion one could say that geotechnical tunnelling problems highly incorporates the stiffness at very small strains and thus a higher shear modulus. The MC model is not applicable for the evaluation of surface settlements and the HS-model constitutes a more conservative approach.

Empfehlungen:

- Modell Abmessungen und Dimensionen:

  Die Abmessungen für das 2D und 3D Modell sind in **Kapitel 5.2.1 und 6.1** näher erläutert. Für genauere Informationen wird auf Möller (2006) verwiesen. Die Länge des 3D Modells wird mit rund **120 bis 140m** empfohlen, hängt aber ebenfalls stark von der Problemstellung und auch der Breite eines Tübbing-Ringes ab. Weiteres hat der Modellrand ein großen Einfluss auf die Länge des Modells. Bei Verwendung eines „whised-in-place" Bereiches in der ersten Phase, beträgt dieser Einfluss rund **20 bis 30m.**

- Modellierung der Wirkung des Ringspaltmörtels:

  Die Modellierung der Wirkung des Ringspaltmörtels erfolgte wie in **Bild 6-3** ersichtlich, in 5 Volumselementen hinter dem offenen Bereich welcher die TBM simuliert. Wobei bereits in diesem offenen Bereich der Einfluss des Mörteldruckes miteinfließt und als Ganzes betrachtet werden muss.

  Grundsätzlich wird in dieser Arbeit zwischen dem die TBM umgebenden Mörtel und den Mörtel im Ringspalt unterschieden. Der simulierte Mörtel im Ringspalt und dessen Gradient, welcher mit der Tiefe zunimmt, hat einen großen Einfluss auf das Verhalten der Tunnelröhre in Längsrichtung. Er beeinflusst die Setzungen an der Oberfläche nur in geringem Ausmaß, jedoch die Verformung der Tübbinge entscheidend. Als Gradiente wird hierbei **5 kN/m²/m** empfohlen. In der Praxis ist dieser meist noch ein wenig höher und führt zum Aufschwimmen der Tübbingringe. Daher sollte auch während des Bauablaufes der Druck der Lisenen 4 und 6 überwacht und möglichst klein gehalten werden. Um dies in der numerischen Simulation vermeiden zu können, wäre es möglich diesen Faktor überhaupt wegzulassen.

  Für die Mörtelsteifigkeit in frischem Zustand wird rund 1000 bis 10 000 kPa empfohlen und für den bereits erhärteten Mörtel ca. 500 000 kPa. Hierbei wird aber auf **Thienert (2010)** verwiesen, welcher dieses Thema genauestens behandelt.

- Mörteldrücke, Reduktionsfaktor für die gemessen Werte:

  Wie in Kapitel 3.4 ausführlich beschrieben, werden die Mörteldrücke nicht an der Stelle gemessen wo ihre Wirkung zum Einsatz kommt, sondern rund 4.5m davor. Was bedeutet, dass der Mörtel bis zum Austritt in den Ringspalt einen weiteren Druckverlust erfährt, welcher nicht gemessen wird und nur abgeschätzt werden kann. Erfahrungswerte schätzen diesen Faktor auf 0.8bar. Für eine grobe Abschätzung wird hierbei auf die Formel in 3.4.3.1.2 verwiesen. Dies beschreibt den Druckverlust einer Strömung in einem geschlossenen Kanal auf Grund der eigenen Scherfestigkeit und der Viskosität. Dieses Ka-

pitel zeigt auch, das ein Wert von 0.8bar etwas zu hoch ist, und daher eher ein Wert von 0.5 bis 0.7bar empfohlen wird. Wobei dies sehr stark vom Material des eingesetzten Mörtels abhängt (2-Komponenten, zementfrei etc). Des Weiteren wurde aufgezeigt, das die Setzungen zumeist infolge vom TBM Stillstand auftreten. Da aber auch das Anfahren der Maschine eine Änderung im Korngefüge hervorruft, hat dies ebenso einen Effekt auf die daraus entstehenden Setzungen. Daher wurde ein simples Verhältnis vorgeschlagen, welches mit 30% die Drücke aus Vortrieb und 70% aus der Tübbing Installation heranzieht und somit auf einen durchschnittlichen Druck kommt welcher für weitere Analysen verwendet werden kann.

- Einfluss der Mörtelströmung um die TBM:

  Die Analyse der Mörtelströmung bezieht sich auf einen 2 dimensionalen empirischen Ansatz, welcher versucht die Strömung und Drücke entlang des TBM-Mantels zu beschreiben. Da diese Vorgänge jedoch 3 dimensional und unstetig von statten gehen, stellt ein analytischer Ansatz nur eine ungenaue Annäherung an das eigentlich Verhalten dar. Dennoch kann damit eine ungefähre Abschätzung getroffen werden, welchen Einfluss der Mörteldruck und die korrespondierende Strömung auf die Druckverteilung und somit in weitere Folge auf Setzungsprognosen hat. Ersichtlich in Kapitel 3.4.2 ist, dass eine Annahme getroffen werden muss, in welche Richtung sich diese erwähnte Strömung bewegt. Die weiterführenden Berechnungen zeigten, dass diese Annahme erheblichen Einfluss auf das Modell und auf die Endsetzungen hat.

  Die Annahme das der Mörteldruck größer als der Stützdruck ist und die Strömung sich in Richtung Ortsbrust bewegt, ergab ungefähr die Hälfte an Setzungen verglichen zur zweiten Annahme mit geringerem Mörteldruck. Der Druckunterschied zwischen beiden Vergleichen liegt bei rund 40 kN/m² oder 0.4 bar. Im Zuge dieser Arbeit wurde festgestellt, dass die Mörteldrücke den Stützdrücken ähneln und sich somit eher ein Fluss Richtung Schildschwanz einstellen wird.

- Einfluss der Wahl des Stoffgesetzes:

  Wie die Ergebnisse in Kapitel 5 und 6 zeigen, hat die Wahl des Stoffgesetzes einen erheblichen Einfluss auf die Endresultate der Setzungsprognose. Im Großen und Ganzen lässt sich jedoch sagen, dass das Mohr-Coulomb model für Tunnel induzierte Setzungsprognosen nicht anwendbar ist. Mohr-Coulomb prognostiziert eine Hebung rund 10 bis 20m vom Modellrand entfernt, was grundsätzlich auf die konstante Steifigkeit mit der Tiefe zurückzuführen ist. Die Berechnungen mit dem HS-model ergeben mehr Setzung als das HS-small model. Des Weiteren kann sich nur das Stoffgesetz mit der small strain stiffness der gemessenen und der empirischen Setzungskurve in Form und Wert annähern.

Kapitel und Seitenverweis anhand von Schlagwörtern:

List of tables

List of figures

Reference list

van Empel, W.H.N.C., de Waal, R.G.A. and van der Veen, C. 2000. Segmental tunnel lining behaviour in axial direction. Rotterdam : Geotechnical Aspects of Underground Construction in Soft Ground, 2000. Pages 357-362.

Anagnostou, G. and Kovari, K. 1994. *Stability Analysis for tunneling with EPB and slurry shields.* Zurich : s.n., 1994.

Bezuijen, Adam and Bakker, K.J. 2007. *Bentonite and grout flow around a TBM.* Prague : ITA, 2007.

Bezuijen, Adam. 2009. The influence of grout and bentonite slurry on the process of TBM tunneling. *Geomechanics and Tunneling.* 2, 2009, No.3, Pages 294-303.

Brinkgreve, R.B.J. and Vermeer, P.A. 2011. *Plaxis Finite Elemente Code for Soil and Rock Analyses.* Rotterdam : A.A. Balkema, 2011.

Gruebl, Fritz. 2009. *Design criteria for segmental linings in soft ground.* Budapest : ITA, 2009.

Institut für Festkörpermechanik, TU-Dresden and Balke, Herbert. 2010. *Einführung in die Technische Mechanik.* Dresden : Springer, 2010.

Luttikholt, Arjan. 2007. Ultimate Limit State Analysis of a segmental tunnel lining. *Results of full-scale tests compared to finite element analysis.* Delft : TU Delft, 2007.

Maidl, et al. 2011. *Mechanised Shield Tunnelling.* Bochum : Ernst&Sohn, 2011.

Mair, R.J. and Taylor, R.N. 1997. *Bored tunneling in urban environment.* London : s.n., 1997.

Möller, Sven. 2006. *Tunnel induced settlements and structural forces in linings.* Stuttgart : P.A. Vermeer, 2006.

Plaxis. 2012. Plaxis 3D Material Model Manual. Delft : Plaxis, 2012.

Schweiger, H. 2012. Lecture notes. *Computational Geotechnics.* Graz : s.n., 2012.

Stack. 1982. *Handbook of Mining and Tunnelling Machinery.* Chichester : Wiley, 1982.

Talmon, A.M. and Bezuijen, A. 2009. Simulating the consolidation fo TBM grout at Noordplaspolder. *Tunnelling and Underground Space Technology.* 2009, Vol. Volume 24, Issue 5, Pages 493-499.

Thewes, Markus. 2009. *TBM drives in soft grounds: Face stability and annular grouting.* Budapest : The international tunnelling association, 2009.

Thewes, Markus und Budach, Christoph. 2009. *Mörtel im Tunnelbau (Grout for tunnel construction).* Bochum : bauportal, www.baumaschine.de, 2009.

Thienert. 2010. *Zementfreie Mörtel für die Ringspaltverpressung beim Schildvortrieb mit flüssigkeitsgestützter Ortsbrust.* Wuppertal : Bergische Universität Wuppertal, 2010.

Thomas, Kasper. 2004. Fininte Elemente Simulation maschineller Tunnelvortriebe in wassergesättigtem Lockergestein. Bochum : Ruhr-Universität Bochum, 2004.

Wikipedia. Wikipedia. [Online] [Zitat vom: 18. August 2012.] www.wikipedia.com.

Winselmann, D., et al. 2000. Aktuelle Berechnungsmethoden für Tunnelauskleidungen mit Tübbingen und deren verfahrenstechnische Voraussetzungen. Hannover : Baugrundtagung Hannover, 2000.

Wood, Muir. 1975. The circular tunnel in elastic ground. s.l. : Geotechnique, 1975. 25.

Internet Reference list:

AG, Herrenknecht. Herrenknecht. [Online] Herrenknecht AG. [Zitat vom: 17. 07 2012.] http://www.herrenknecht.de/meta-navigation/home.html.

Engineers, Babendererde. 2008. facesupport. *facesupport.* [Online] Babendererde Engineers GmbH, 2008. [Zitat vom: 5. Juni 2012.] http://www.facesupport.org/home.

Habermann, Arthur. habermann-gmbh.de. [Online] Habermann Arthur GmbH & Co KG. [Zitat vom: 11. 07 2012.] http://www.habermann-gmbh.de/.

Schwing. [Online] Schwing GmbH. [Zitat vom: 15. Juni 2012.] http://www.schwing.de/.

Google. Google maps. [Online] [Zitat vom: 15. Juni 2012.] www.google.com/maps.

Wikipedia. Wikipedia. [Online] [Zitat vom: 18. August 2012.] www.wikipedia.com.